AD-A093 803 MCDONNELL AIRCRAFT CO ST LOUIS MO F/G 11/6
ENVIRONMENT-LOAD INTERACTION EFFECTS ON CRACK GROWTH IN LANDING--ETC(U)
OCT 80 C R SAFF N62269-79-C-0275
UNCLASSIFIED NADC-79095-60 NL

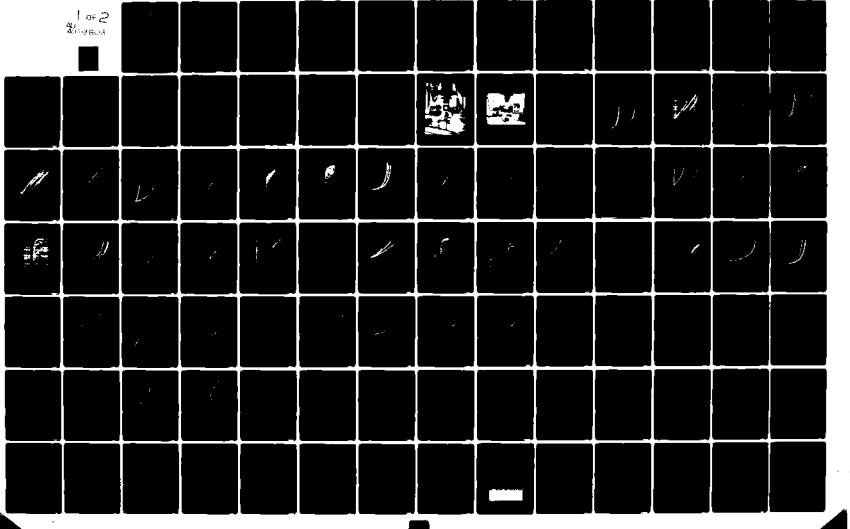

REPORT NO. NADC-79095-60

AD A093803

12

LEVEL II

ENVIRONMENT-LOAD INTERACTION EFFECTS ON CRACK GROWTH IN LANDING GEAR STEELS

DECEMBER 1980

C.R. SAFF

MCDONNELL AIRCRAFT COMPANY
MCDONNELL DOUGLAS CORPORATION
P.O. BOX 516
ST. LOUIS, MISSOURI 63166

APPROVED FOR PUBLIC RELEASE; DISTRIBUTION UNLIMITED

PREPARED FOR
UNITED STATES NAVY
NAVAL AIR DEVELOPMENT CENTER
WARMINSTER, PA 18974

NOTICES

REPORT NUMBERING SYSTEM - The numbering of technical project reports issued by the Naval Air Development Center is arranged for specific identification purposes. Each number consists of the Center acronym, the calendar year in which the number was assigned, the sequence number of the report within the specific calendar year, and the official 2-digit correspondence code of the Command Office or the Functional Directorate responsible for the report. For example: Report No. NADC-78015-20 indicates the fifteenth Center report for the year 1978, and prepared by the Systems Directorate. The numerical codes are as follows:

CODE	OFFICE OR DIRECTORATE
00	Commander, Naval Air Development Center
01	Technical Director, Naval Air Development Center
02	Comptroller
10	Directorate Command Projects
20	Systems Directorate
30	Sensors & Avionics Technology Directorate
40	Communication & Navigation Technology Directorate
50	Software Computer Directorate
60	Aircraft & Crew Systems Technology Directorate
70	Planning Assessment Resources
80	Engineering Support Group

PRODUCT ENDORSEMENT - The discussion or instructions concerning commercial products herein do not constitute an endorsement by the Government nor do they convey or imply the license or right to use such products.

APPROVED BY: E. J. Sturm DATE: 11/17/80

E. J. Sturm
CAPT USN

SECURITY CLASSIFICATION OF THIS PAGE *(When Data Entered)*

19 **REPORT DOCUMENTATION PAGE**

READ INSTRUCTIONS BEFORE COMPLETING FORM

1. REPORT NUMBER: NADC-79095-60 (18)	2. GOVT ACCESSION NO.: AD-A093 803
3. RECIPIENT'S CATALOG NUMBER:	
4. TITLE *(and Subtitle)*: ENVIRONMENT-LOAD INTERACTION EFFECTS ON CRACK GROWTH IN LANDING GEAR STEELS (6)	5. TYPE OF REPORT & PERIOD COVERED: Final Report, Aug 1979-Aug 1980 (13)
	6. PERFORMING ORG. REPORT NUMBER:
7. AUTHOR(s): C. R. Saff (10)	8. CONTRACT OR GRANT NUMBER(s): N62269-79-C-0275 (15)
9. PERFORMING ORGANIZATION NAME AND ADDRESS: McDonnell Aircraft Company, P.O. Box 516, St. Louis, Missouri 63066 (16) F41441	10. PROGRAM ELEMENT, PROJECT, TASK AREA & WORK UNIT NUMBERS: 62241 N (12), Air Task WF41-400-000, Work Unit 2A-601
11. CONTROLLING OFFICE NAME AND ADDRESS: Commander Naval Air Development Center, Warminster, Pennsylvania 18974 (11)	12. REPORT DATE: Oct 1980 (12) 15
	13. NUMBER OF PAGES: 139
14. MONITORING AGENCY NAME & ADDRESS *(if different from Controlling Office)*:	15. SECURITY CLASS. *(of this report)*: Unclassified
	15a. DECLASSIFICATION/DOWNGRADING SCHEDULE:

16. DISTRIBUTION STATEMENT *(of this Report)*

Approved for public release: distribution unlimited.

17. DISTRIBUTION STATEMENT *(of the abstract entered in Block 20, if different from Report)*

18. SUPPLEMENTARY NOTES

19. KEY WORDS *(Continue on reverse side if necessary and identify by block number)*

Crack Growth	Surface flaws
Steels	Crack Growth Prediction
Environmental Acceleration	Landing Gear
	Spectrum Loads

20. ABSTRACT *(Continue on reverse side if necessary and identify by block number)*

The objective of this program was to investigate chemical environment-load interaction effects on crack propagation. Dry air (<10 percent relative humidity) was used as a reference environment. Alternate immersion in synthetic sea water was used to simulate the aggressive chemical environment to which Navy carrier based aircraft are subjected. Tests were performed to determine the behavior of 300M and HP-9-4-.30 steels in both environments under a variety of stress ratios and load wave shapes. A crack growth

DD FORM 1 JAN 73 1473

4 111

SECURITY CLASSIFICATION OF THIS PAGE *(When Data Entered)*

20. ABSTRACT (continued)

prediction capability developed through analysis and test accounts for environment and load interaction effects. A flight-by-flight test stress history was developed for a landing gear of a carrier based Navy aircraft. Crack growth predictions were prepared and tests performed to verify the chemical environment-spectrum loading analysis capability. A comparison of landing gear spectra under Air Force and Navy design conditions is presented.

FOREWORD

This report was prepared by McDonnell Aircraft Company (MCAIR), St. Louis, Missouri, for the Structures Research Branch of the Naval Air Development Center (NADC), Warminster, Pennsylvania, under Contract No. N62269-79-C-0275. Mr. M. S. Rosenfeld was the Project Engineer.

The Structural Research Department of McDonnell Aircraft Company had responsibility for performance of this program. The program manager for MCAIR was H. D. Dill. Principal author of this report is C. R. Saff. W. D. Nowak, MCAIR, was a consultant for development of the landing gear load spectrum. K. C. Garland and F. J. Coffey, MCAIR Metallurgical Laboratories, performed the test program.

This report covers work accomplished during the period August 1979 through August 1980.

This report was released by the author in October 1980 for publication.

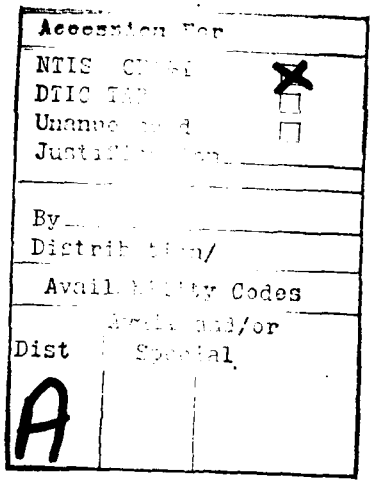

TABLE OF CONTENTS

TABLE OF CONTENTS (Concluded)

LIST OF ILLUSTRATIONS

LIST OF ILLUSTRATIONS (Continued)

LIST OF ILLUSTRATIONS (Continued)

LIST OF ILLUSTRATIONS (Concluded)

LIST OF TABLES

SECTION I

INTRODUCTION

Aircraft are subjected to a combination of environmental attack and varying loads. Structural integrity can be impaired by surface degradation due to corrosive action or when crack damage is developed or aggravated by the environment.

Landing gear of Navy aircraft are subjected to an extreme combination of aggressive chemical environment and high load levels, particularly during carrier operations. Landing gear structure usually consists of a series of nonredundant elements. Weight and geometrical constraints require that landing gear be fabricated from high strength materials, even though these materials may be susceptible to environmentally accelerated crack growth.

Great care is taken during manufacturing and processing to ensure that these nonredundant structural elements are as flaw-free as possible. However, even with good quality control, minute cracks can be developed, for example during grinding and plating of nigh strength steel parts. Also, as with any aircraft structural subsystem, small cracks can be initiated during service life from latent damage sites developed by fretting, pitting, intergranular stress corrosion cracking (for aluminum alloys) and fatigue.

In landing gear structural components, the cracks of principal concern initiate on the surface of the component. Cracks, whether initially present or service developed, can propagate to failure in these highly-loaded nonredundant structural subsystems and cause system failure.

The objective of this program was to systematically investigate crack growth behavior under chemical environment and loading combinations typical of Navy aircraft. Both constant amplitude and spectrum tests were performed. Stress histories were selected to represent usage conditions for a landing gear component of a multi-mission, carrier-based Navy aircraft. Experimental results were used to evaluate the ability of available analysis procedures to predict crack growth behavior under aggressive environments.

In Task I, Model Calibration and Evaluation Test Program, constant amplitude and spectrum crack growth data were obtained to calibrate and evaluate the current analysis procedure. Twenty-eight specimens were tested in dry air and alternate immersion in sea water environments under a variety of loading frequencies. Results of the alternate immersion tests were used to revise the crack growth analysis methodology to include analysis of the decaying rate of crack growth which occurs during drying in the alternate immersion tests of 300M steel. Materials studied were 300M and HP-9Ni-4Co-.30 steels.

In Task II, Landing Gear Stress History, a flight-by-flight test stress history was prepared for a landing gear component. The F-4J main landing gear was selected to determine the stress values and to estimate times associated with each stress condition. This stress history was developed based on design loads and not on field measurements.

In Task III, Crack Growth Prediction, the methodology developed and revised in Task I was used to predict spectrum crack growth in dry air and alternate immersion in sea water environments. Predictions were prepared for the flight-by-flight stress history both including and ignoring sustained loads.

In Task IV, Verification Test Program, ten tests were performed to verify the crack growth prediction methodology. Spectrum fatigue tests were performed on center cracked and surface flawed panels in both dry air and synthetic sea water environments using both accelerated and sustained load stress histories.

In Task V, Comparison of Analysis and Test Results, results of the verification test program were compared with predicted crack growth from Task III. These comparisons indicate that the prediction methodology provides accurate assessment of crack growth under aggressive environments under varying loading conditions.

SECTION II

MODEL CALIBRATION AND EVALUATION PROGRAM

1. TEST PROGRAM SUMMARY - The purpose of this program was to obtain experimental data necessary for calibrating and evaluating a set of crack growth prediction algorithms. Table 1 summarizes the crack growth program. Two steels (300M and HP-9-4-.30) were each subjected to 14 tests. Data were obtained to determine material behavior, verify stress intensity solutions for part-through elliptical flaw geometries, and develop crack growth prediction algorithms. The test series was identical for each material with the exception of Specimen 13 for which test conditions were selected independently in each case. The tests had four objectives:

- o Characterize each material by developing constant amplitude fatigue crack growth rate data in a dry air environment. (Specimens 1-3).
- o Evaluate a linear summation model of environmentally accelerated crack growth. (Specimens 4-11). Specimens 4-6 were used to evaluate the effects of frequency on environmentally accelerated crack growth rates. Specimens 7-11 were used to evaluate wave shape effects under an aggressive environment and the interaction of wave shape with frequency and stress ratio.
- o Calibrate the load interaction model for the landing gear stress history used in the verification test program. Center cracked panel specimens were tested in dry air to the landing gear stress history without sustained loads (Specimen 12). Specimen 13 was used to duplicate any one test in each material which appeared to give results which are inconsistent with expected trends.
- o Evaluate the stress intensity solution for semi-elliptical surface flaw specimens used in verification testing (Specimen 14).

2. TEST MATERIALS - Materials used in this program were 300M and HP-9-4-.30 steels. 300M steel is used in landing gear of several Navy aircraft. These materials were selected to represent the range of environmental sensitivity found in landing gear steels. Crack growth in 300M steel is significantly accelerated by exposure to salt water or sea water under loading cycles involving sustained loads (Reference 1). Crack growth in HP-9-4-.30 steel has been shown to be relatively insensitive to immersion in sea or salt water.

TABLE 1. MODEL CALIBRATION AND EVALUATION TEST PROGRAM SUMMARY

Specimen Number	Specimen Type	Environment	Stress Ratio	Frequency (cps)	Wave Shape	Test Type	Objectives
1	Center Cracked Panel	<10% RH Air	0	10	Sinusoidal	Const-Amp	Develop da/dn and Evaluate Stress Ratio
2	↓	↓	0.5	10	↓	↓	↓
3	↓	↓	−1	10	↓	↓	↓
4	↓	Sea Water	0	10	↓	↓	Evaluate Frequency
5	↓	↓	0	1	↓	↓	↓
6	↓	↓	0	0.1	↓	↓	↓
7	↓	Sea Water	0	10	Trapezoidal	↓	Evaluate Wave Shape
8	↓	↓	0	1	↓	↓	↓
9	↓	↓	0	0.1	↓	↓	↓
10	↓	↓	0.5	0.1	↓	↓	↓
11	↓	↓	−1	0.1	↓	↓	↓
12	↓	<10% RH Air	–	10	Sinusoidal	Spectrum	Calibrate Model
13	↓	↓	–	↓	↓	↓	Duplicate Test
14	Elliptical Flaw	<10% RH Air	0	10	Sinusoidal	Const-Amp	Evaluate K

Test series is identical for both materials

GP03-0838-2

Tensile test results for the steel materials used in this program are presented in Table 2. Three tests were performed for each material. The strength levels found are typical of those used in these materials for landing gear applications.

TABLE 2. TENSILE TEST RESULTS

Alloy	Specimen	Yield Strength (ksi)	Ultimate Strength (ksi)	Percent Elongation	Percent Reduction of Area	Modulus of Elasticity (psi x 10^6)
300M	1	248.0	296.0	11	37	29.5
	2	248.0	296.0	11	37	29.2
	3	248.0	295.0	11	38	28.5
	Average	248.0	295 5	11	37	29.1
HP 9-4-0.30	1	210.0	228.0	16	59	28.5
	2	210.0	229.0	14	56	28.3
	3	211.0	229.0	15	62	28.4
	Average	210.5	228.5	15	59	28.4

GP03-0838-3

3. TEST SPECIMENS - The specimens were of two types: center cracked panels and surface flawed panels. Test specimens are shown in Figures 1 and 2.

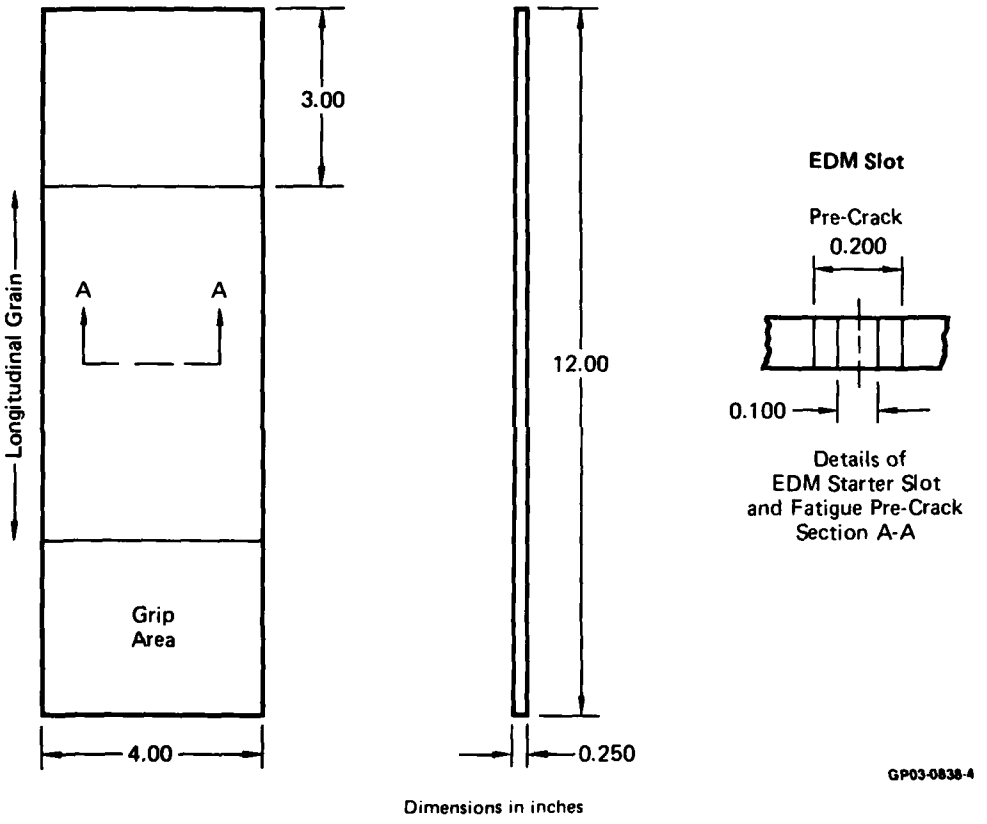

Figure 1. Center Cracked Panel Specimen

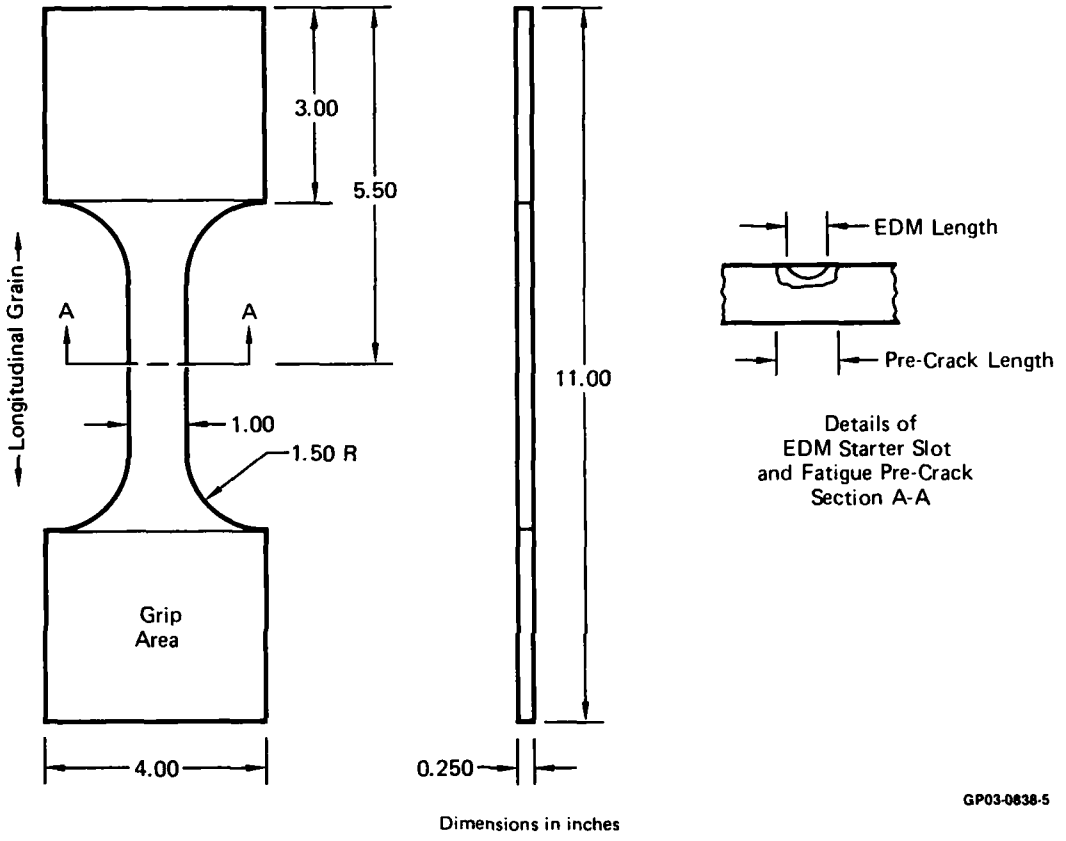

Figure 2. Surface Flawed Panel Specimen

Surface flaw specimens were used for stress intensity calibration of part-through cracks and to determine environment-load interaction effects on part-through flaws representative of flaws found in landing gear structure (Reference 2). The reduced section (Figure 2) was required to properly simulate stresses experienced in landing gear components, and maintain load levels within the capacity of available fatigue test equipment. The predicted finite width effect on crack growth was small.

4. TEST PROCEDURES

a. Precracking Procedures - Center cracked panel specimens were precracked at zero stress ratio until the total crack length was approximately 0.20 inch. The final 0.05 inch of crack growth was performed at a stress level equal to or less than that at which the subsequent test was performed. For alternate immersion tests, the cracked section of the specimen was immersed during the final 0.05 inch of precracking. Specimens were immersed during the final stages of precracking to avoid an artificial increase in crack growth rate found to occur when specimens precracked in a laboratory air environment are immersed in salt water for test (Reference 1).

Semi-elliptic surface flaw specimens had EDM notches having 0.05 inch surface length and 0.025 inch depth to insure that the surface flaw would initiate at all points along the EDM slot periphery during precracking to 0.1 inch surface length. The initial flaw geometry was selected to insure that crack growth in the depth dimension is accompanied by growth on the surface. Specimens were precracked at zero stress ratio. The final 0.025 inch of precrack growth was obtained using a load level equal to or less than that used for subsequent testing. Final precracking was performed in sea water, if the test was to involve the alternate immersion environment.

b. Specimen Loading and Instrumentation - Cyclic testing was performed in an MTS test system, consisting of a hydraulic power supply, load frame assembly, electronic control console, and tele-printer. The specimens were loaded through self-aligning hydraulic grips. Teflon roller guides were installed against the specimen surface to prevent buckling during application of compression loads.

During testing, crack lengths were optically monitored using a linear displacement transducer with a 30X microscope. During constant amplitude tests in dry air, crack growth measurements were made after every .05 inches of crack growth (approximately). During alternate immersion tests, crack lengths were measured before immersion, after immersion, and at the midpoint of the drying cycle (25 minutes). During spectrum tests, crack lengths were measured every 100 landings until 2000 landings were obtained, measurements were made every 500 landings thereafter.

c. Environmental Control - Two environments were used for tests in this program: low humidity dry air (10% R.H.) and alternate immersion in ASTM standard synthetic sea water (10 minutes immersed 50 minutes blown dry by filtered shop air). The containment method used for the low humidity air environment is shown in Figure 3. Low humidity air was obtained using silica jell dessicant.

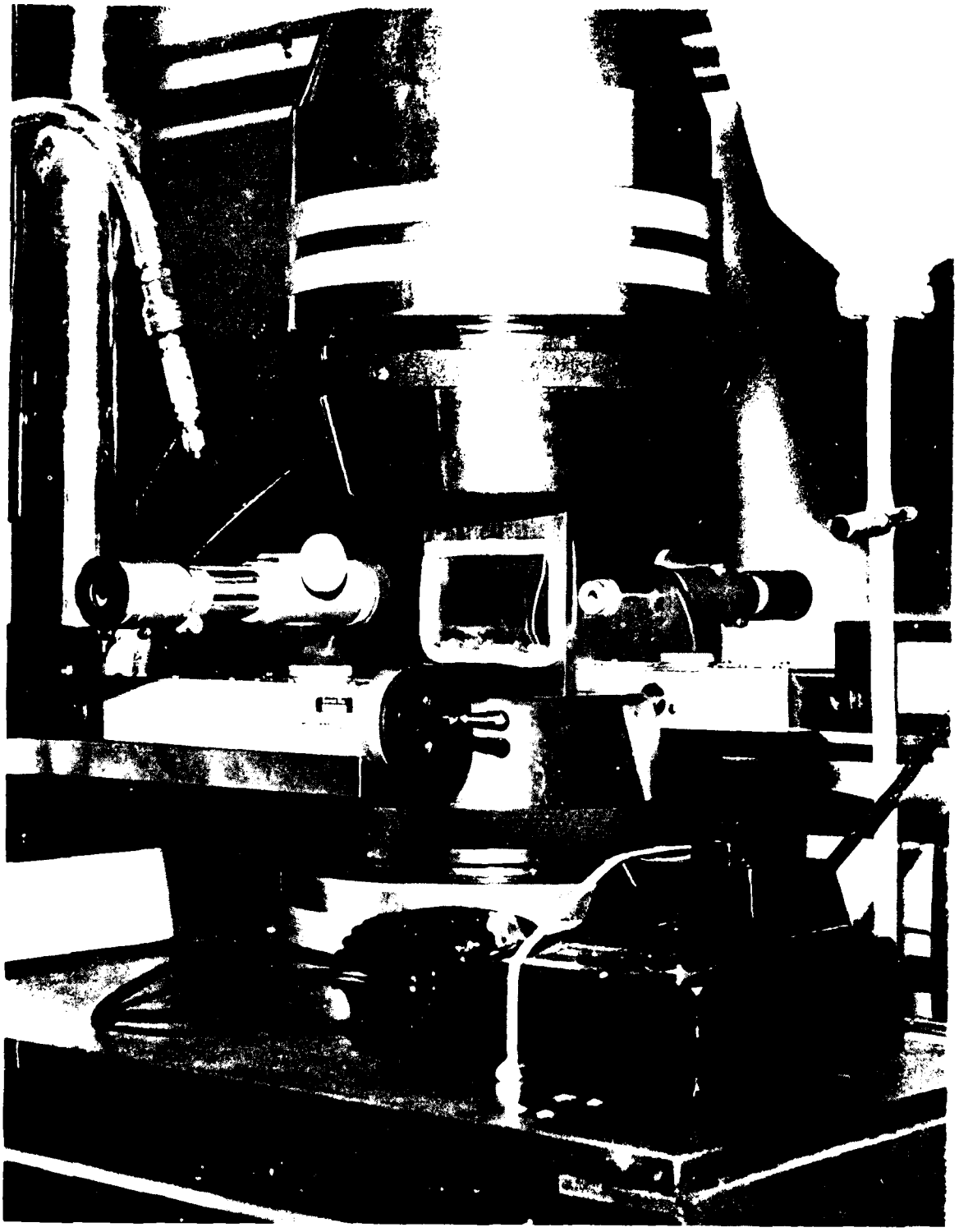

GP03 0838 5

Figure 3. Containment Method for Low Humidity Air Tests

The container used for alternate immersion tests is shown in Figure 4. The plexiglass container is wide enough to accept the specimen and a nylon tube which encircles the specimen to provide air for the drying cycle. Synthetic sea water was introduced through a plastic tube and stainless steel port. The synthetic sea water used was ASTM D 1141-75 substitute ocean water without heavy metals. This water is commonly used for salt water spray tests.

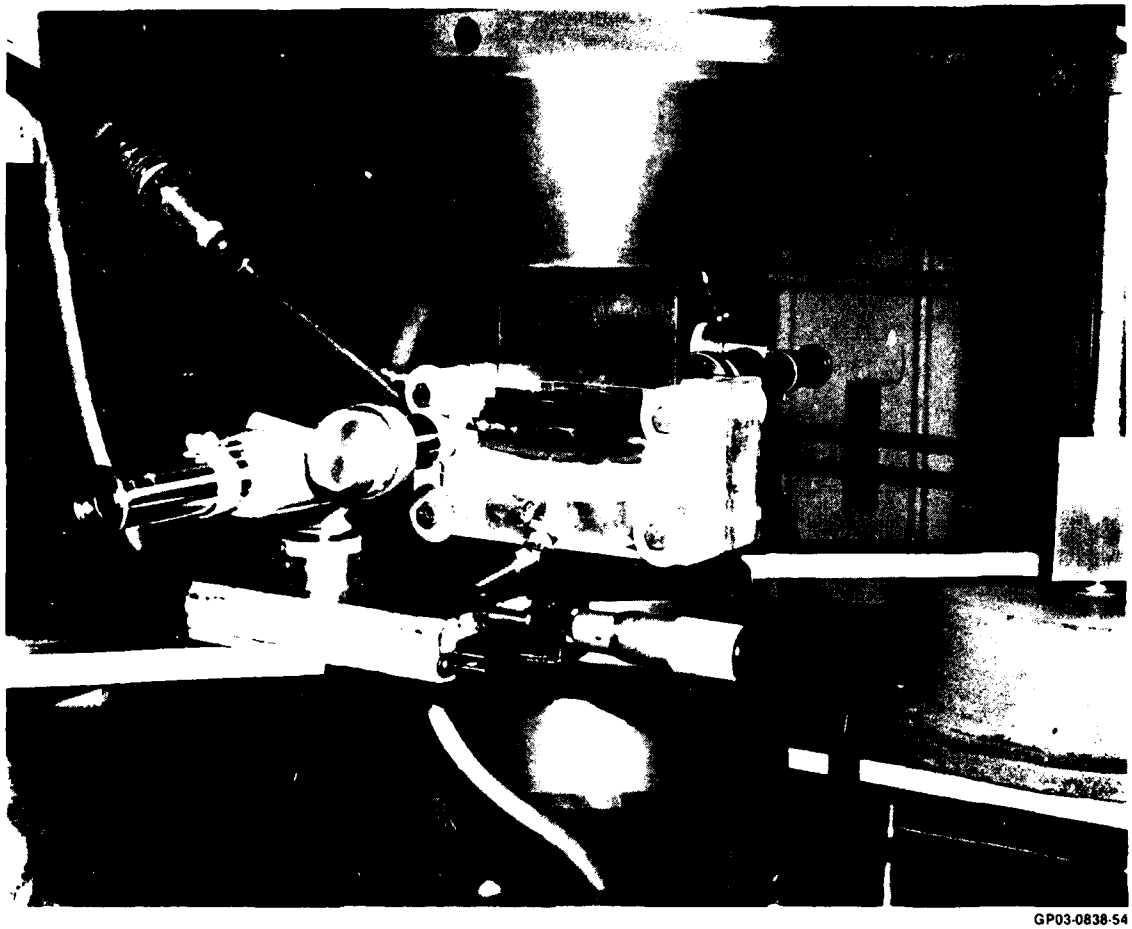

GP03-0838-54

Figure 4. Container Used for Alternate Immersion Tests

The crack was totally immersed during the 10 minute immersion cycle. The sea water was released through a second stainless steel drain port. After immersion filtered shop air at 10 psia was used to blow the specimen dry. This procedure rapidly dried the specimen surface and container. Rapid drying provided better control of the environment than simply allowing the specimen and container to dry in laboratory air.

5. SUMMARY OF CONSTANT AMPLITUDE TEST RESULTS - The results of constant amplitude crack growth testing were summarized using the procedure shown in Figure 5. They are presented in Table 3 in terms of number of cycles to grow a center crack over the range of crack lengths shown for each material.

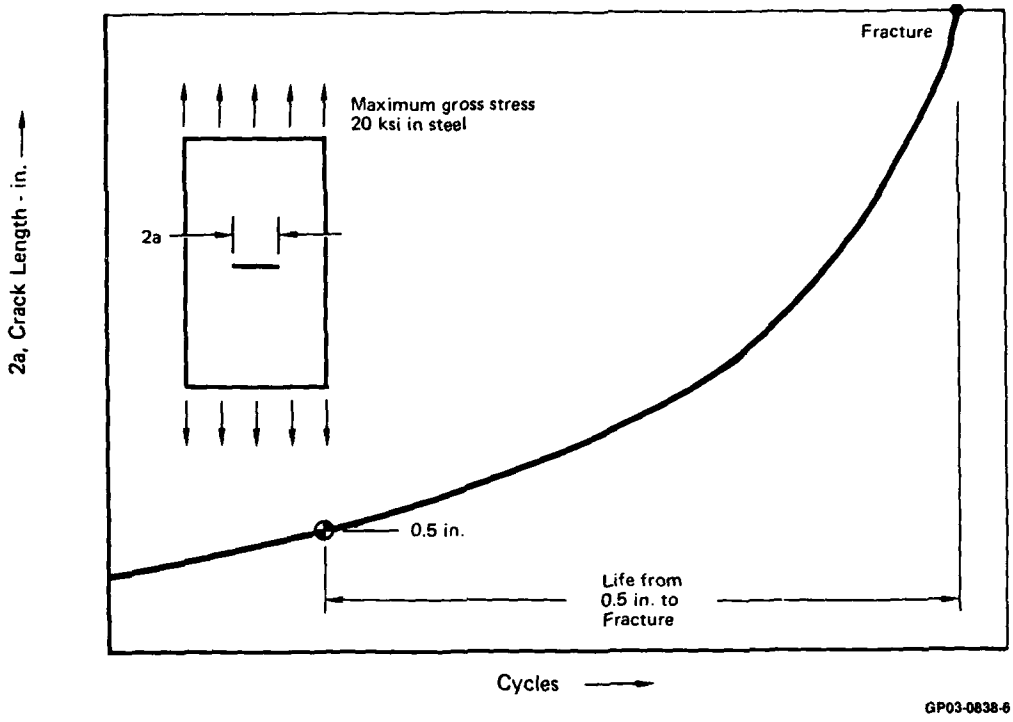

Figure 5. Algorithm Test Program Summary Procedure

TABLE 3. SUMMARY OF CONSTANT AMPLITUDE LIVES
Results of Model Calibration and Evaluation Tests

Specimen Number	Specimen Type	Environment	Stress Ratio	Frequency (cps)	Wave Shape	Test Type	300M Cycles to Grow Crack from 0.5 to 2.6 in.	HP 9-4-0.30 Cycles to Grow Crack from 0.5 to 2.6 in.
1	Center Cracked Panel	< 10% RH Air	0	10	Sinusoidal	Const-Amp	140,000	137,000
2			0.5	10			370,000	390,000
3			−1	10			122,000	115,800
4		Alternate Immersion in Sea Water	0	10			155,000	131,000
5			0	1			94,000	101,900
6			0	0.1			22,900	22,500 (1)
7			0	10	Trapezoidal		140,000	108,500
8			0	1			62,700	149,400
9			0	0.1			6,210	35,000 (1)
10			0.5	0.1			7,380	76,500 (1)
11			−1	0.1			4,010	32,000 (1)

Note: (1) These flaws did not grow until precracked beyond 1.25 in. Lives shown are based on 1.70 in. to 2.6 in. of growth GP03-0838-78
2. Maximum gross stress in each test was 20 ksi

6. CONSTANT AMPLITUDE FATIGUE STRESS RATIO EVALUATIONS - (Specimens 1-3) - Constant amplitude fatigue tests were performed on 6 center crack panels (three per material) to determine the effect of stress ratio on crack growth rate and to verify an analytical stress ratio correction. Tests were performed at stress ratios of 0, 0.5, and -1 for both of the materials in a low-humidity air environment (10% R.H.). The wave shape used for these tests was a sinusoid, applied at a frequency of 10 Hz. During the tests, crack growth was visually monitored and crack length recorded at approximately 0.05 inch intervals.

The results of the tests used to evaluate the effects of stress ratio are summarized in Table 3, and Figures 6 through 11. The figures also present predictions based on an analysis procedure discussed in Section III. Plots of crack growth rate versus ΔK (stress intensity factor range) are presented in Figures 7 and 10 to show the effect of stress ratio on growth rate as commonly presented. Figures 8 and 11 show the same data plotted versus K_{max} so that crack growth rates show the same behavior as that shown in the plots of crack growth measurements (Figures 6 and 9).

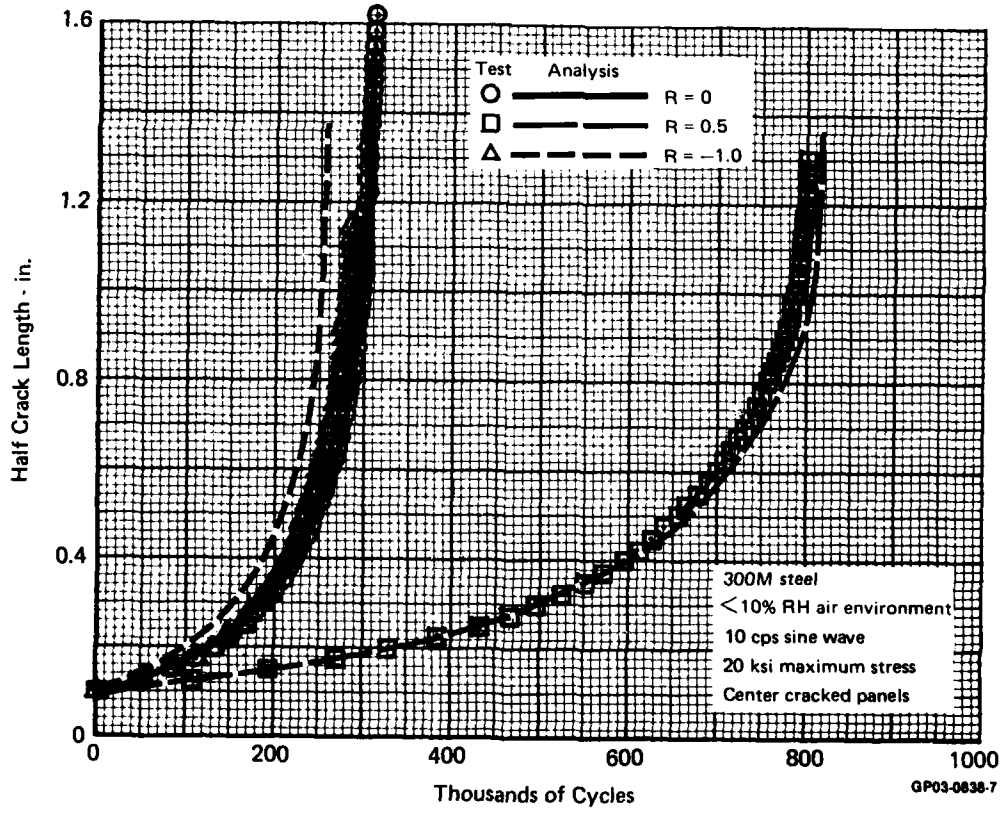

Figure 6. Effect of Stress Ratio on Crack Growth in 300M Steel

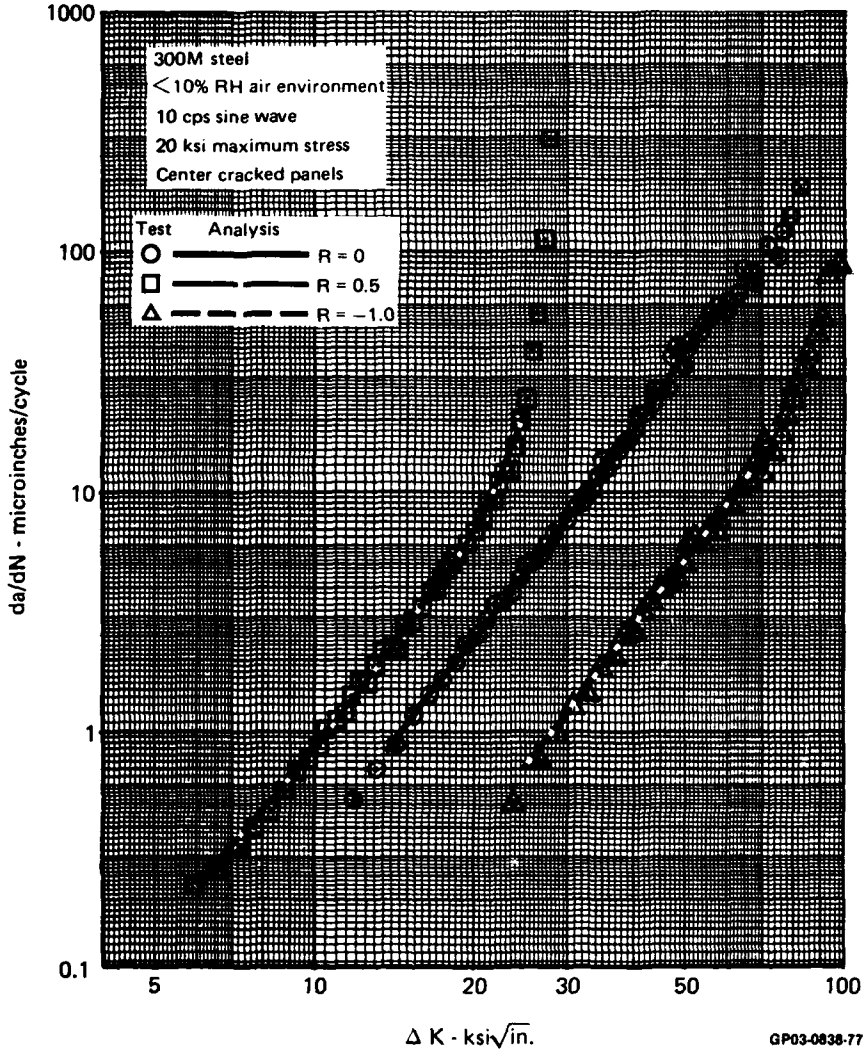

Figure 7. Effect of Stress Ratio on Crack Growth Rate in 300M Steel

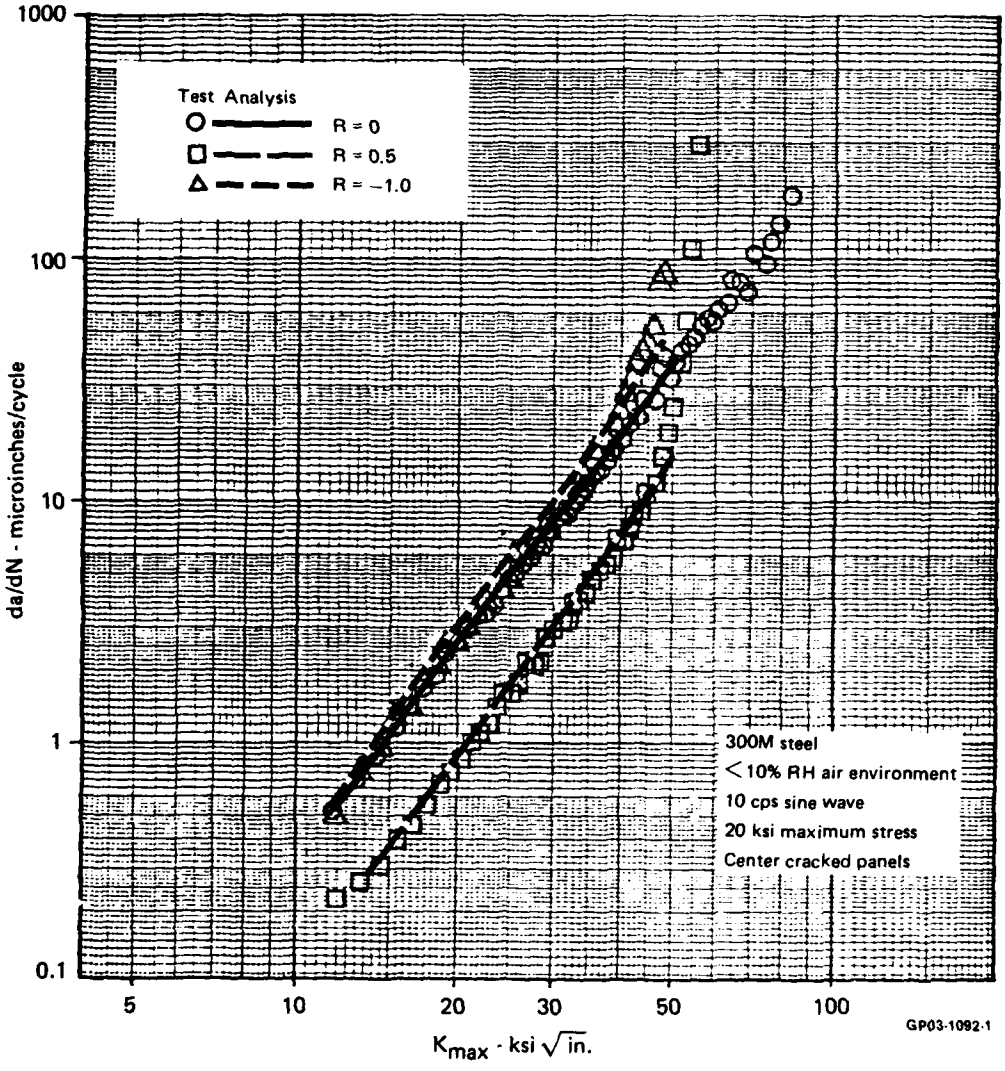

Figure 8. Effect of Stress Ratio on Crack Growth Rate in 300M Steel (Plotted vs K_{max})

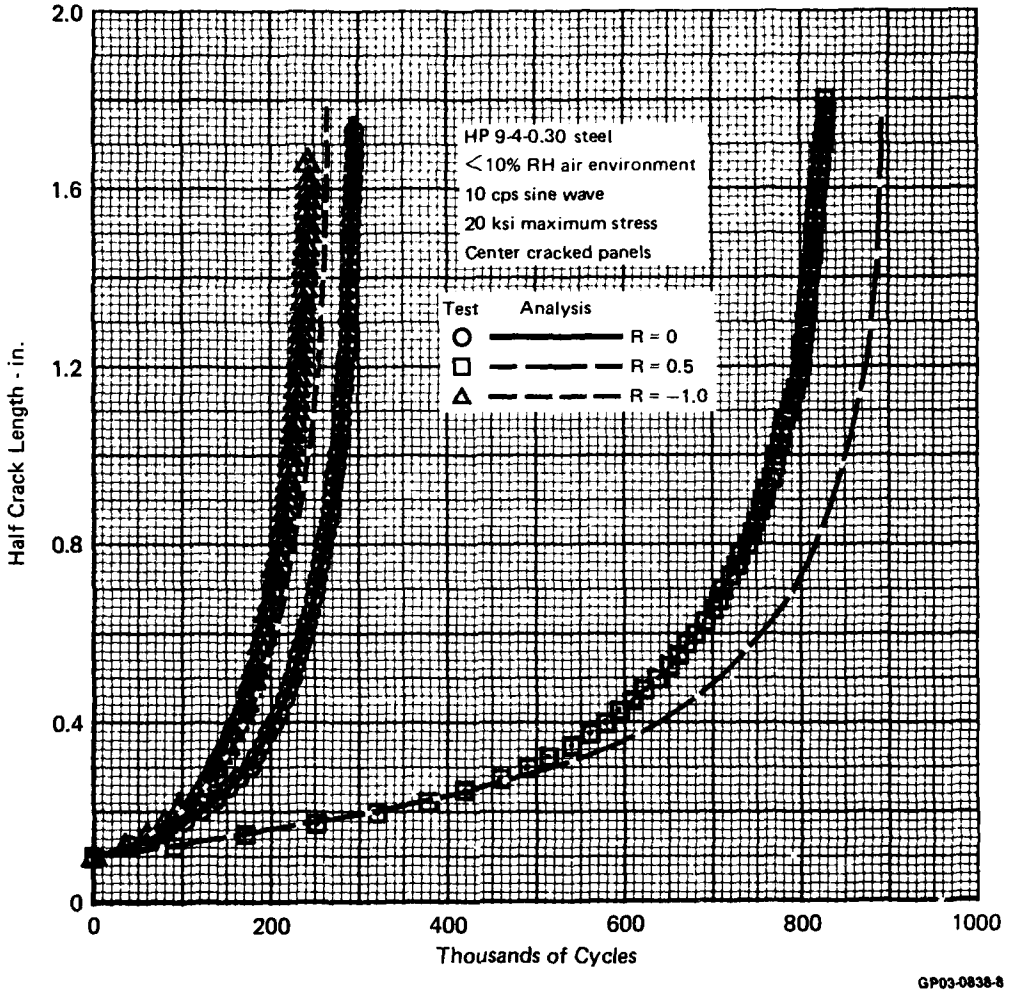

Figure 9. Effect of Stress Ratio on Crack Growth in HP 9-4-0.30 Steel

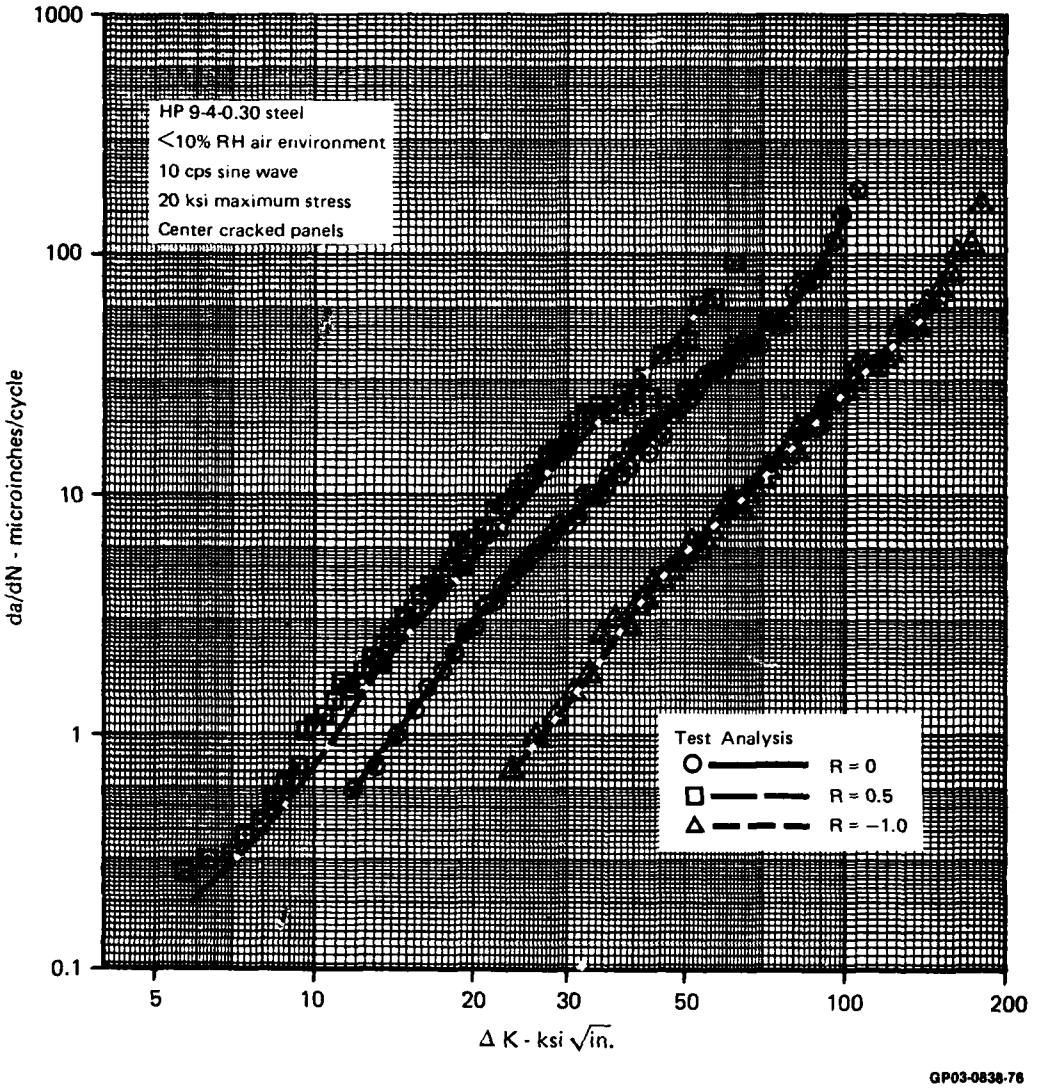

Figure 10. Effect of Stress Ratio on Crack Growth Rate in HP 9-4-0.30 Steel

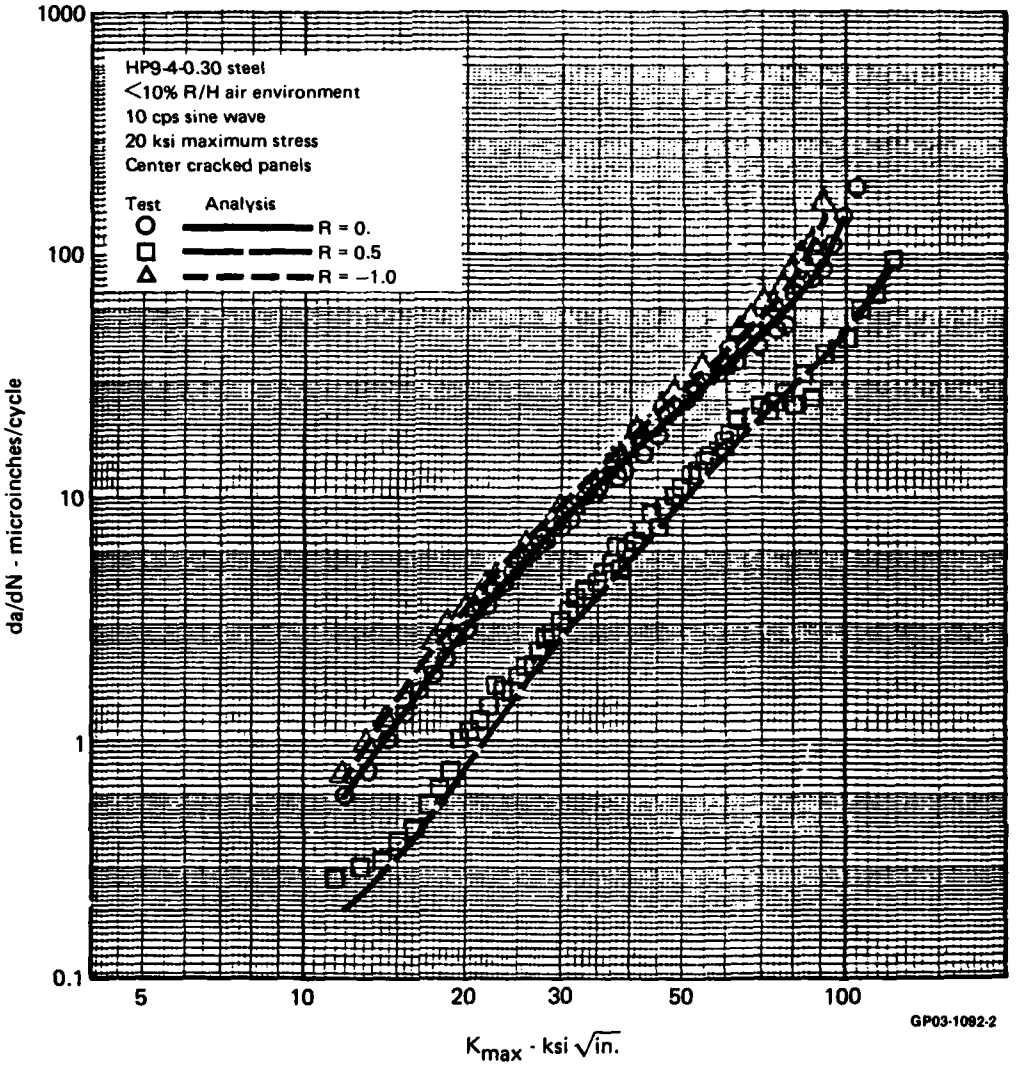

Figure 11. Effect of Stress Ratio on Crack Growth Rate in HP 9-4-0.30 Steel (Plotted vs K_{max})

7. CONSTANT AMPLITUDE FATIGUE FREQUENCY EVALUATIONS - (Specimens 4-6) - Constant amplitude fatigue tests were performed on 6 center crack panels (3 per material) to determine the effect of cyclic frequency on crack growth rate and to verify crack growth predictions obtained with a linear superposition model (Section III). Specimens were tested at frequencies of 10 cps, 1 cps, and 0.1 cps for each material. Each specimen was subjected to an aggressive environment (alternate immersion in sea water) during test. The wave shape was sinusoidal. During the tests, crack growth was visually monitored and crack length recorded before immersion, after immersion, and 25 minutes into the drying cycle. In addition, crack length measurements were recorded at approximately 0.05 inch intervals.

The results of this series of tests are summarized in Table 3 (Page 10) and Figures 12 through 19. 300M steel shows a much larger effect of test frequency in the sea water environment than HP-9-4-.30. The 300M shows a factor of 7 decrease in crack growth life as the frequency is reduced from 10 cps to 0.1 cps. HP-9-4-.30 shows little effect of either environment or frequency. Crack growth life for HP-9-4-.30 varies less than 50 percent as frequency decreases from 10 cps to 0.1 cps. At 0.1 cps and stress intensity factors less than 25 ksi $\sqrt{in}$, crack growth in HP-9-4-.30 stopped during the drying portion of the alternate immersion cycle. This phenomenon occurred in trapezoidal wave tests also and is discussed in detail in the next section.

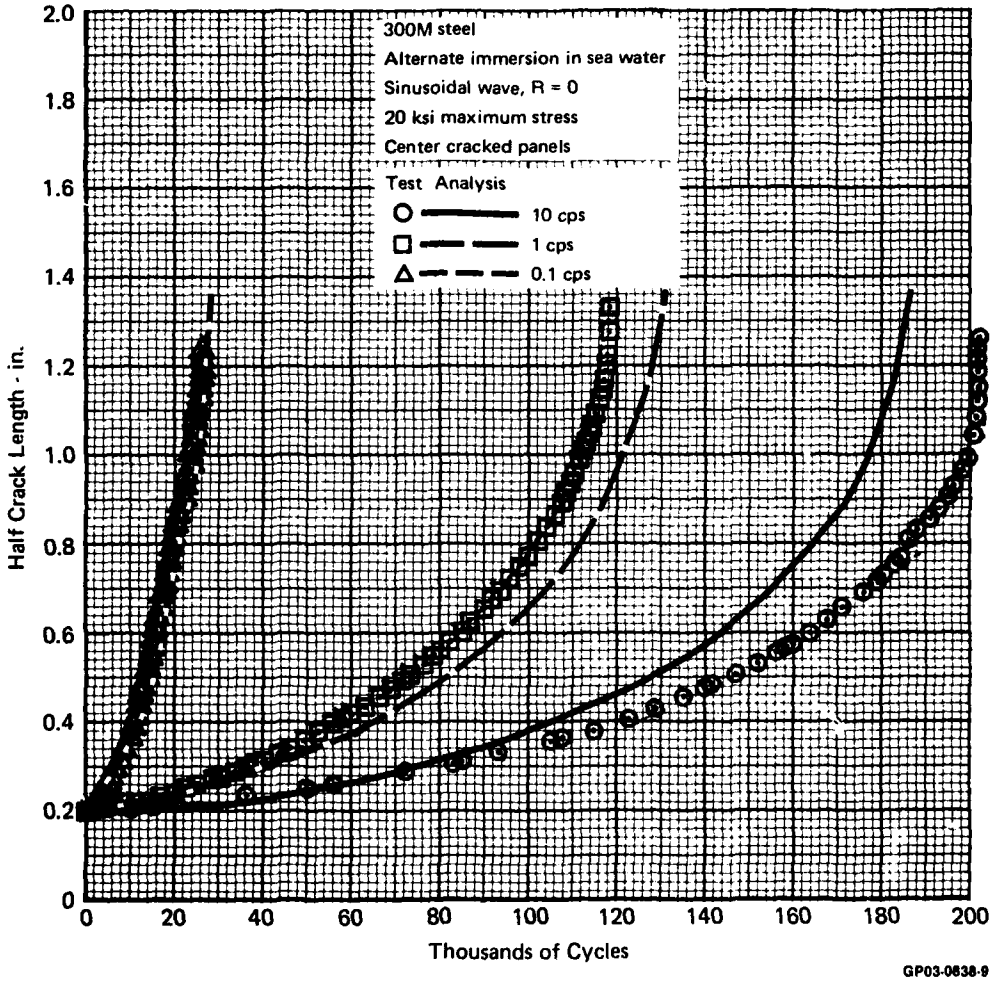

Figure 12. Effect of Sine Wave Loading Frequency on Crack Growth in 300M Steel

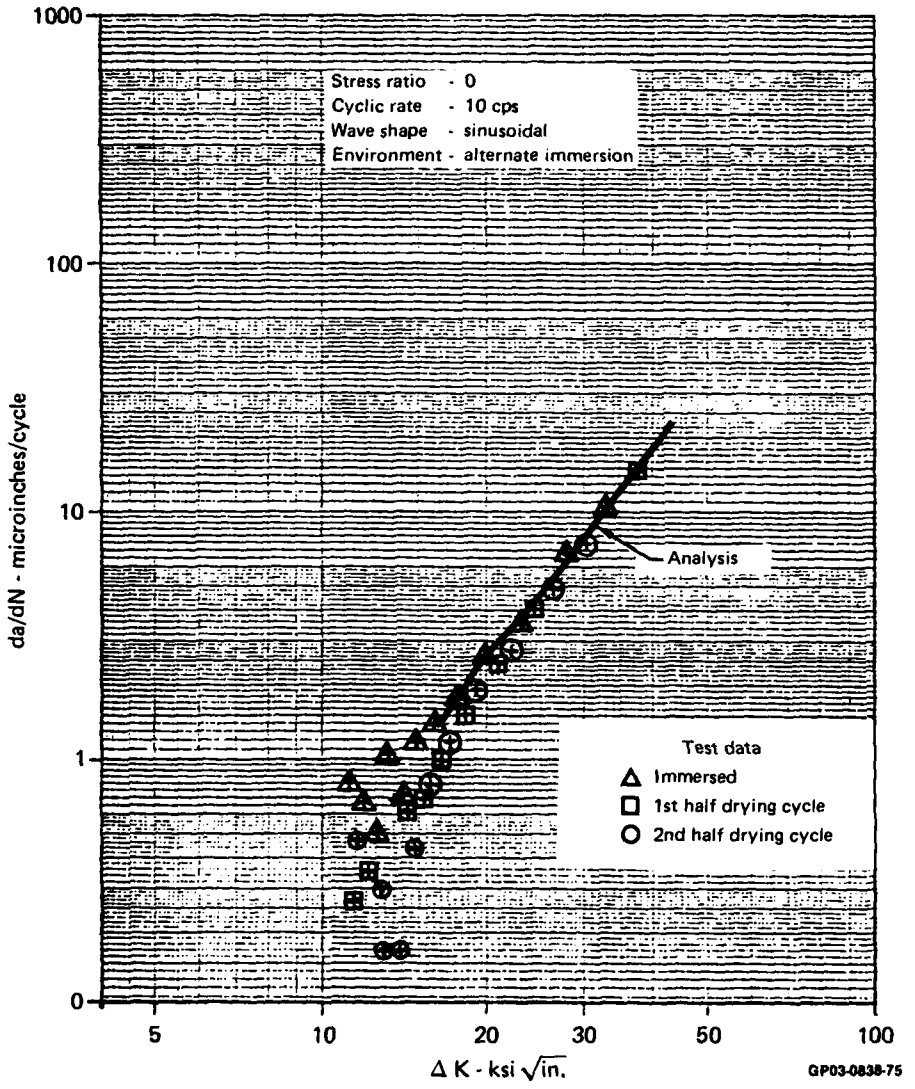

Figure 13. Effect on Sine Wave Loading at 10 cps on Crack Growth Rate in 300M Steel in Sea Water

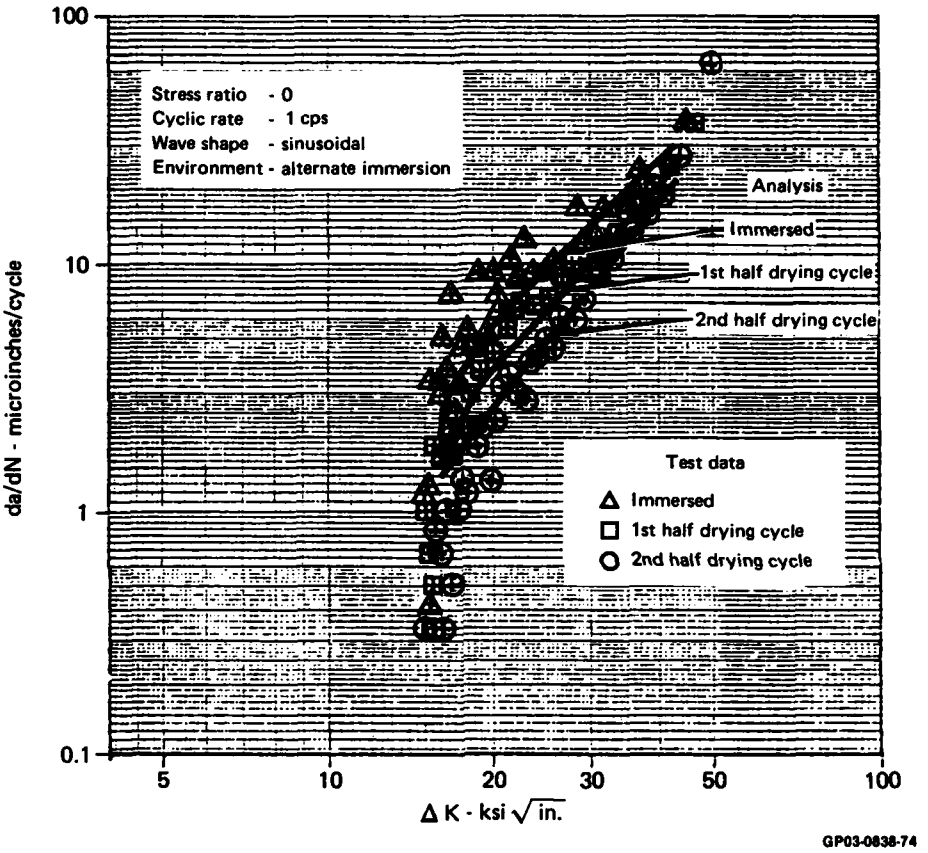

Figure 14. Effect of Sine Wave Loading at 1 cps on Crack Growth Rate in 300M Steel in Sea Water

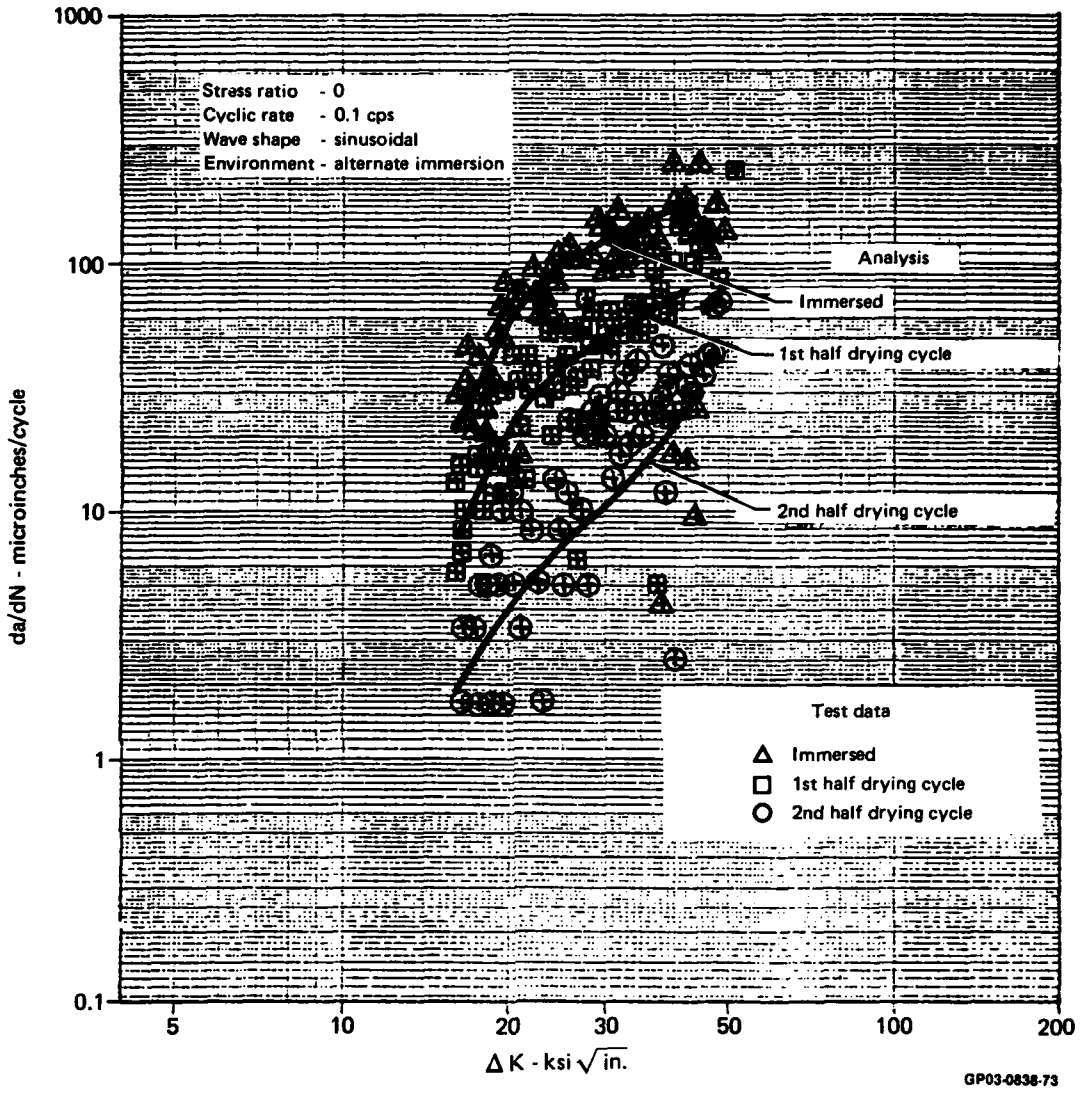

Figure 15. Effect of Sine Wave Loading at 0.1 cps on Crack Growth Rate in 300M Steel in Sea Water

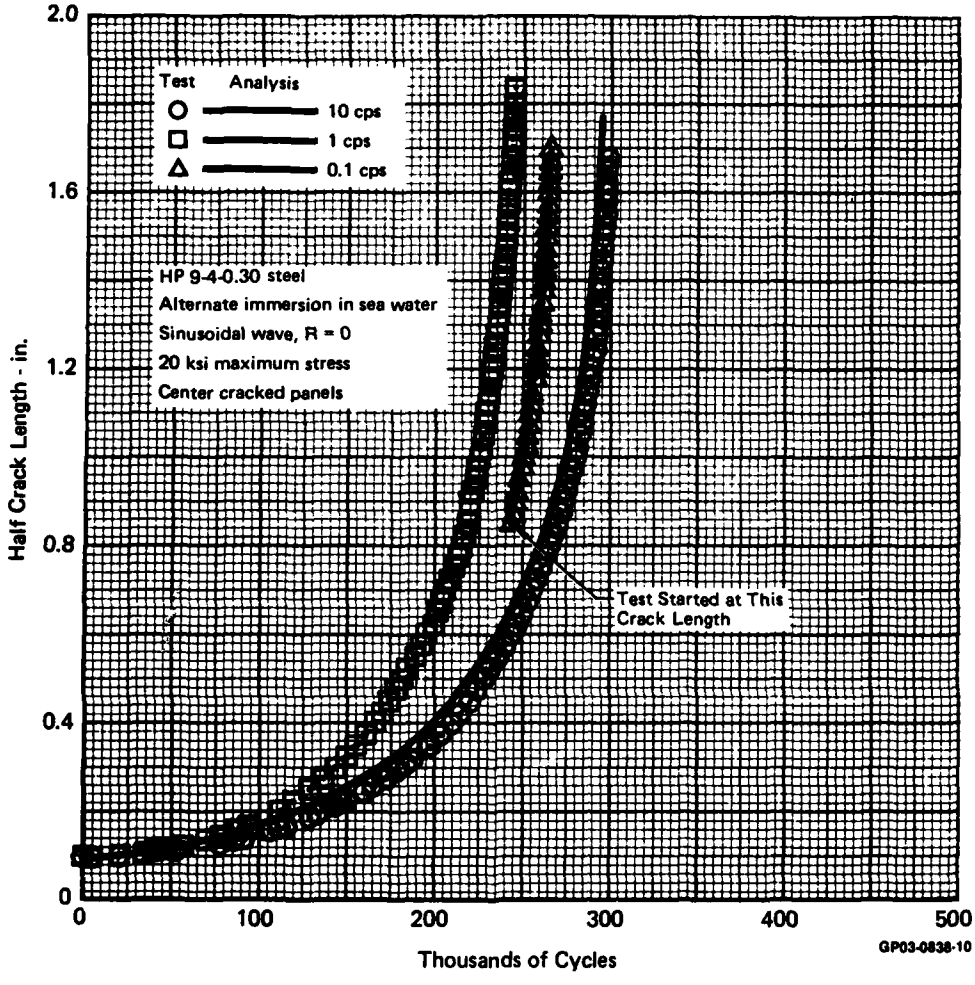

Figure 16. Effect of Sine Wave Loading Frequency on Crack Growth in HP 9-4-0.30 Steel

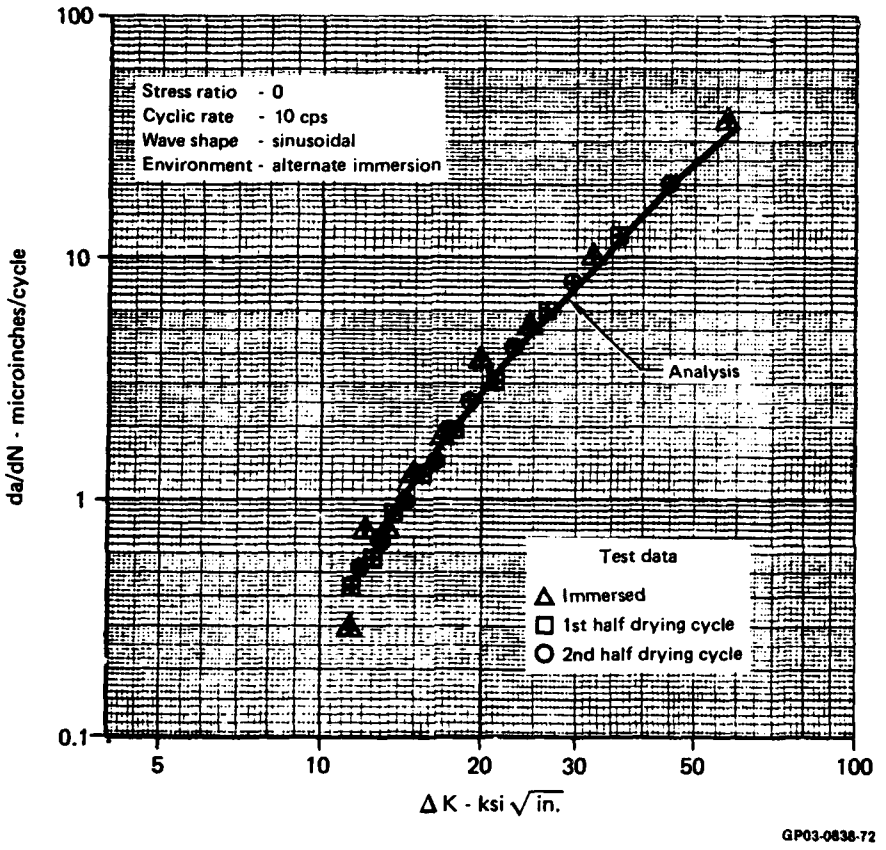

Figure 17. Effect of Sine Wave Loading at 10 cps on Crack Growth Rate in HP 9-4-0.30 Steel in Sea Water

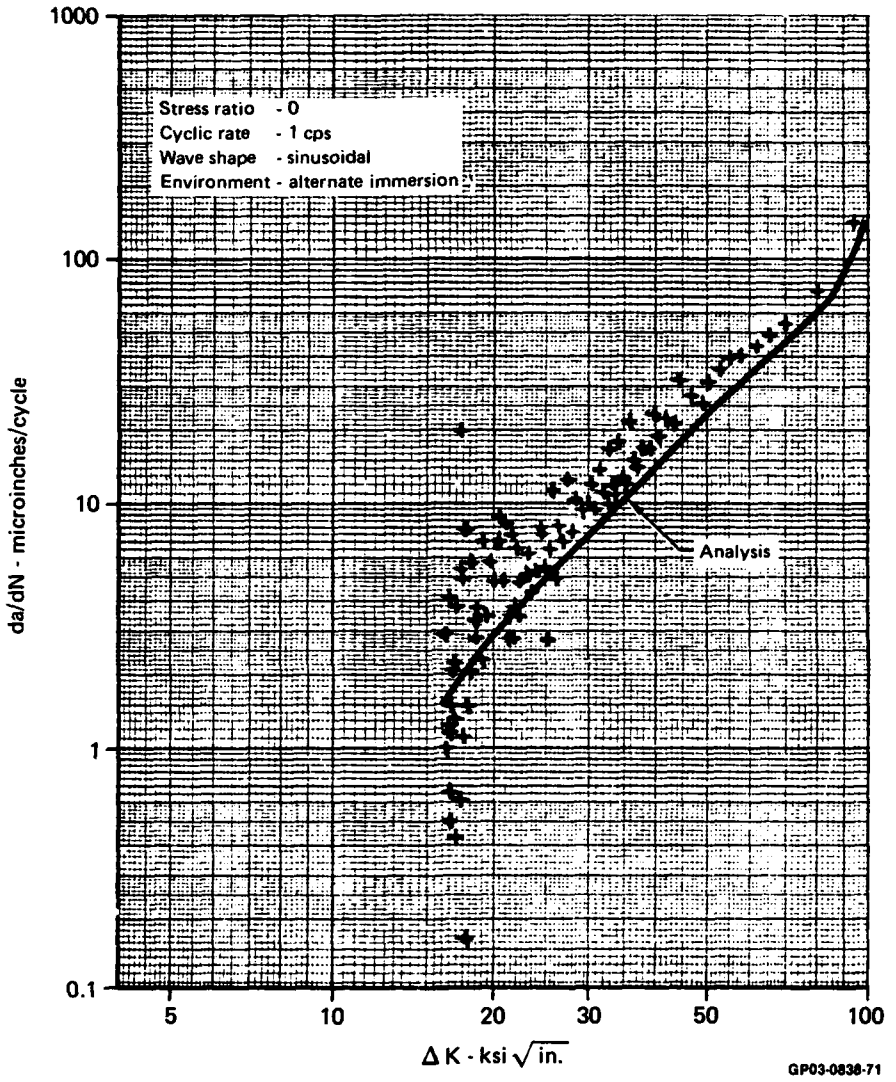

Figure 18. Effect of Sine Wave Loading at 1 cps on Crack Growth Rate in HP 9-4-0.30 Steel iin Sea Water

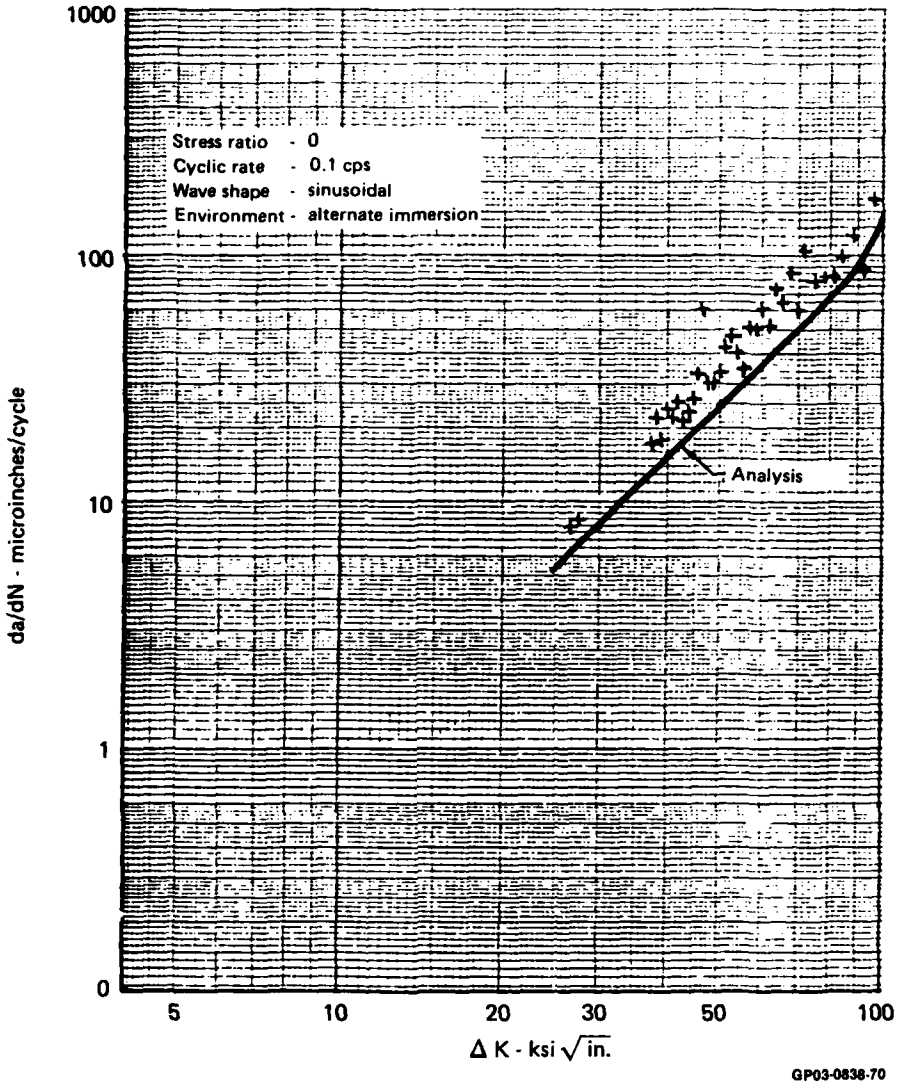

Figure 19. Effect of Sine Wave Loading at 0.1 cps on Crack Growth Rate in HP 9-4-0.30 Steel in Sea Water

Because of the slow crack growth rate in HP-9-4-.30 at 0.1 cps, many immersion cycles are applied prior to obtaining appreciable crack growth. Plots of crack growth and growth rate are based on data obtained after each 0.05 inch of crack growth. Since each point represents many environmental cycles, crack growth rates during immersion cannot be separated from total growth.

8. CONSTANT AMPLITUDE FATIGUE WAVE SHAPE EVALUATIONS - (Specimens 7-11) - Ten constant amplitude fatigue tests were performed on center crack panels to assess the interaction of environment, stress ratio, cyclic frequency, and wave shape on crack growth. Five tests were performed on specimens from each material using a trapezoidal wave form, Figure 20, in which the load rate allowed a great portion of the cycle to be held at a constant peak stress. Tests with the trapezoidal wave shape were run at frequencies ranging from 0.1 cps to 10 cps. Tests at 0.1 cps were run at stress ratios of 0, 0.5, and -1. All specimens were subjected to the aggressive environment (alternate immersion in sea water) during the test.

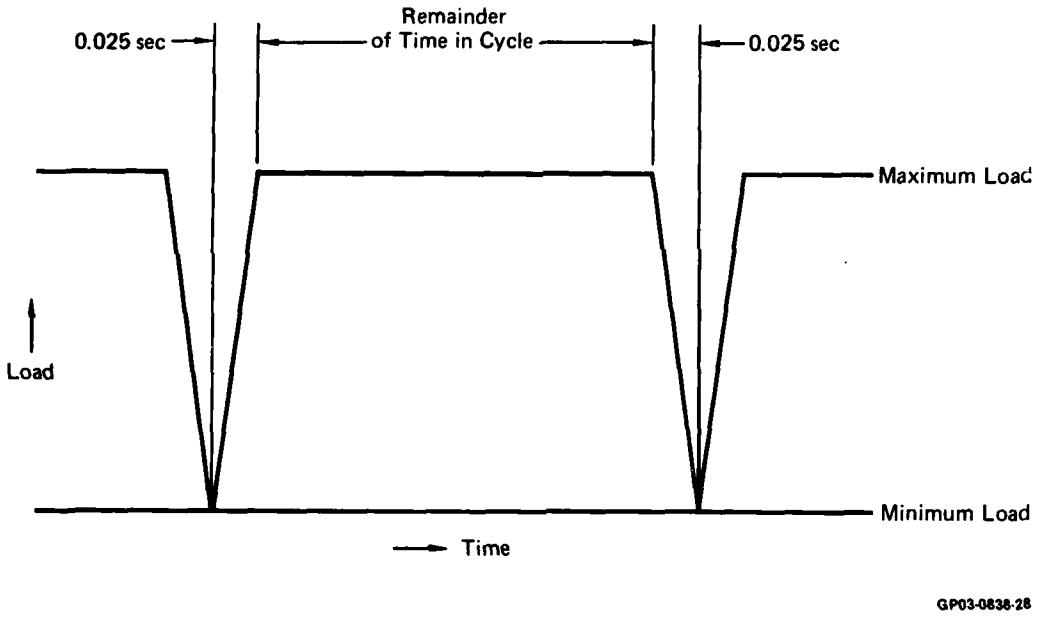

Figure 20. Trapezoidal Wave Shape

The effect of sustained load duration are presented in Figures 21-28. In 300M steel, increasing the sustained load time in the alternate immersion environment shortened life considerably. Crack growth life under trapezoidal wave loading at 0.1 cps is about five percent of that for 10 cps loading.

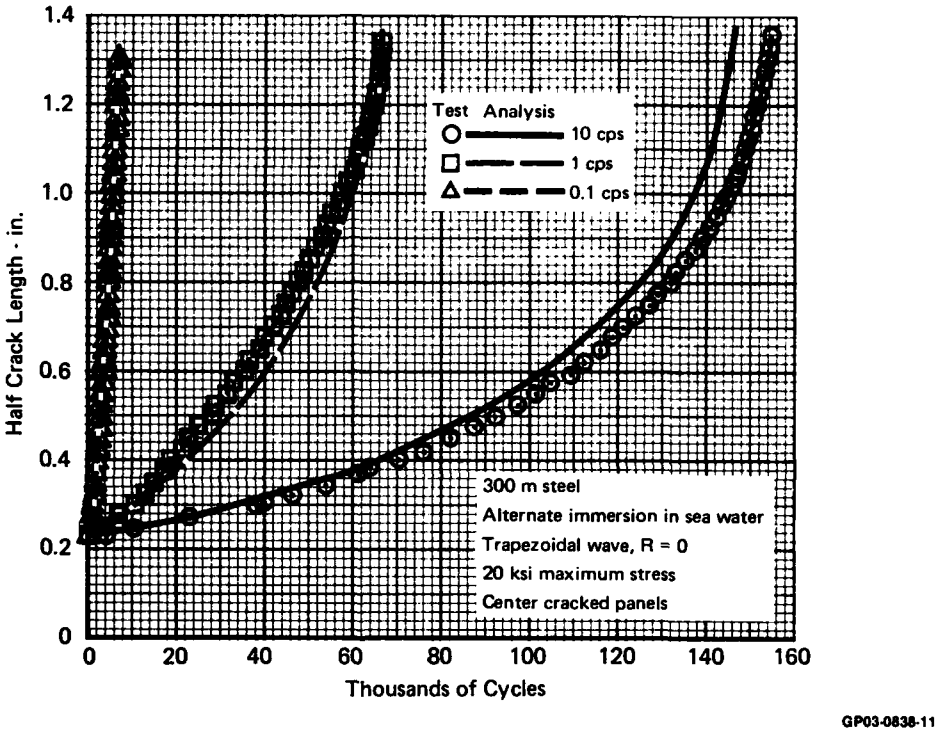

Figure 21. Effect of Trapezoidal Wave Loading Frequency on Crack Growth in 300M Steel

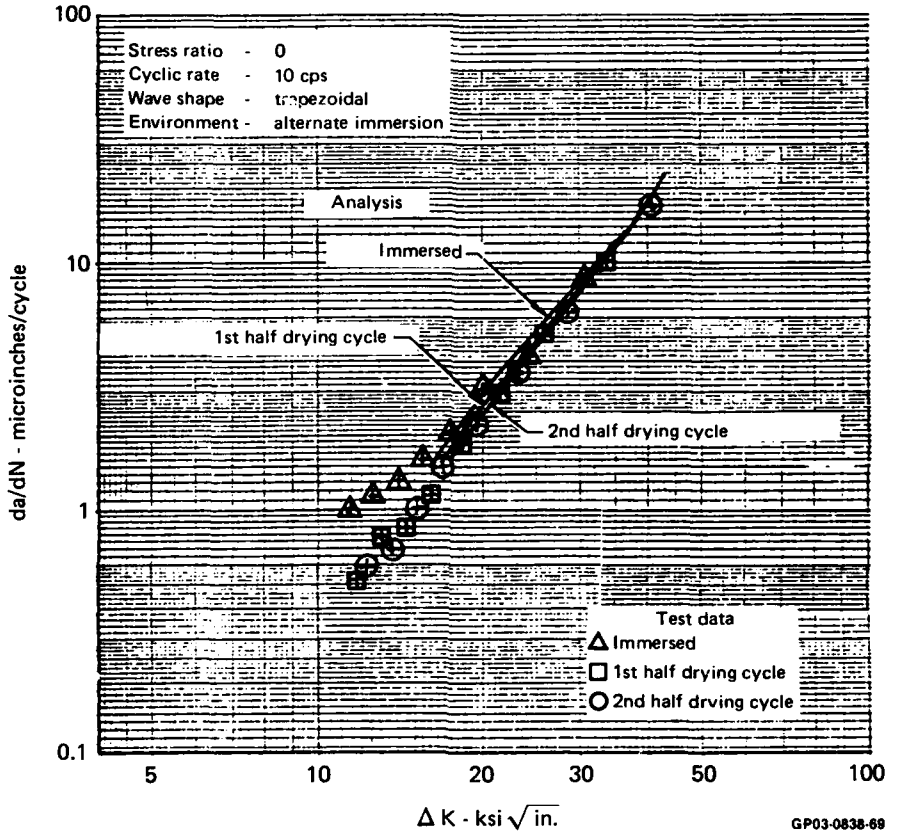

Figure 22. Effect of Alternate Immersion Environment on Crack Growth Rate on 300M Steel - 10 cps Trapezoidal Wave Loading

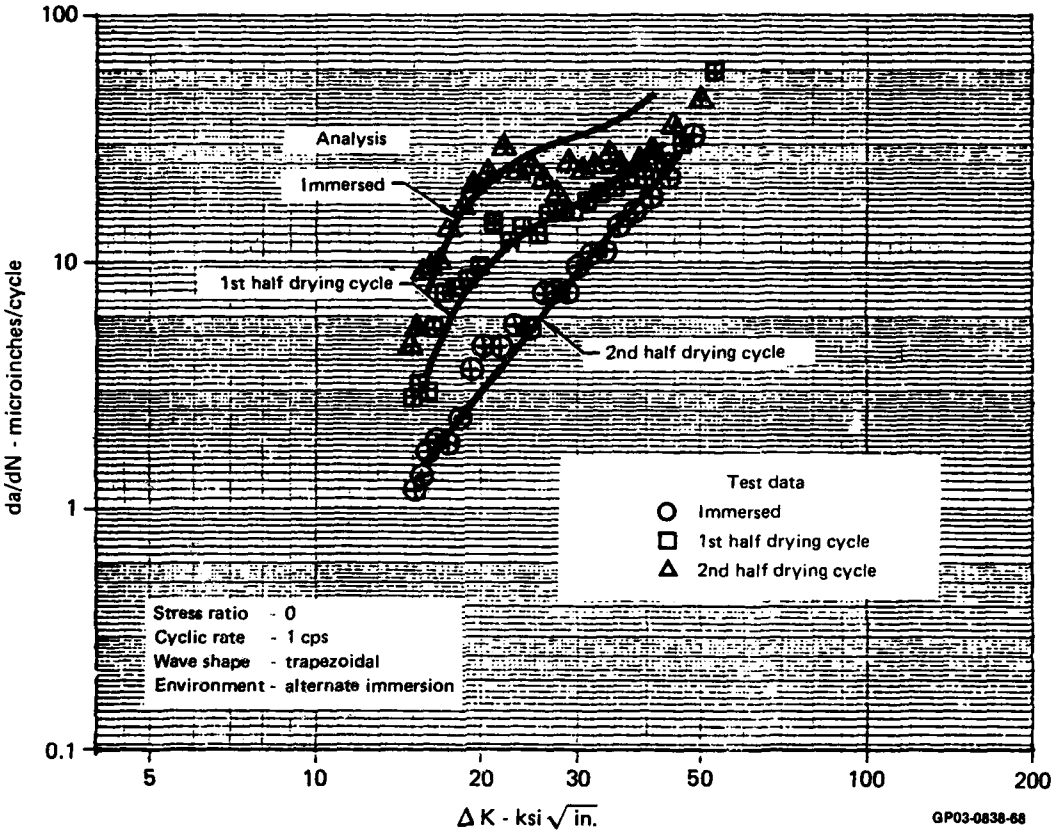

Figure 23. Effect of Alternate Immersion Environment on Crack Growth Rate in 300M Steel - 1 cps Trapezoidal Wave Loading

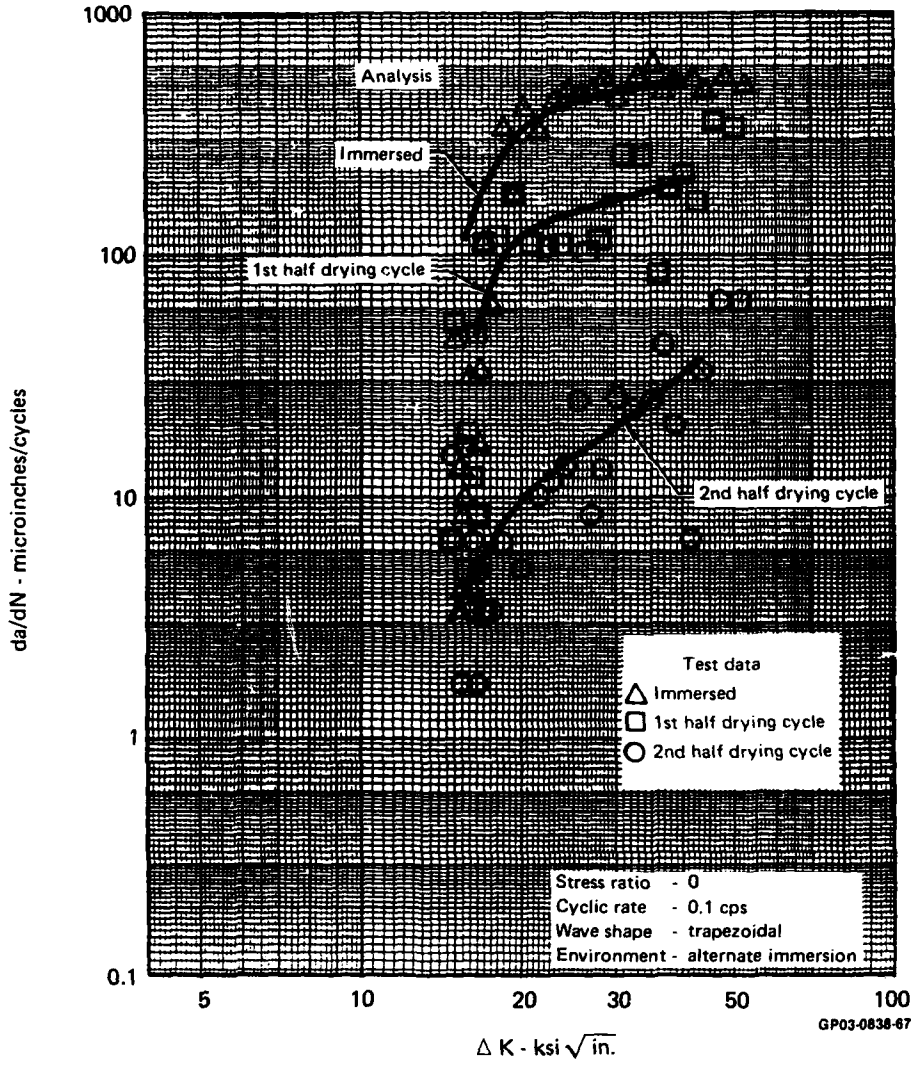

Figure 24. Effect of Alternate Immersion Environment on Crack Growth in 300M Steel - 0.1 cps Trapezoidal Wave Loading

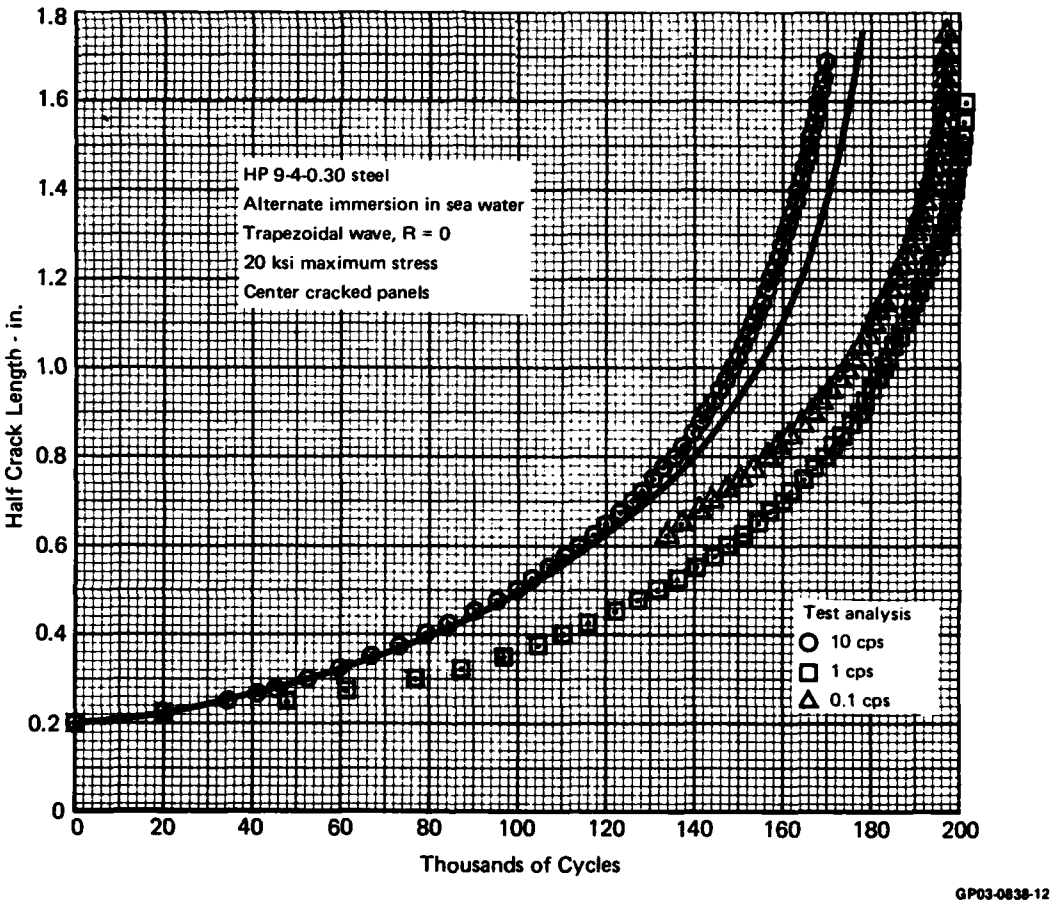

Figure 25. Effect of Trapezoidal Wave Loading Frequency Growth on HP 9-4-0.30 Steel

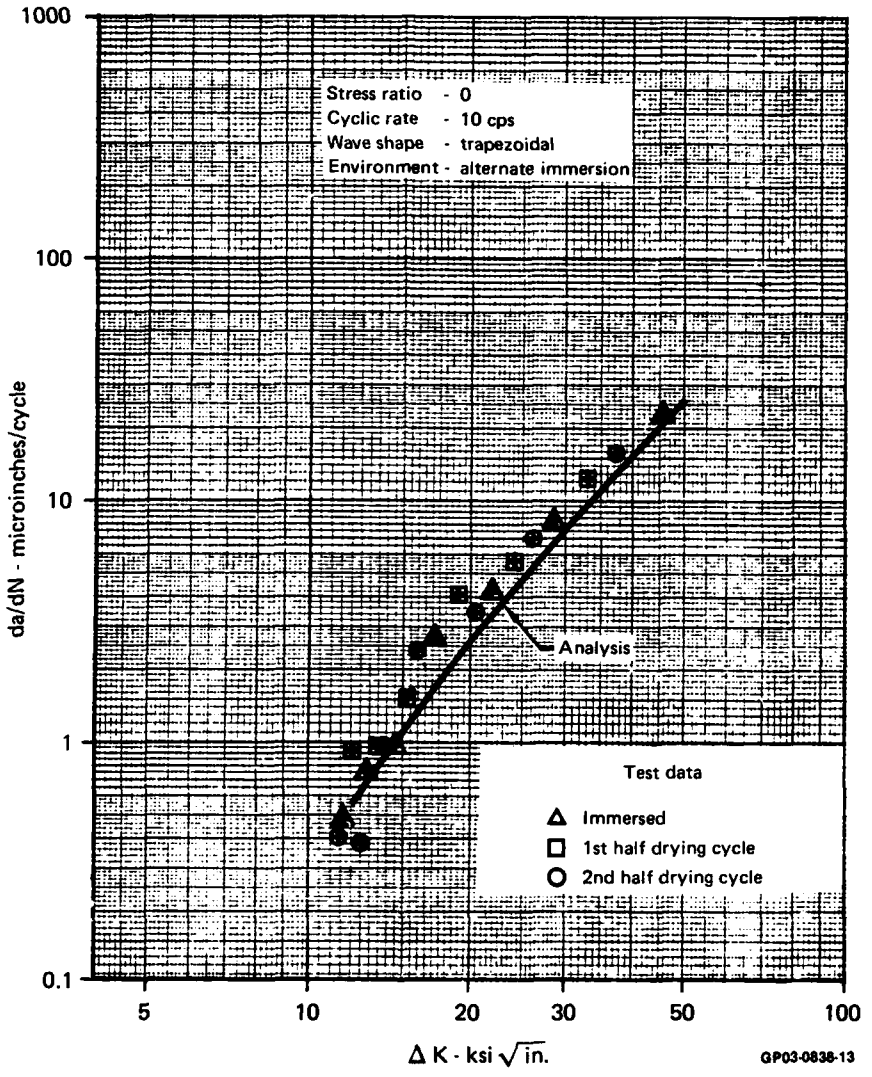

Figure 26. Effect of Trapezoidal Wave Loading at 10 cps on Crack Growth Rate in HP 9-4-0.30 Steel

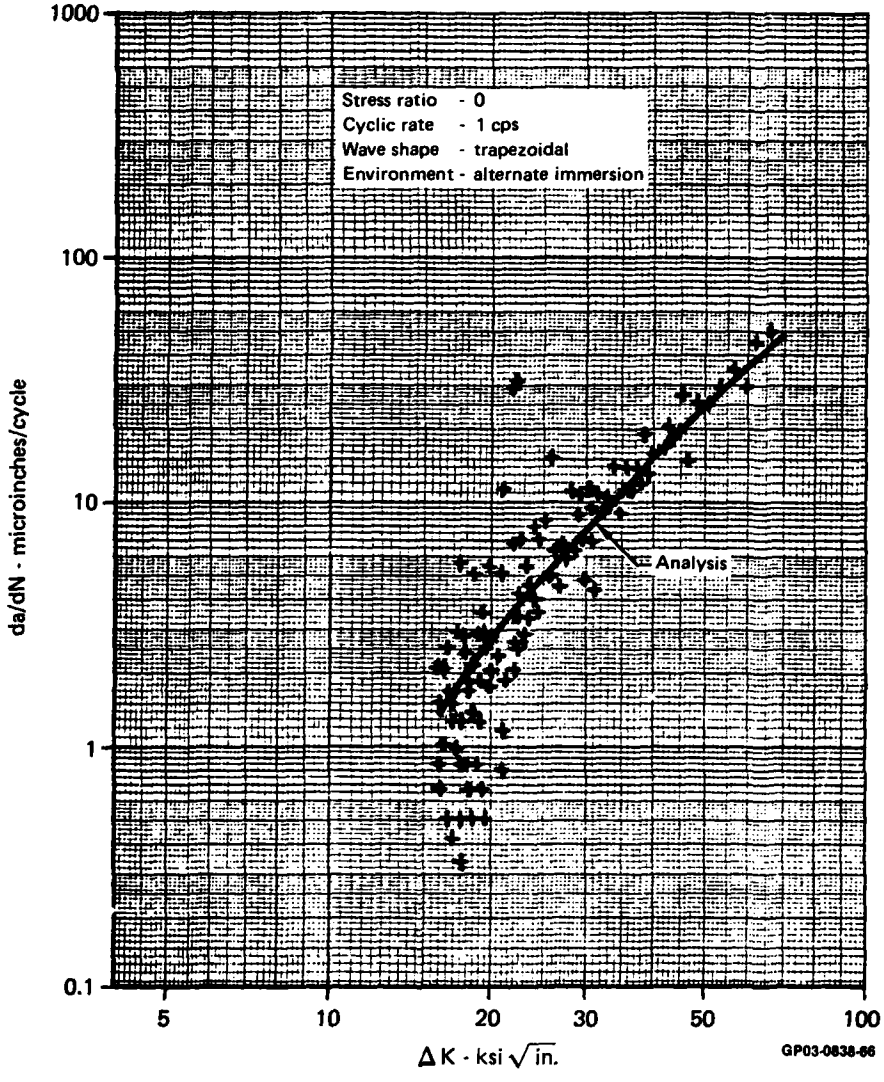

Figure 27. Effect of Trapezoidal Wave Loading at 1 cps on Crack Growth Rate in HP 9-4-0.30 Steel

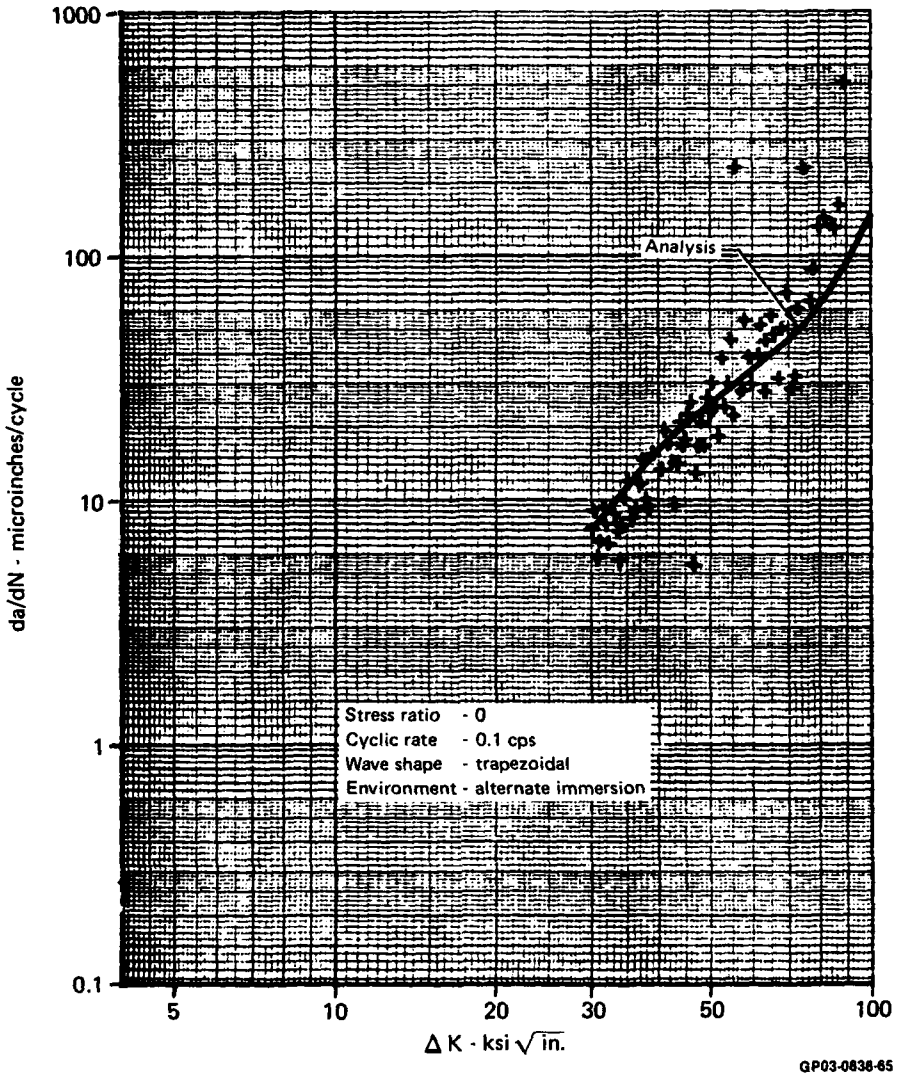

Figure 28. Crack Growth Rate in HP 9-4-0.30 Steel in Alternate Immersion Environment Using 0.1 cps Trapezoidal Wave Loading

HP-9-4-.30 steel does not show the environmental acceleration found in 300M steel, and consequently does not show much effect of frequency or environment. However, under the 0.1 cps trapezoidal wave test of HP-9-4-.30 specimen 9 (R=0), the threshold stress intensity factor in the alternate immersion environment was found to increase to about 25 ksi $\sqrt{in}$., Figure 28. Below this threshold value, the specimen was precracked in sea water in 0.05 inch increments and then subjected to the alternate immersion environment and the 0.1 cps trapezoidal wave loading; the crack stopped growing once the specimen was dried and did not start growing during immersion. Thousands of precracking cycles were required to reinitiate the crack growth when precracking in salt water.

Currently, our conjecture is that corrosion products, created on the crack faces during immersion, solidify during drying. These corrosion products reduce the stress intensity factor ranges applied to the crack tip (i.e. increasing crack closure) causing the crack growth to slow or stop. During immersion, these corrosion products are formed but are kept in solution in the sea water and do not significantly affect the crack tip behavior. This would explain the negligible impact of continuous immersion environment on crack growth in HP-9-4-.30 steel found in previous work, Reference 1.

In the alternate immersion environment, high cycle rates may tend to reduce the buildup of corrosion products near the crack tip during drying, producing little impact on crack growth at low stress intensity factors. At low cycle rates, the crack tip is held open long enough during drying that corrosion products solidify and, acting like a wedge in the crack, prevent growth. Evidently, the ten minute immersion period used in these tests is not sufficient to dissolve the corrosion products. At the threshold stress intensity factor range, the crack begins to grow, in spite of the corrosion product wedge. Once crack growth begins the crack tip grows away from the corrosion products during the drying cycle and crack growth rates rapidly approach those found in dry air.

The combined effects of wave shape, stress ratio, and alternate immersion environment are demonstrated in the crack growth results presented in Figures 29 through 34. The data presented in Figures 29 and 32 show that the effects of stress ratio under trapezoidal wave shape loading are somewhat less for 300M than for HP 9-4-.30.

Stress ratio effects for HP 9-4-.30 steel are relatively insensitive to environment and load frequency. This is demonstrated by the agreement between the crack growth rate data and analysis shown in Figures 33 and 34. The analysis results shown are based on dry air data. Also shown in Figures 33 and 34 is the variation of threshold stress intensity factor range (ΔK), with stress ratio. The little data taken at low ΔK's indicates that crack growth rates in the alternate immersion environment are very close to those in dry air whenever K_{max} exceeds about 25 ksi $\sqrt{in}$ (ΔK = 12.5 ksi $\sqrt{in}$ at R = 0.5, ΔK = 50 ksi $\sqrt{in}$ at -1.0).

High frequency trapezoidal wave loading has little effect on crack growth life in either steel in an alternate immersion environment (Figures 35 and 36). At low frequencies, both sine and trapezoidal wave loadings have significant effect on crack growth behavior (Figures 37 and 38). In HP 9-4-.30 low frequency loadings of either wave shape in alternate immersion tests raised the threshold stress intensity factor above the initial stress intensity factors used in the high frequency tests (Figures 25 and 26, pages 30 and 31).

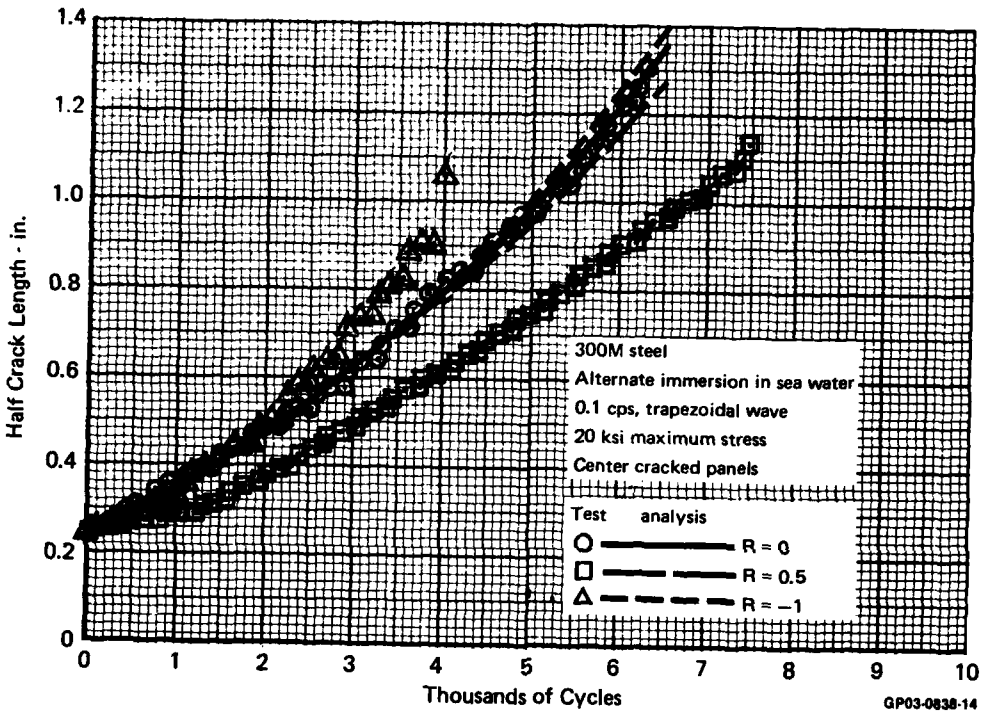

Figure 29. Effect of Stress Ratio on Crack Growth in Alternate Immersion Environment - 300M Steel

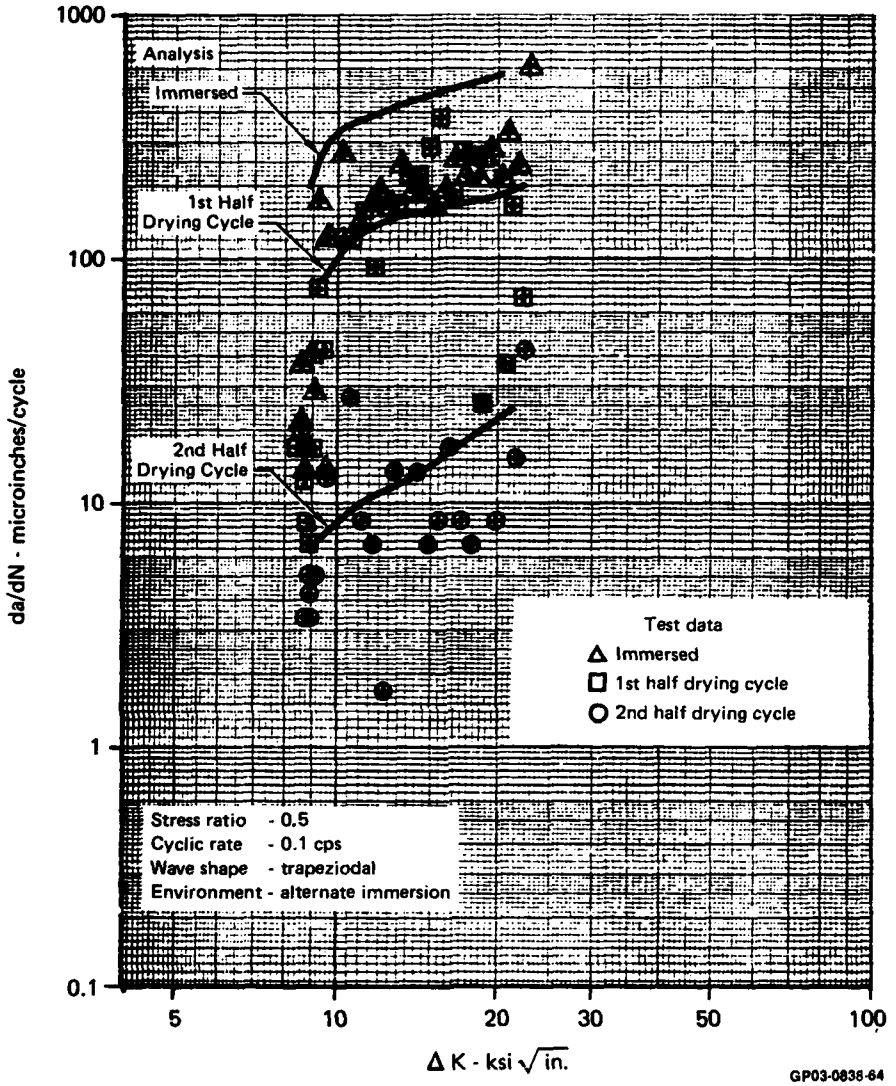

Figure 30. Crack Growth Rate for 300M Steel in Alternate Immersion Environment, R = 0.5

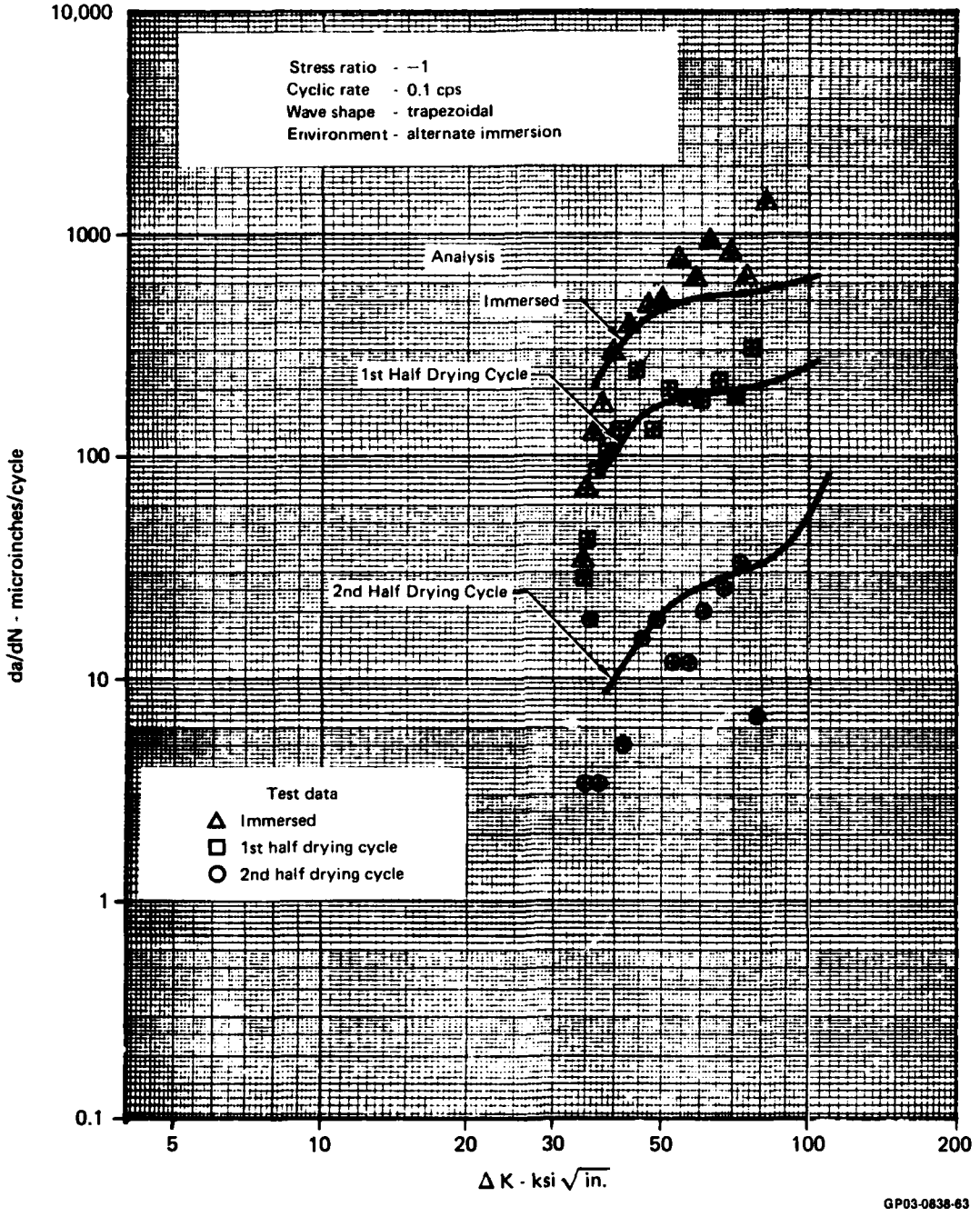

Figure 31. Crack Growth Rate for 300M Steel in Alternate Immersion Environment, R = −1.0

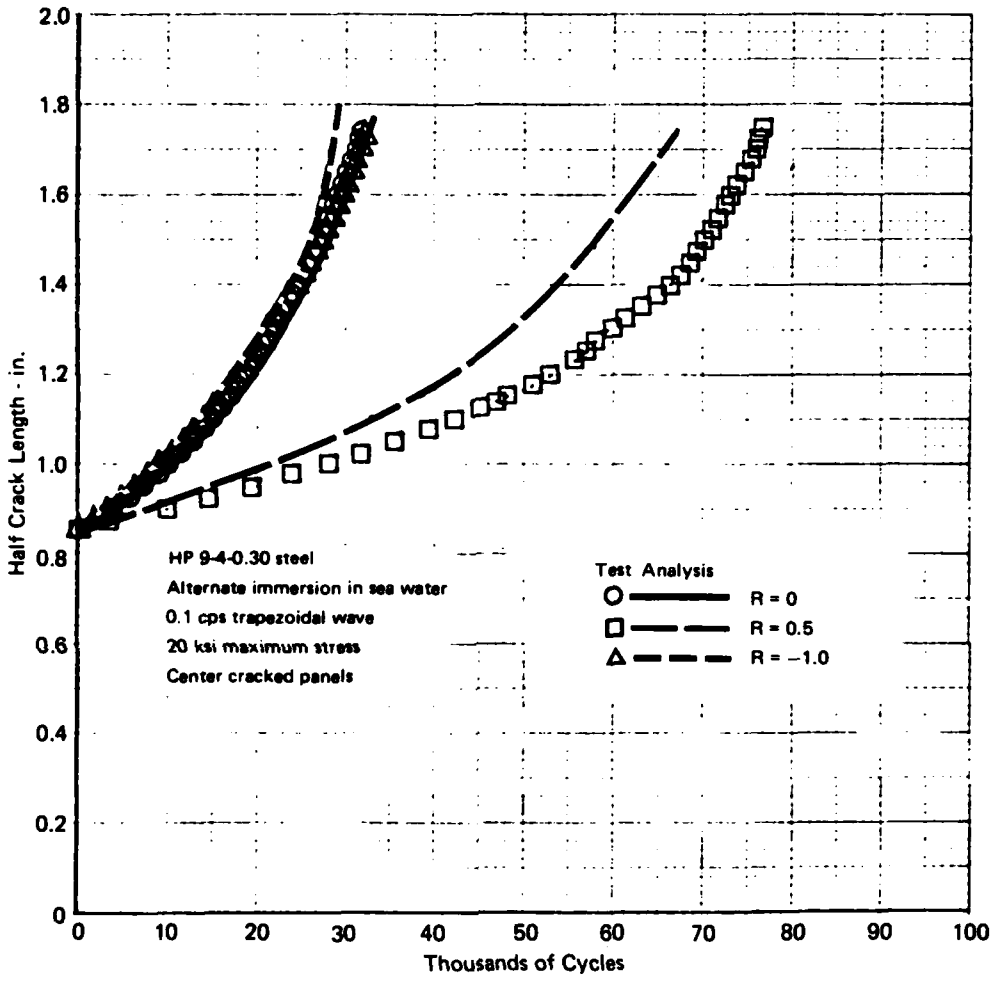

Figure 32. Effect of Stress Ratio on Crack Growth in Alternate Immersion Environment - HP 9-4-0.30 Steel

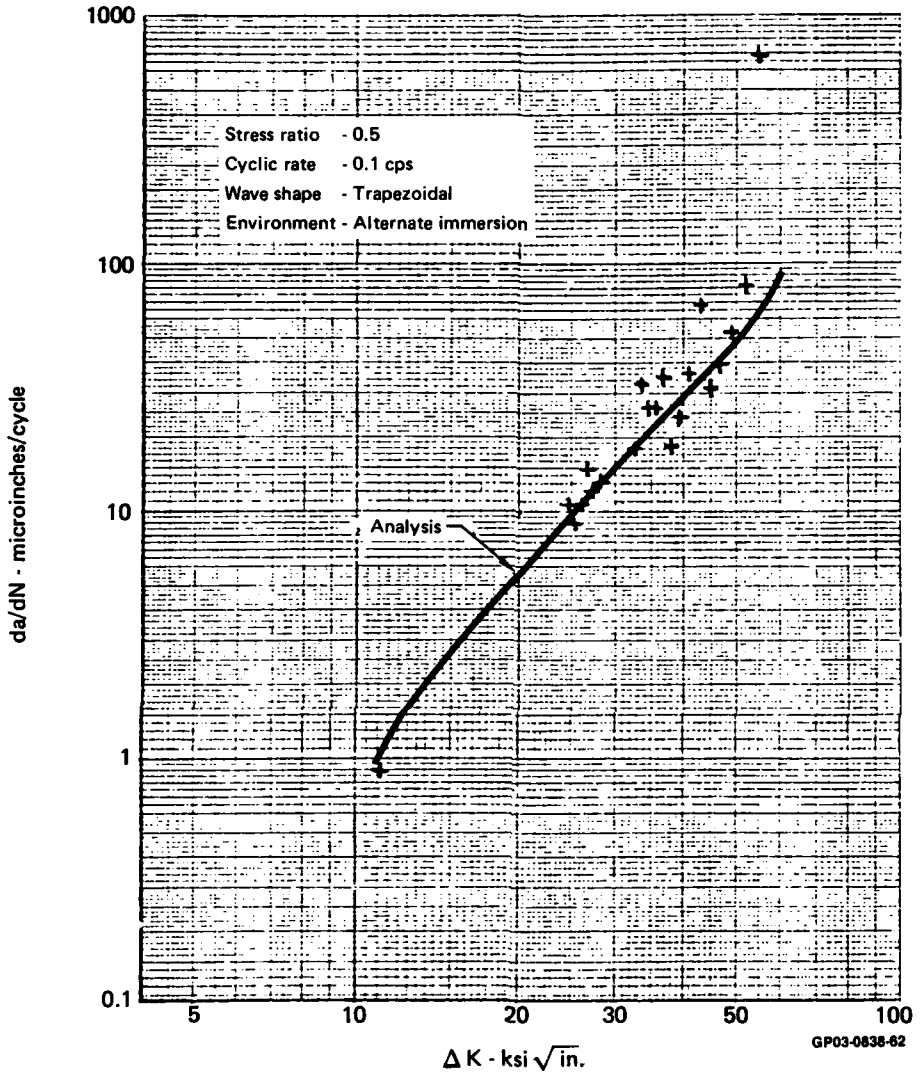

Figure 33. Crack Growth Rate in HP 9-4-0.30 Steel in Alternate Immersion Environment, R = 0.5

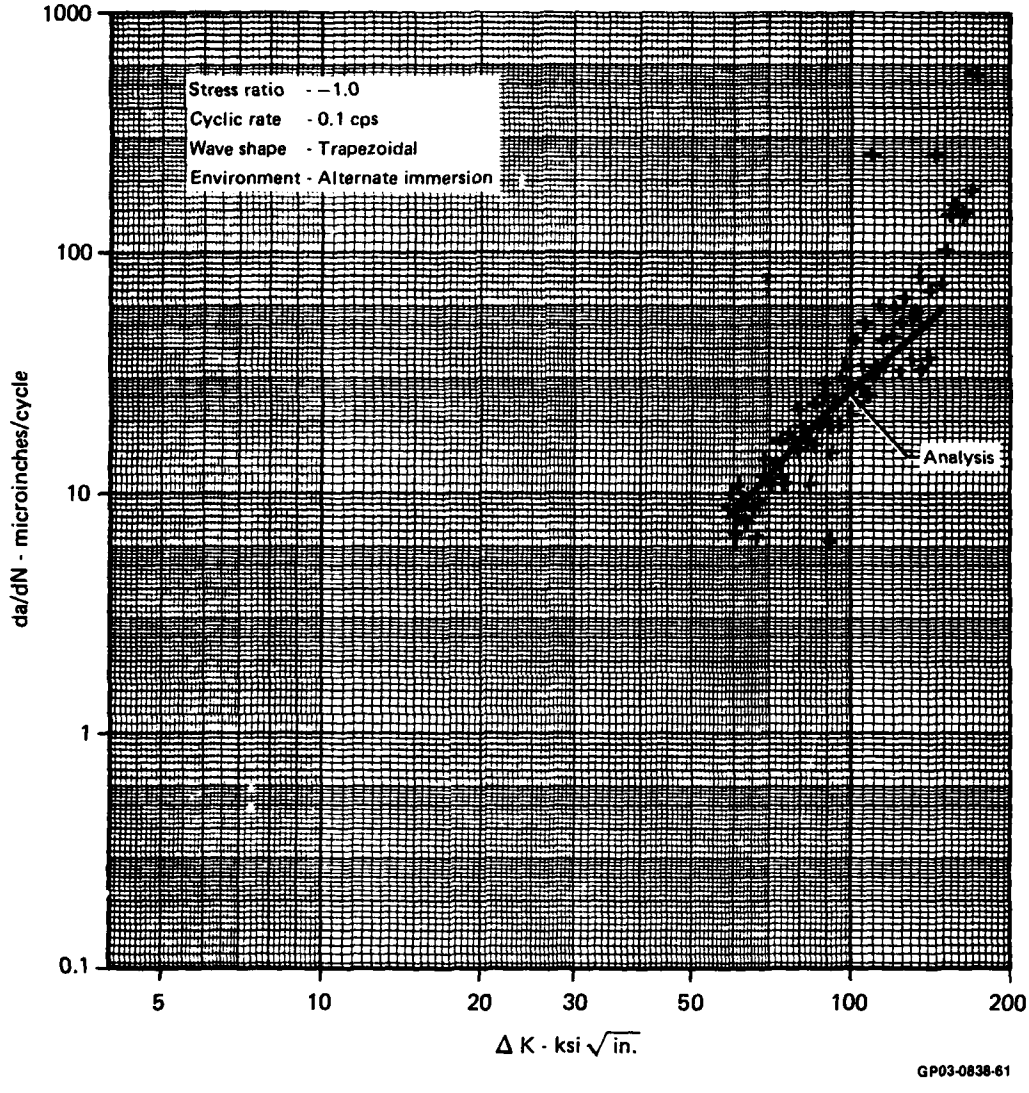

Figure 34. Crack Growth Rate in HP 9-4-0.30 Steel in Alternate Immersion Environment, R = − 1.0

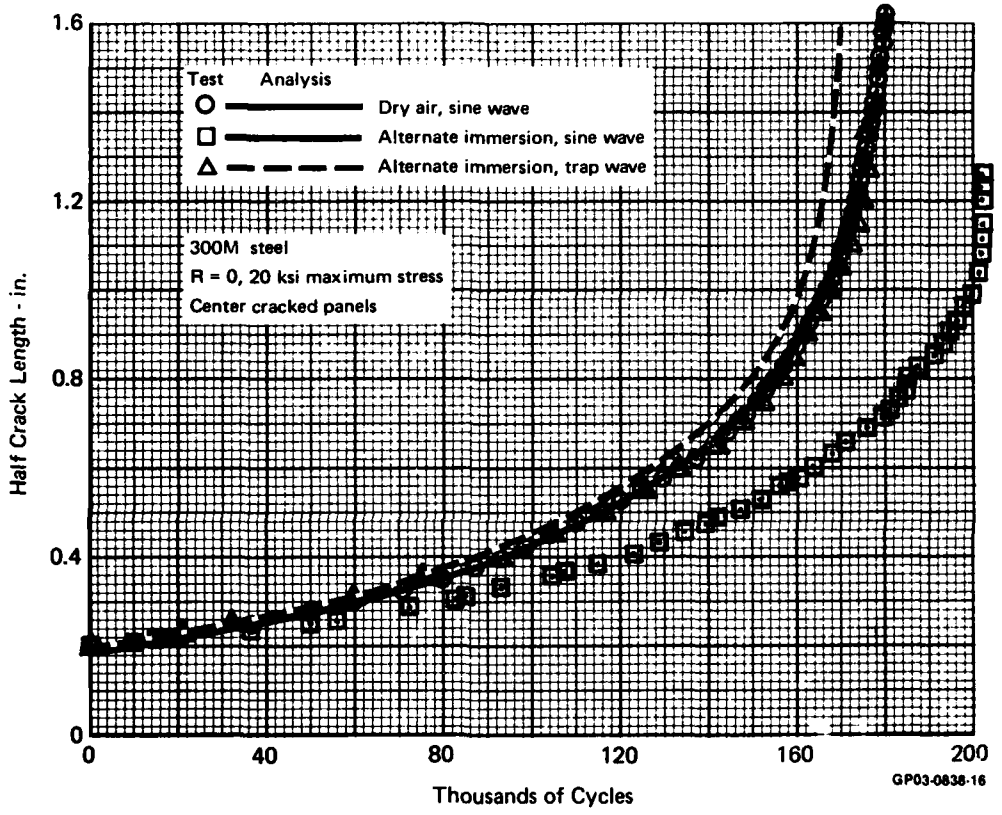

Figure 35. Effect of Wave Shape and Environment on Crack Growth in 300M Steel at 10 cps

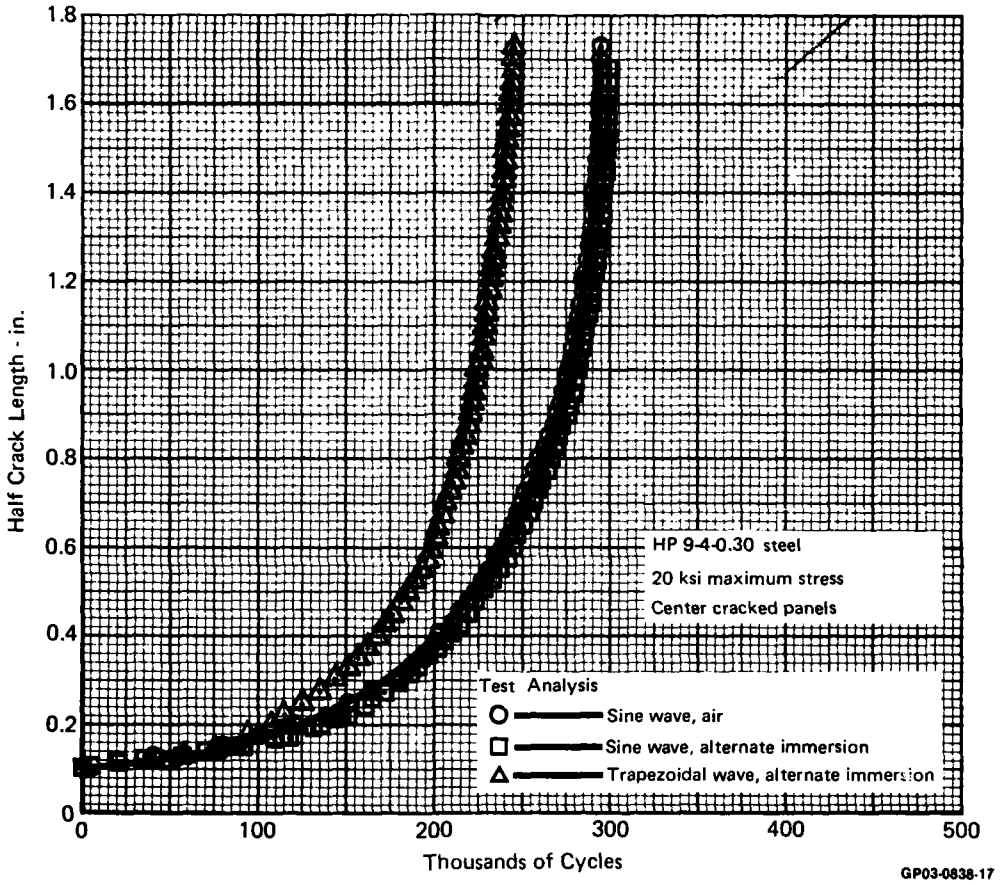

Figure 36. Effect of Environment and Wave Shape on Crack Growth in HP 9-4-0.30 Steel at 10 cps

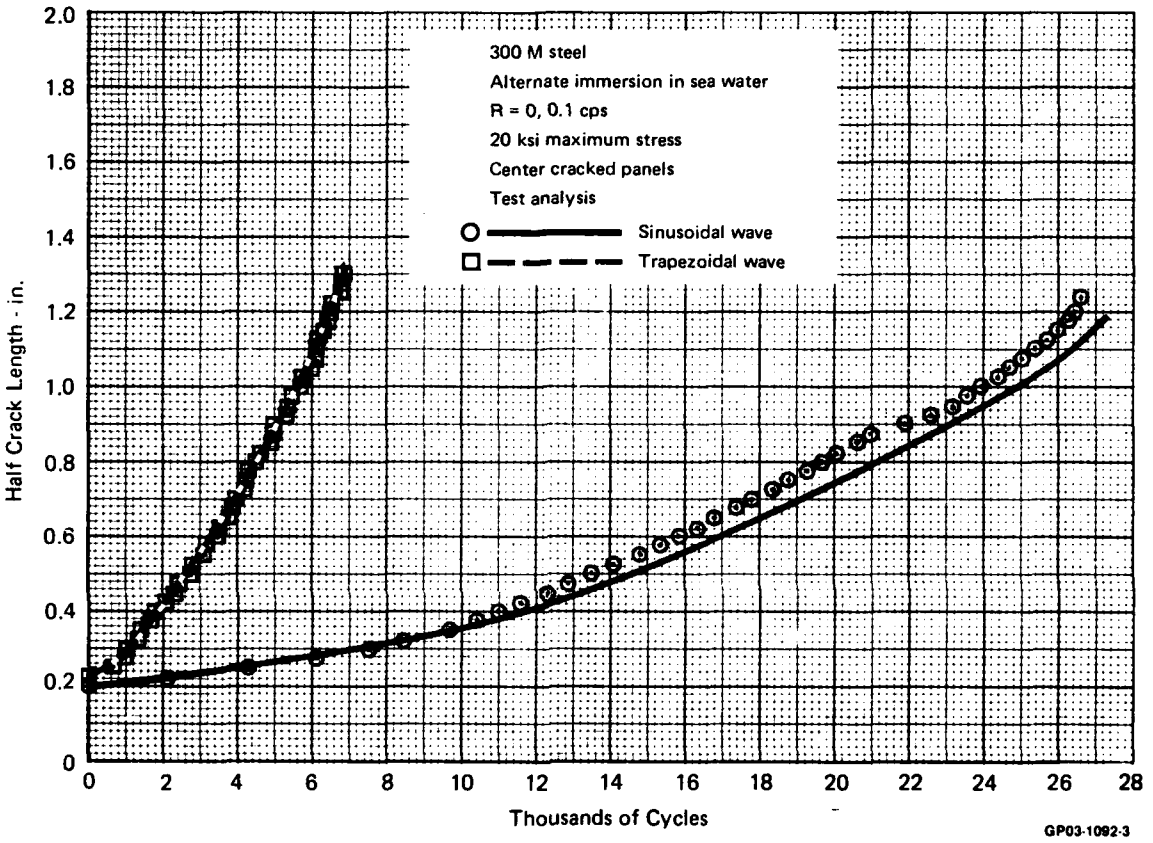

Figure 37. Effect of Wave Shape on Crack Growth in 300M Steel in Sea Water at 0.1 cps

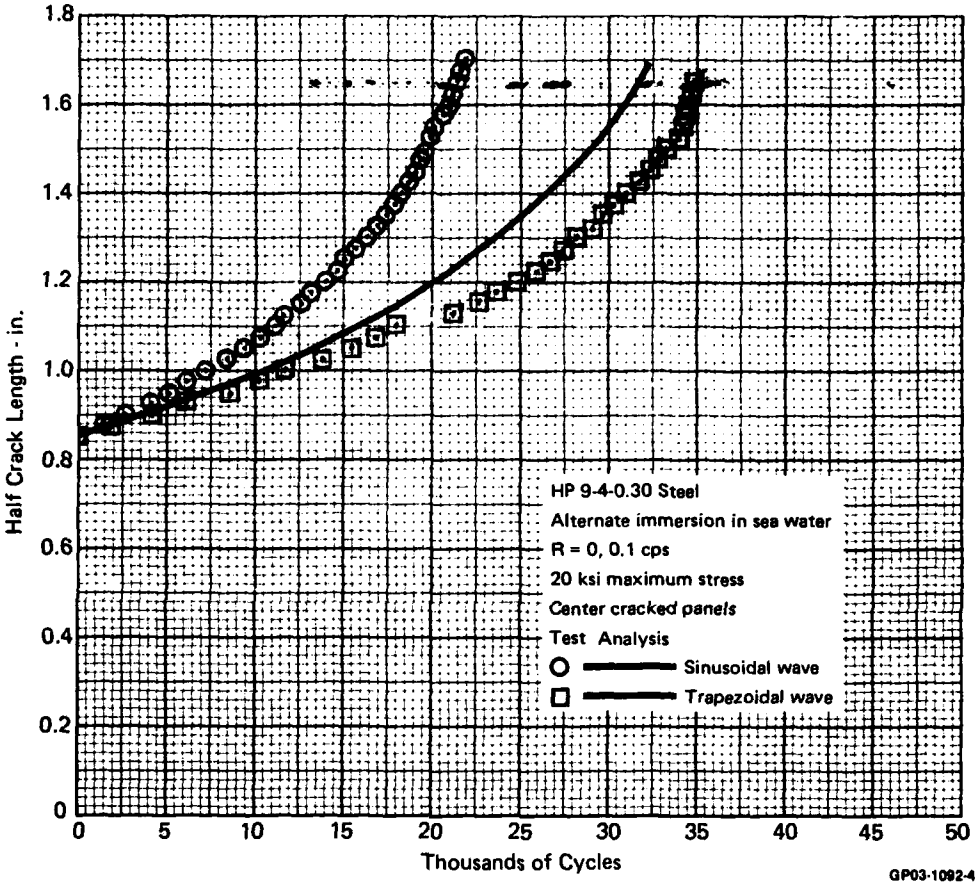

Figure 38. Effect of Wave Shape on Crack Growth in HP 9-4-0.30 Steel in Sea Water at 0.1 cps

In 300M steel, at low frequency, a trapezoidal wave causes faster crack growth than a sine wave at a similar frequency. As shown in Table 3 (page 10) the crack growth life for a 0.1 cps trapezoidal wave is about one fourth that under an 0.1 cps sinusoidal wave. This is expected since 300M exhibits large sustained load cracking rates in a salt water environment (References 1, 3, and 4).

9. SPECTRUM AND DUPLICATE TESTS - (Specimens 12-13) - Specimens 12 and 13 were used to evaluate crack growth retardation under landing gear spectrum loads in center crack panels. Two tests in each material were performed in the dry air environment using the spectrum defined in Section V. The test frequency was approximately 10 cps.

In HP-9-4-.30, spectrum tests were performed at 40 ksi and 48 ksi maximum stress levels. The results presented in Figure 39 indicate the sensitivity of crack growth lives to stress level variations. Analysis results indicate that the effect on life of such variations is adequately predicted. Some accelerated growth can be noticed in both results prior to the occurrence of the maximum stress level at about 3800 landings. This is probably due to the low precracking stress level (12 ksi) used for these tests.

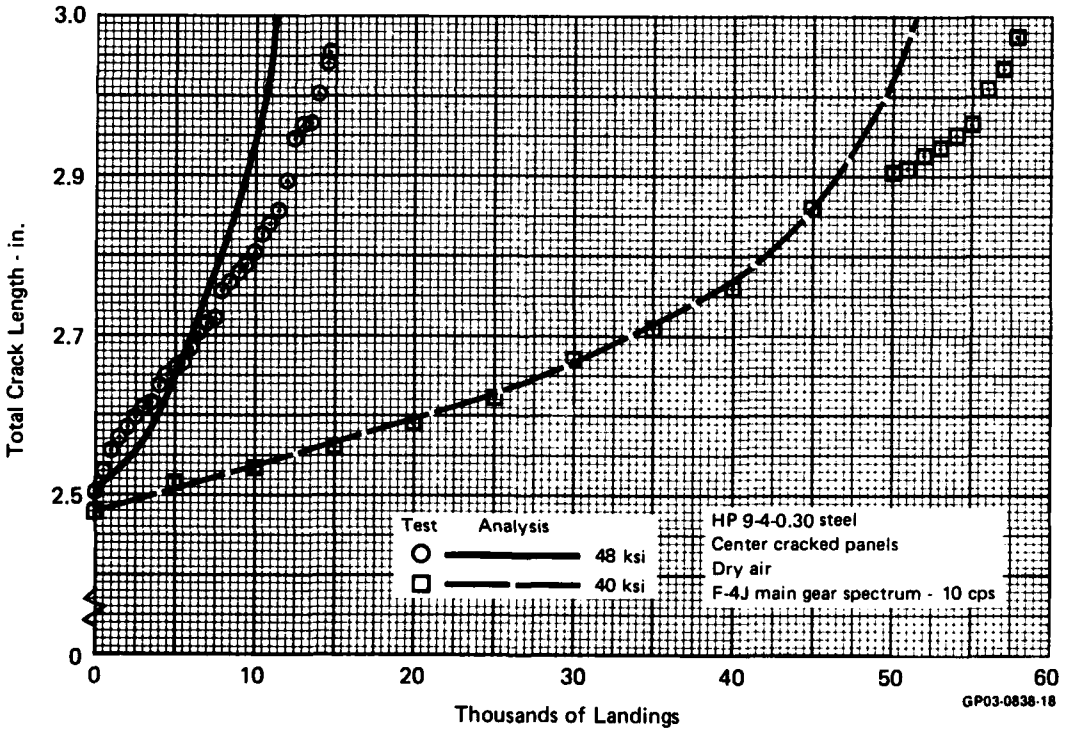

Figure 39. Spectrum Test Results for HP 9-4-0.30 in Dry Air

In 300M steel, both spectrum tests were performed at 48 ksi and two initial crack lengths were used (1.0 inch and 1.14 inch). Results from both tests are presented in Figure 40. The first test took 20,000 landings to reach a crack of 1.14 inches. Data from the second test are plotted starting at this point to simplify comparison of the two test results. The results presented in Figure 40 indicate the specimen-to-specimen variation in crack growth under the landing gear spectrum. Reasonably good correlation between analysis and both test results was obtained. Initial acceleration is not evident in these results.

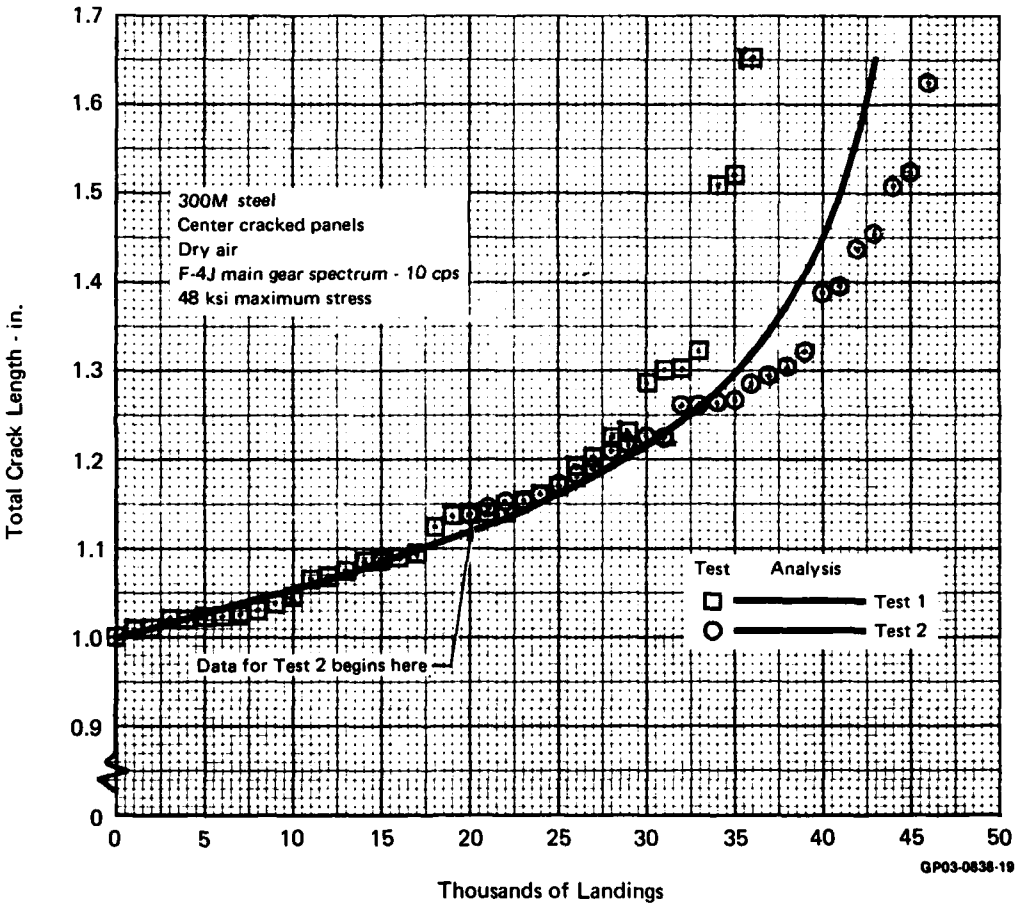

Figure 40. Spectrum Test Results for 300M in Dry Air

These test results permitted selection of overload interaction zone sizes for both materials, which were used to predict the crack growth behavior expected in the verification test. The prediction methodology is discussed in Section III.

10. SURFACE FLAW TESTS (Specimen 14) - Two tests of surface flawed panels were used to verify the crack growth analysis procedure for surface flaws. One constant amplitude test in each material was performed in the dry air environment. The test frequency was approximately 10 cps. Tests were intended to last approximately 10,000 cycles at 100 ksi and crack lengths were measured after 500 cycle increments.

Comparisons of predicted and measured crack growth on the specimen surface are presented in Figures 41 and 42. Predicted and measured growth rates are compared with center cracked panel growth rates in Figures 43 and 44. Measured growth rates in both tests are initially lower than predicted. In 300M the growth rate rapidly approaches predicted values and good agreement between predicted and measured growth is obtained (Figure 41). In HP 9-4-.30 the initial growth rates are low enough that the crack growth curve comparison of Figure 42 is not as good as for 300M. In both cases the initial low growth rates measured may be due to differences between assumed and actual initial flaw shapes. These differences rapidly disappear as the flaw shapes approach natural flaw shapes. The generally good agreement between predicted and measured results indicates the accuracy of the surface flaw analysis procedure.

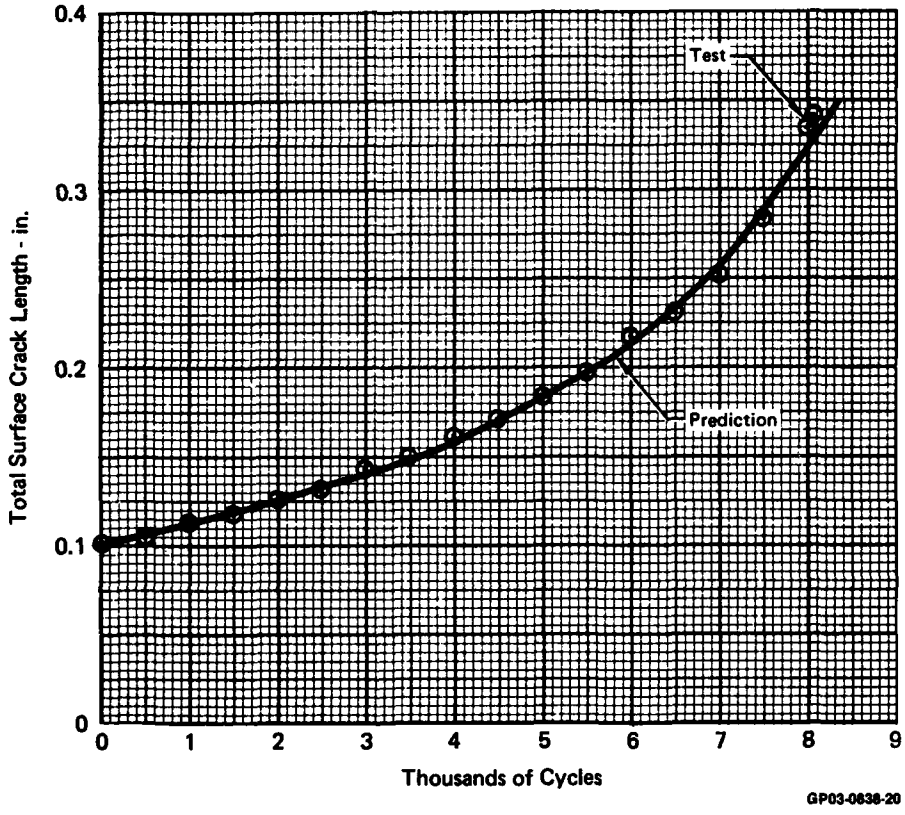

Figure 41. Comparison of Surface Flaw Test and Analysis Results in 300M Steel

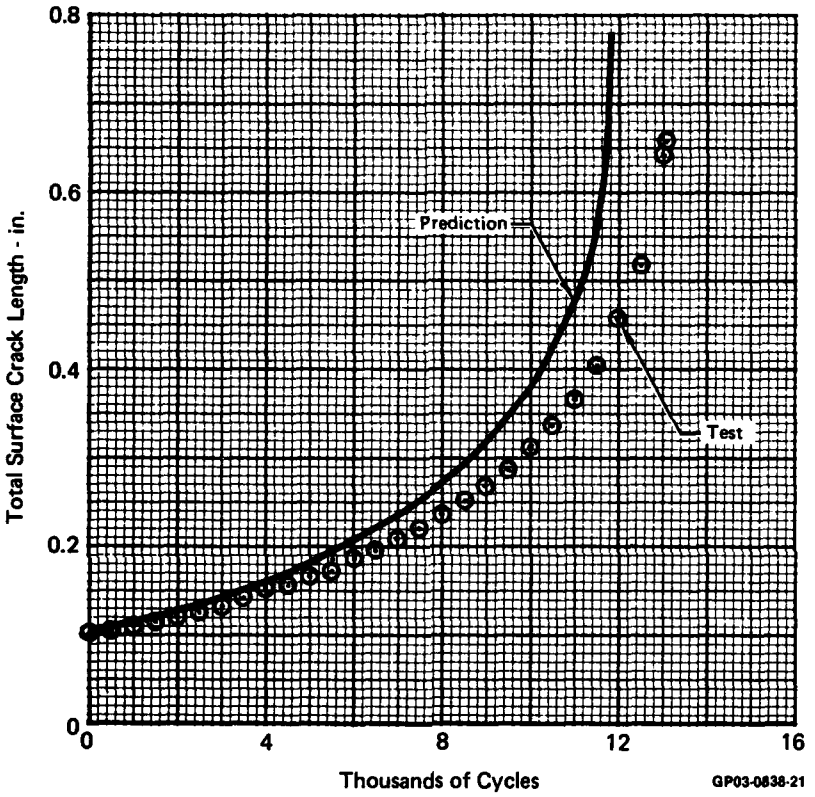

Figure 42. Comparison of Surface Flaw Test and Analysis Results in HP 9-4-0.30 Steel

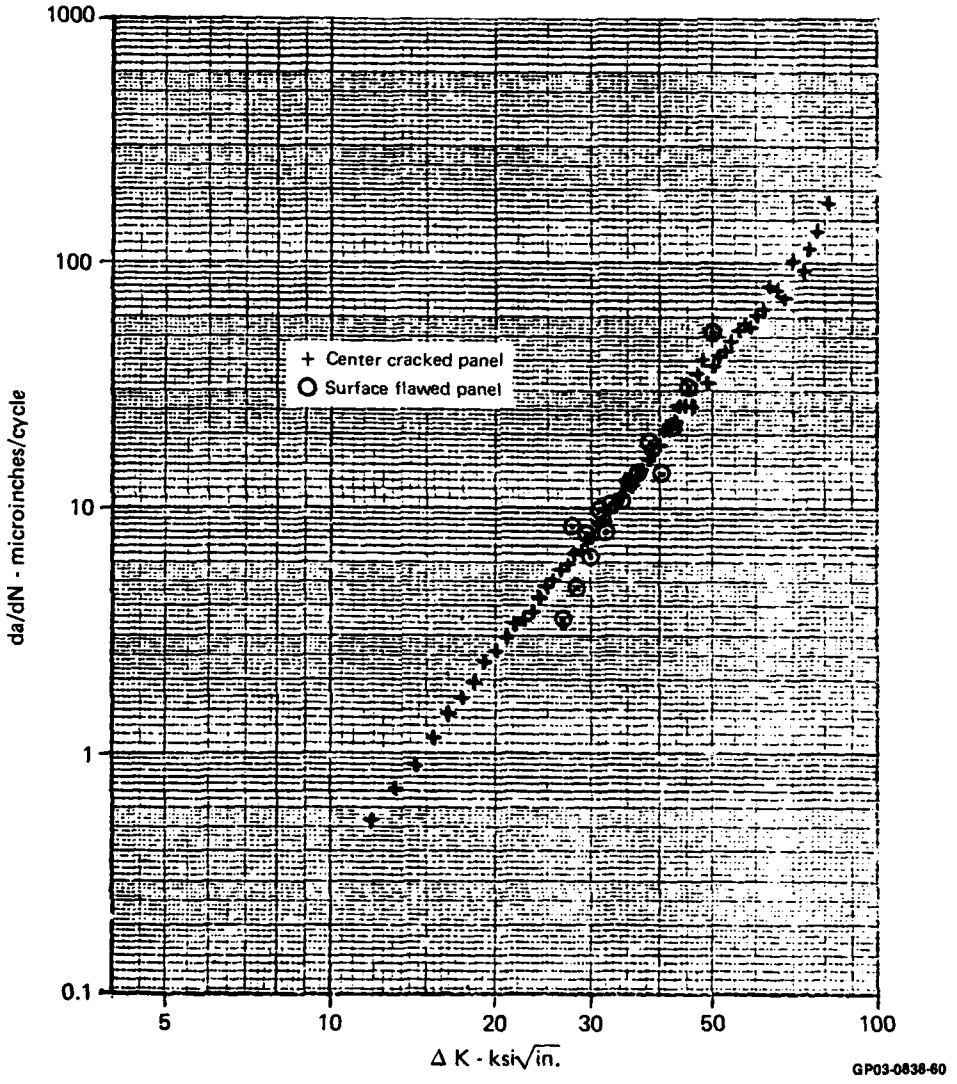

Figure 43. Comparison of Surface Flaw and Center Crack Growth Rates for 300M

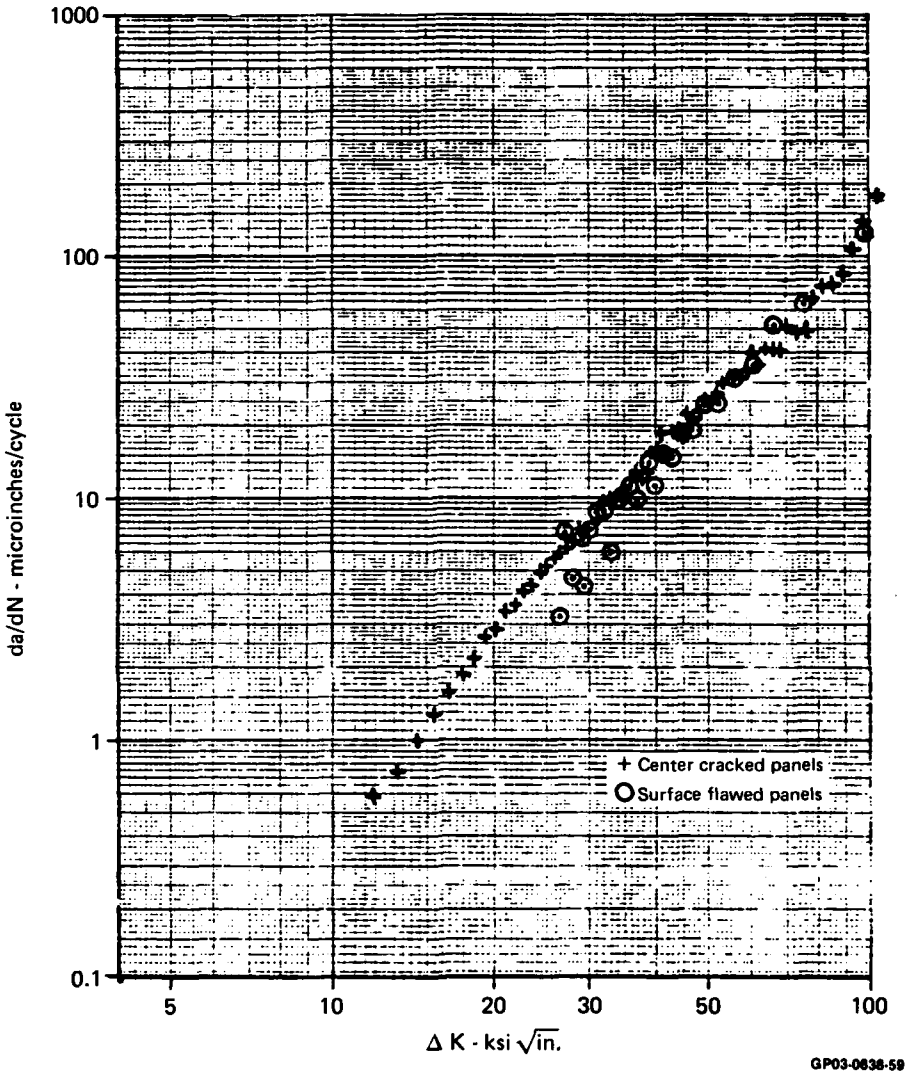

Figure 44. Comparison of Surface Flaw and Center Crack Growth Rates for HP 9-4-0.30

SECTION III

ENVIRONMENT-LOAD INTERACTION MODEL

1. SUMMARY - The analysis of environmental acceleration of crack growth is based on a linear superposition of cyclic load and sustained load crack growth. Stress ratio effects are accounted for by using an effective stress intensity range concept based on closure. Crack growth analysis using the combination of these two algorithms shows good correlation with the results of the model evaluation and calibration tests.

The Willenborg model was the basis for extension of the crack growth analysis to spectrum loadings. Spectrum test results from center crack panels were used to calibrate the model for predictions of surface flaw and center crack growth under spectrum loadings for the verification tests. Stress intensity factor solutions for semi-elliptical surface flaws were determined using a slice synthesis model, validated by comparisons with finite element solutions.

2. STRESS RATIO EFFECTS - The method used herein to predict the effect of stress ratio on crack growth rate is based on analysis of crack closure caused by crack surface displacements. Crack closure determines the stress intensity range which is effective in propagating the crack. This effective stress intensity range is obtained from a curve fit to the analyses of Reference 5.

$$\Delta K_{eff} = \left(\frac{1-R}{1-K^\circ}\right) [1 - (1-R)\, K^\circ]\, K_{max} \quad \text{for } R \geq 0 \qquad (1)$$

$$\Delta K_{eff} = \frac{1}{1-K^\circ} [1 - K^\circ e^{0.1R}]\, K_{max} \quad \text{for } R < 0 \qquad (2)$$

where R and K_{max} are defined by the remote loading conditions and K° is the ratio of closure stress intensity to K_{max} at R=0, generalized as

$$K^\circ = (0.33045 + 0.15164\, r_p - 0.01476\, r_p^2) \qquad (3)$$

$$[1 + 0.6\, (f_c/f_m - 1) - 0.156\, (f_c/f_m - 1)^2]$$

where

f_m = monotonic yield stress

f_c = cyclic yield stress

The parameter, r_p, was used to "tune" Equations (1) and (3) for each material analyzed so that constant amplitude test lives for R=0 and R=0.5 were matched. In the closure analysis of Reference 5, r_p, was related to plastic zone conditions, r_p=1 for plane stress, r_p=0 for plane strain. As presented in Table 4, r_p=0 (K_o=0.33) was found to provide good correlation with the R=0 and R=0.5 crack growth results in both 300M and HP 9-4-.30. This differs somewhat from the values found in Reference 1 where K_o for 300M was 0 and for HP 9-4-.30 was 0.242. However, because of heat treating difficulties noted in Reference 1, the material used in that program was less well behaved than that used in this program: This probably accounts for the differences in behavior at various stress ratios.

TABLE 4. PARAMETERS USED FOR STRESS RATIO CORRECTIONS

Material	r_p (1)	f_m ksi (2)	f_c ksi (3)	K^o (4)
HP 9-4-0.30	0	210	210	0.330
300M	0	248	228	0.330

Notes:
(1) Plastic zone size correction factor
(2) Monotonic yield stress
(3) Cyclic yield stress
(4) Ratio of $K_{max\text{-}eff} - \Delta K_{eff}$ to $K_{max\text{-}applied}$ for R = 0, constant amplitude loading

GP03-0838-29

The closure based approach, as empirically used in this program, has two advantages over the Forman equation, Reference 6: (1) predicted effects of stress ratio on crack growth rate can be varied to account for variations in material behavior, and (2) negative stress ratios generally are predicted to accelerate crack growth. As shown in Figures 6-9 (Pages 11-14), this analysis agrees well with the test data from this program.

3. LINEAR SUPERPOSITION APPROACH FOR PREDICTION OF ENVIRONMENTAL ACCELERATION

a. Modification of Wei-Landes Approach - The Wei-Landes linear summation hypothesis, Reference 7, suggests that environmentally accelerated crack growth rates can be predicted by adding the crack growth due to the individual mechanisms of environmental attack and cyclic loading. This hypothesis, when used to account for frequency effects, can be expressed:

$$\left(\frac{da}{dN}\right)_{total} = \frac{1}{f}\left(\frac{da}{dt}\right)_{environment} + \left(\frac{da}{dN}\right)_{fatigue} \qquad (4)$$

The $da/dt_{environment}$ is obtained from sustained load or low frequency cyclic tests in the environment, and $da/dN_{fatigue}$ is obtained from cyclic load tests conducted at high frequencies in air or a non-aggressive environment.

The modification of the linear summation hypothesis used in this program is that for any environment the total crack growth rate for any cycle is the sum of two components; one due to mechanical loading in the reference environment (less than ten percent relative humidity), and one due to sustained load in an aggressive environment. This model is formulated as:

$$\frac{da}{dN} = \frac{da}{dN}\Big|_{ref} + \frac{da}{dN}\Big|_{env} \tag{5}$$

where,

$$\frac{da}{dN}_{\substack{env \\ immersed}} = \int_{t_1}^{t_2} \frac{da}{dt}_{immersed} dt \quad \text{(during immersion)} \tag{6a}$$

$$\frac{da}{dN}_{\substack{env \\ drying}} = \int_{t_1}^{t_2} \frac{da}{dt}_{immersed} e^{-\alpha t} dt \quad \text{(during drying)} \tag{6b}$$

Where the load period is t_2-t_1.

The sustained load crack growth rate during immersion is determined from 0.1 cps trapezoidal wave test data by:

$$\frac{da}{dt}_{immersed} \cong \frac{1}{10}\left[\frac{da}{dN}_{\substack{immersed \\ 0.1\ cps}} - \frac{da}{dN}_{\substack{ref \\ 10\ cps}}\right] \tag{7}$$

Equation (6a) was numerically integrated for a 1 cps, R=0, sine wave loading to determine the crack growth rate for sine waves of various K_{max} values. Only crack growth rates during the loading portion of the sine wave are integrated because it is assumed that the unloading portion of the cycle contributes no growth.

During the drying cycle, the environmental acceleration decays exponentially with time after immersion. This results in a stair-step crack growth curve at low frequencies, Figure 45. Using the exponential decay function, Equation (6b), the crack growth rate for a cycle during the drying period having sustained load from time, t_1 to t_2, can be approximated from integration of Equation (6b) as

$$\frac{da}{dN}_{drying} = \frac{da}{dN}_{\substack{ref \\ 10\ cps}} + \frac{1}{\alpha f}\frac{da}{dt}_{immersed}\left(e^{-\alpha t_1} - e^{-\alpha t_2}\right) \qquad (8)$$

where $\frac{da}{dt}$ immersed is assumed not to change significantly during a single cycle. The exponent, α, in Equation (6b) was determined empirically by correlation with the crack growth rates measured during the drying cycle of the trapezoidal wave test using R=0 at 0.1 cps (Specimen 9). In 300M steel α was found to be 0.00175. In HP-9-4-.30, no environmental acceleration was found and α is zero.

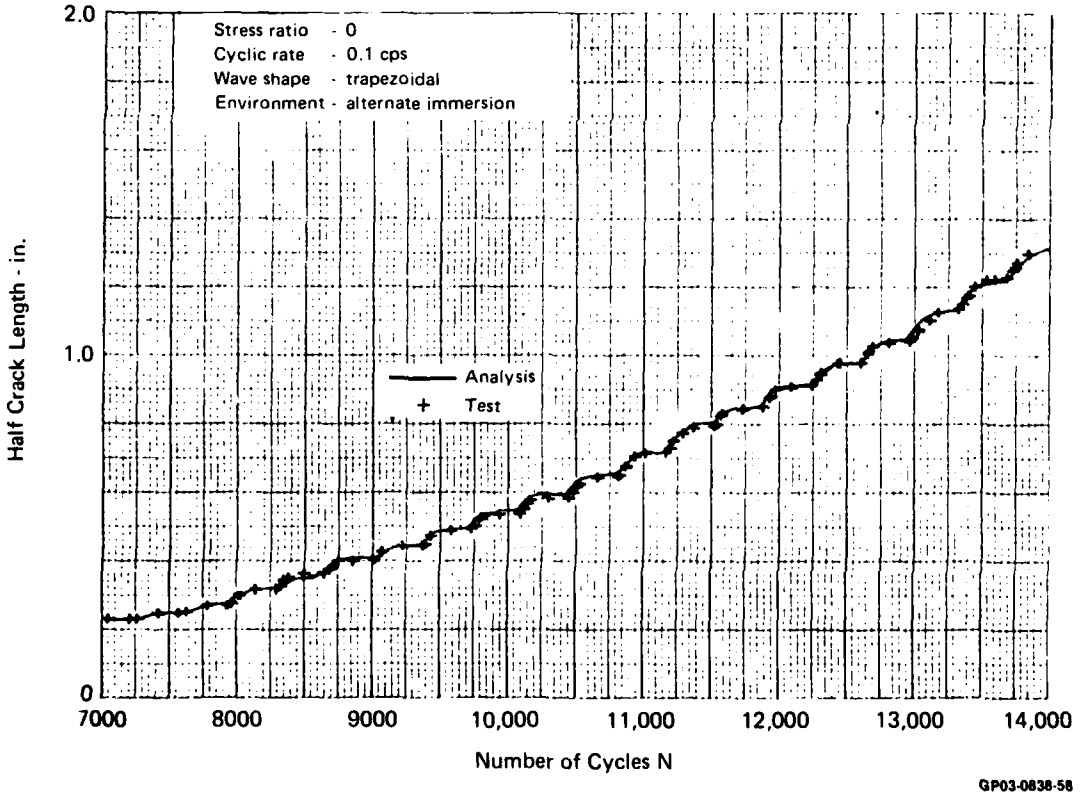

Figure 45. Crack Growth Behavior of 300M Steel in Alternate Immersion in Sea Water at Low Cycle Rates

The prediction of sustained load crack growth by Equation (6a) was found to adequately describe crack growth behavior in continuous immersion tests (Reference 1). However, in alternate immersion tests, the sustained load crack growth rate during immersion was less than that predicted by Equation (6a) for 1 cps and 10 cps load frequencies. Sustained load crack growth rates for both alternate immersion and continuous immersion tests are compared in Figure 46. An empirical correction is applied to Equation (6a) to improve correlation with the test results. The corrected expression is:

$$\left(\frac{da}{dt}\right)_{\text{immersed}} = (0.1t_h)^{0.25} \left(\frac{da}{dt}\right)_{\substack{\text{immersed} \\ 0.1\ \text{cps}}} \qquad (9)$$

where t_h is the hold time in a given load cycle.

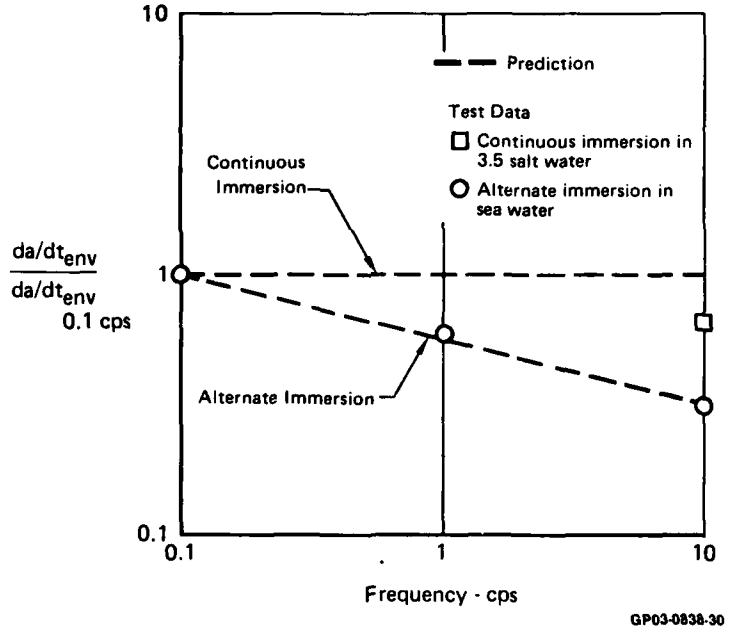

Figure 46. Comparison of Sustained Load Crack Growth Rates in 300M Steel for Alternate and Continuous Immersion Environments

Sustained load cracking during immersion is assumed to occur only during the loading portion of the cycle. When a trapezoidal wave is applied, predicted crack growth is the sum of three components; cyclic growth during loading, sustained load growth during loading (analyzed as a sine wave), and sustained load growth during the hold time. The unloading portion of a cycle is assumed to produce no crack growth and is ignored in the analysis.

This model was used for all analyses presented herein. Comparison of analysis and test results for 300M steel, Figures 21-24, and 45, indicate the accuracy of the model to describe the crack growth behavior of 300M steel in the alternate immersion environment at several loading frequencies. Predicted and measured lives for all constant amplitude crack growth tests in 300M steel are summarized in Table 5. Good correlation is evident.

TABLE 5. COMPARISON OF TEST AND ANALYSIS RESULTS IN 300M STEEL

Specimen Number	Specimen Type	Environment	Stress Ratio	Frequency (cps)	Wave Shape	Test Type	300M Test Cycles to Grow Crack from 0.5 to 2.6 in.	300M Analysis Cycles to Grow Crack from 0.5 to 2.6 in.
1	Center Cracked Panel	< 10% RH Air	0	10	Sinusoidal	Const-Amp	140,000	139,000
2			0.5	10			370,000	378,000
3			−1	10			122,000	126,000
4		Alternate Immersion in Sea Water	0	10			155,000	135,000
5			0	1			94,000	104,000
6			0	0.1			22,900	22,500
7			0	10	Trapezoidal		140,000	132,000
8			0	1			62,700	59,300
9			0	0.1			6,210	6,350
10			0.5	0.1			7,380	6,630
11			−1	0.1			4,010	6,320

Note: Maximum stress level was 20 ksi for each test.

GP03-0838-31

The effect of stress ratio on life in 300M steel in the alternate immersion environment is indicated in Figures 29-31. The correlation of predicted and measured lives in the alternate immersion environment, Figure 29, is not as good as that of the other comparisons shown. Evidently stress ratio has more impact on crack growth in the aggressive environment than is computed from Equation (5). The correlation is considered adequate since the analysis does predict the more significant reduction in life produced by the aggressive environment.

Predicted and measured crack growth lives for HP-9-4-.30 steel are compared in Table 6. These predictions assume that there is no impact of the aggressive environment. This assumption is confirmed by the test data. However, the 0.1 cps trapezoidal wave shape test results show a significant increase in threshold stress intensity factor. Plots summarizing the effects of frequency and stress ratio on crack growth life in HP-9-4-.30 steel are presented in Figures 25 and 32. These plots indicate the accuracy of the technique.

TABLE 6. COMPARISON OF TEST AND ANALYSIS RESULTS IN HP 9-4-0.30 STEEL

Specimen Number	Specimen Type	Environment	Stress Ratio	Frequency (cps)	Wave Shape	Test Type	HP 9-4-0.30 Test Cycles to Grow Crack from 0.5 to 2.6 in.	HP 9-4-0.30 Analysis Cycles to Grow Crack from 0.5 to 2.6 in.
1	Center Cracked Panel	< 10% RH Air	0	10	Sinusoidal	Const-Amp	137,000	139,000
2			0.5	10			390,000	370,000
3			−1	10			115,800	127,000
4		Alternate Immersion in Sea Water	0	10			131,000	139,000
5			0	1			101,900	139,000
6			0	0.1			22,500	32,000 (1)
7			0	10	Trapezoidal		108,500	139,000
8			0	1			149,400	139,000
9			0	0.1			35,000	32,000 (1)
10			0.5	0.1			76,500	67,000 (1)
11			−1	0.1			32,000	29,000 (1)

GP03-0838-32

Notes: (1) Cracks did not grow until precracked beyond 1.25 inches. Lives presented here are from 1.7 to 2.6 inches.
(2) Maximum stress level was 20 ksi for each test.

b. Simple Approach to Load-Environment Interaction Analysis - A less complicated analysis technique, presented in Reference 1, which does not account for the decay in crack growth rates after immersion in an aggressive environment, was also evaluated using the test data presented in Section II. This second technique is similar to that presented previously but uses average crack growth rate data from the 0.1 cps, alternate immersion tests to determine the sustained load crack growth rate via Equation (7). In this case, the alternate immersion cycle in total is considered the aggressive environment and computation of the acceleration due to the environment is made using only Equation (6a).

Comparison of analysis results using this technique with alternate immersion test data for 300M steel at three different frequencies is presented in Figure 47. Correlation is even better than that for the more detailed analysis shown in Figure 21, Page 26. Correlation with the remainder of constant amplitude tests in 300M and HP-9-4-.30 is as good as that shown for the more detailed analysis technique previously presented. Thus, the simple load-environment interaction analysis presented in Reference 1, while it is not capable of predicting detailed crack growth behavior in alternate immersion tests, is an accurate method for predicting the gross behavior in constant amplitude tests.

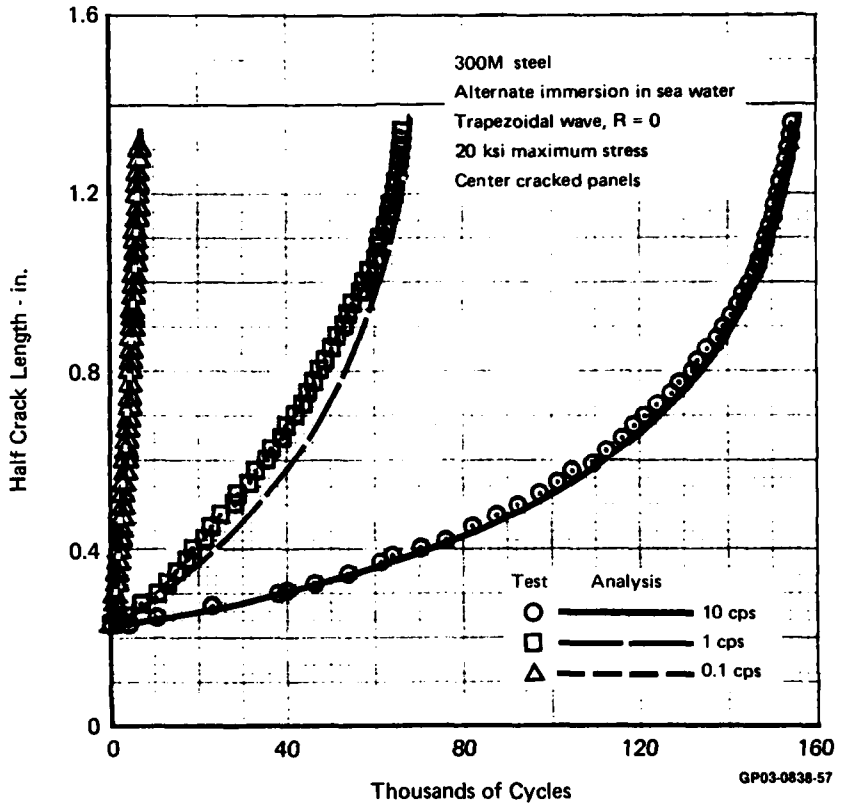

Figure 47. Comparison of Results of Simple Load-Environment Analysis With Crack Growth Behavior of 300M Steel

The average crack growth rate curve used for these analyses is compared with the test data for 0.1 cps, alternate immersion test of 300M steel in Figure 48. This comparison indicates the inability of this technique to account for the transitory acceleration which occurs in alternate immersion tests. This is not a major handicap for analysis of constant amplitude behavior, where many load cycles and immersion cycles are applied during the specimen life. However, in spectrum crack growth analyses, where the coupling of high sustained loads and immersion in salt or sea water provide significant acceleration of crack growth rates in 300M steel, this simple technique could provide erroneous predictions of crack growth behavior. Therefore, the simple technique was not used for prediction of crack growth behavior under spectrum loadings in this program.

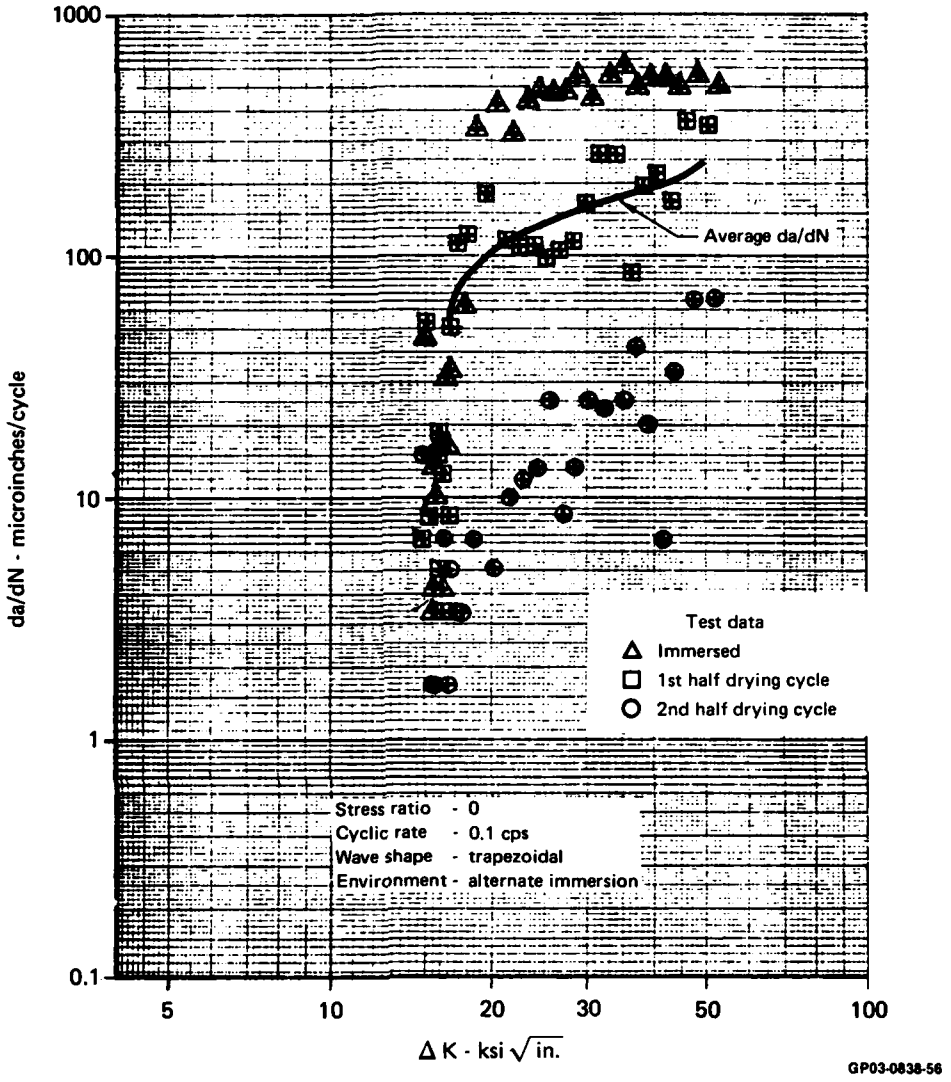

Figure 48. Comparison of Average da / dN Curve with Crack Growth Rate Test Data

c. Spectrum Analysis with Environmental Acceleration - Application of the crack growth algorithms to spectrum analysis was straightforward. The spectrum was input as a series of stresses and corresponding time increments to peak stress (Section IV). Stress levels were joined by haversine waves as shown in Figure 49. Sustained stress levels are represented by two adjoining peaks having the same stress level, the peak to peak time being the hold time.

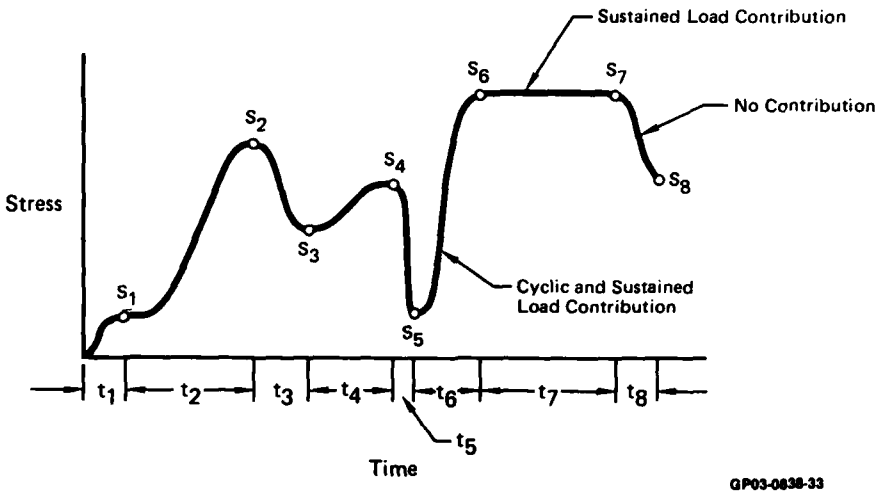

Figure 49. Spectrum Load Definitions Used for Analysis

The stress history was simplified so that it contains only peaks and valleys and the times at which they are applied. Thus, during simplification, the stress level s_o is the first valley, stress level s_1 is dropped and s_2 is the peak for the first half cycle. The time increment for the first cycle is the sum of t_1 and t_2.

Under spectrum loadings, da/dN_{ref} and da/dN_{env} are assumed to depend on the effective loading parameters, $K_{max-eff}$ and $K_{min-eff}$, computed by the Willenborg model.

The following assumptions are also inherent in the analysis:

(a) The unloading portion of the stress cycle produces no crack growth and is ignored in the analysis. The stress intensity range and stress ratio used for analysis are determined by a valley stress and the subsequent peak stress.

(b) Any half cycle having a stress ratio greater than 0.9 is treated as a sustained load.

(c) In the computation of sustained load crack growth, a cycle has a peak stress intensity factor of $K_{max-eff}$, as determined by the Willenborg model, and $R_{eff}=0$.

(d) Fracture is assumed to occur whenever the stress intensity factor exceeds K_c.

Computation of cyclic crack growth considers only the loading portion of the cycle, i.e., s_5 to s_6 is a load cycle, s_6 to s_7 or s_7 to s_8 are assumed to produce no cyclic growth. Similarly, computation of sustained load crack growth uses only the loading half cycle and sustained load, the growth is predicted by Equations (5) through (9). The cyclic frequency is determined from the loading period, i.e.,

$$f = \frac{1}{2t_4} \text{ for } s_3 \text{ to } s_4, \tag{10}$$

For sustained load, i.e., half cycles having $R \geq 0.90$,

$$\frac{da}{dN} = \Delta t \frac{da}{dN_{env}} \tag{11}$$

where for s_6 to s_7, $\Delta t = t_7$.

4. WILLENBORG MODEL

a. Generalized Willenborg Model - The Willenborg, et al, model, Reference 8, as generalized by Gallagher and Hughes (Reference 9) is the load interaction model extended to the analysis of environmental effects. The original Willenborg Model was developed to describe crack growth retardation following high-low block loadings. It is based on observations of the following phenomena:

(a) Retarded crack growth occurs whenever the maximum applied stress intensity is reduced.

(b) Such retardation is directly related to the reduction in maximum stress intensity.

(c) The length over which crack growth is retarded, i.e., the load interaction zone, is proportional to the plastic zone created by the maximum stress intensity.

(d) There is no retardation of growth if the current maximum stress creates a load interaction zone which extends out to or beyond a previously established interaction zone.

Based on these observations, Willenborg, et al, assumed that the load interaction effects were caused by variations in local stress intensity as the crack grows through the residual stress field produced by the overload(s).

Mathematically, the effective stress intensity for the Willenborg model is expressed in Reference 8 as:

$$K_{eff} = K^{\infty} - K_{RED} \tag{12}$$

$$K_{RED} = K_{max}^{OL} \left(1 - \frac{\Delta a}{z_{OL}}\right)^{1/2} - K_{max}^{\infty} \tag{13}$$

where K^{∞} is the applied stress intensity, K_{RED} is the additional stress intensity required to extend the current interaction zone to that created by the overload, Δa is the growth following the overload, and z_{OL} is the overload interaction zone size. The effective stress intensity range and stress ratio are computed as,

$$\Delta K_{eff} = K_{eff}^{max} - K_{eff}^{min} = K_{max}^{\infty} - K_{RED} - (K_{min}^{\infty} - K_{RED}) = \Delta K^{\infty} \tag{14}$$

$$R_{eff} = \frac{K_{eff}^{min}}{K_{eff}^{max}} = \frac{K_{min} - K_{RED}}{K_{max} - K_{RED}} \tag{15}$$

Thus, as noted in Reference 8, the Willenborg model predicts retardation by depressing the effective stress ratio below that remotely applied while leaving the stress intensity range intact. Since K_{RED} decreases as the crack grows through the overload interaction zone, the Willenborg model predicts that maximum retardation will occur just after the overload and that the growth rate will return to constant amplitude when the current interaction zone extends to the end of the overload interaction zone.

Due to the dependence of the Willenborg retardation on effective stress ratio, a crack growth rate relationship which interrelates the influence of stress ratio with stress intensity range must be used. This relationship is discussed in Paragraph 2. Overload ratio is defined as the ratio of overload stress intensity to maximum stress intensity, for the current load, and shut-off ratio as the overload ratio that prevents subsequent crack growth.

The Willenborg model predicts zero value for the maximum effective stress intensity, and thus no growth should occur when the overload ratio is two, that is, when K_{RED} equals K_{max}^{∞} in Equation (12). This can be shown by rewriting (12) for the maximum effective stress intensity as:

$$K_{max}^{eff} = K_{max}^{\infty} - \left[K_{max}^{OL} \left(1 - \frac{\Delta a}{z_{OL}}\right)^{1/2} - K_{max}^{\infty}\right] \tag{16}$$

where K_{max}^{OL} is the maximum overload stress intensity, Δa is growth following overload and z_{OL} is overload interaction zone size. Immediately following the overload, Δa is usually very close to zero so that K_{max}^{eff} is zero when K_{max}^{OL} is twice K_{max}.

Test results obtained by several investigators, References 10 through 13, show that the actual crack growth shut-off ratio can be greater than two. Gallagher and Hughes, Reference 9, generalized the Willenborg model to correct prediction of the overload to maximum load ratio required to produce cessation of crack growth. They proposed modifying Equation (16) so that for R=0:

$$K_{max}^{eff} = K_{max}^{\infty} - \Phi \left[K_{max}^{OL} \left(1 - \frac{\Delta a}{z_{OL}}\right)^{1/2} - K_{max}^{\infty}\right] \qquad (17)$$

For the condition of no growth, a=0, $K_{max}^{eff} = K_{maxTH}$ (threshold stress intensity) so that,

$$\Phi = \frac{1 - \dfrac{K_{maxTH}}{K_{max}^{\infty}}}{\dfrac{K_{max}^{OL}}{K_{max}^{\infty}} - 1} \qquad (18)$$

where the shut-off overload ratio ($K_{max}^{OL}/K_{max}^{\infty}$) must be obtained from tests for the given material, thickness, and stress ratio (underload condition).

Gallagher and Hughes used the generalized model quite successfully to predict the number of cycles required to return to constant amplitude growth rate following an overload in two steels having different yield strengths. Gallagher and Stalnaker, Reference 14, also used the generalized model to predict magnitude and trends of crack growth rate data generated under transport-wing simulation loading. The correlation of test and analysis was significantly improved over that of the original model.

The computer routine for the generalized Willenborg Model was extracted from the Air Force's CRACKS II computer program, Reference 15.

b. Compression Loads Analysis - There are two effects of compression loading. One effect is to increase the stress intensity amplitude of the cycle following compression; analysis of this stress ratio effect was discussed in Paragraph 2. The second, and frequently greater effect is to accelerate the crack growth caused by subsequent load cycles. In the program "Effects of Fighter Attack Spectrum on Crack Growth", Reference 16, modifications were made to the Willenborg model to better account for the accelerated growth following compression. The approach is to reduce the overload plastic zone size based on the minimum stress intensity applied prior to the overload:

$$z_{OL} = [(K^{\infty}_{max})^2 - \frac{3}{32} (K^{\infty}_{min})^2] \frac{\gamma}{2\pi} F^2_{ty} \qquad (19)$$

where K_{min} is the minimum stress intensity applied prior to the overload, F_{ty} is the material yield strength, and γ is the plane stress-plane strain coefficient; $\gamma = 1$ for plane stress and $= 1/2\sqrt{2}$ for plane strain. The multiplier 3/32 was empirically selected to correlate predictions with the compression loads test data presented in Reference 17.

The improvement in prediction accuracy obtained by including compression in spectrum loading analysis is shown in Figure 50. The test data was obtained from the program "Effects of Fighter Attack Spectrum on Crack Growth", and in this series of tests the ground load was varied to investigate the effects of compression. The earlier Willenborg model predicted small impact of this variation, the improved model more accurately predicted the acceleration observed in test.

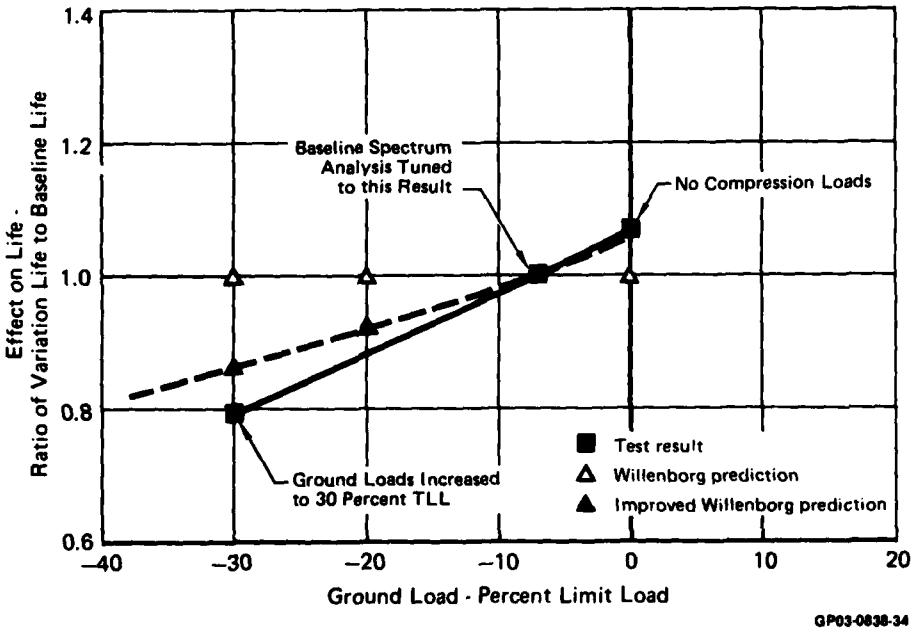

Figure 50. Improved Analysis of Compression Effects With Residual Stress Intensity Model

The complete environment-load interaction analysis routine is presented in the form of a user's manual in Appendix A.

5. MODEL CALIBRATION - The generalized Willenborg model was used to account for the effect of high loads in a spectrum to retard the crack growth produced by subsequent low load cycles. The Willenborg model accounts for this retardation by using two parameters; the overload interaction zone size, z_{OL}, and the shut-off overload ratio. The overload interaction zone size determines the amount of crack growth affected by an overload. Increasing the interaction zone size retards the predicted crack.

Values of both of these parameters were selected by correlation with results obtained with tests of center crack panels. The shut-off overload ratio selection was based on results of single overload tests reported in Reference 1. The overload interaction zone size was selected to correlate with the spectrum tests in dry air. The premise of the Willenborg model application in this program was that once parameter values were found which correlated spectrum analysis and test results, they could be used with confidence to predict the results of similar spectrum tests. The Willenborg model parameters used to make all spectrum crack growth predictions presented herein are shown in Table 7.

TABLE 7. WILLENBORG MODEL PARAMETERS USED FOR ANALYSIS

Material	ROOT2 (1)	OLMAX (2)
HP 9-4-0.30	0.100	3.50
300M	0.028	3.50

Notes:

(1) ROOT2 is an overload interaction zone size factor
The interaction zone size is defined as

$$Z_{OL} = \frac{ROOT2}{2\pi}\left\{\frac{K^{OL}_{max}}{F_{ty}}\right\}^2$$

(2) OLMAX is the overload ratio $\frac{K^{OL}_{max}}{K^{\infty}_{max}}$ which is determined from tests to shut-off subsequent crack growth

GP03-0838-35

a. Determination of Shut-off Ratio Using Overloads Tests - To determine the overload ratio which shuts-off subsequent constant amplitude crack growth, a series of single overload tests was performed and reported in Reference 1. The constant amplitude crack growth between overload applications was sufficient to preclude interactions of the overload effects.

The correlation of predicted and measured delay cycles for overload tests in both 300M and HP 9-4-.30 were used to select shut-off ratio of 3.5 for both steels. The correlation of measured and predicted delay cycles for HP 9-4-.30 tests in both air and salt water is shown in Figure 51. As shown, the shut-off ratio of 3.5 used for analysis of HP 9-4-.30 steel correlates well with the higher overload ratios but predicts much less delay than measured for lower overload ratios. This should result in conservative analysis when applied to spectrum loadings.

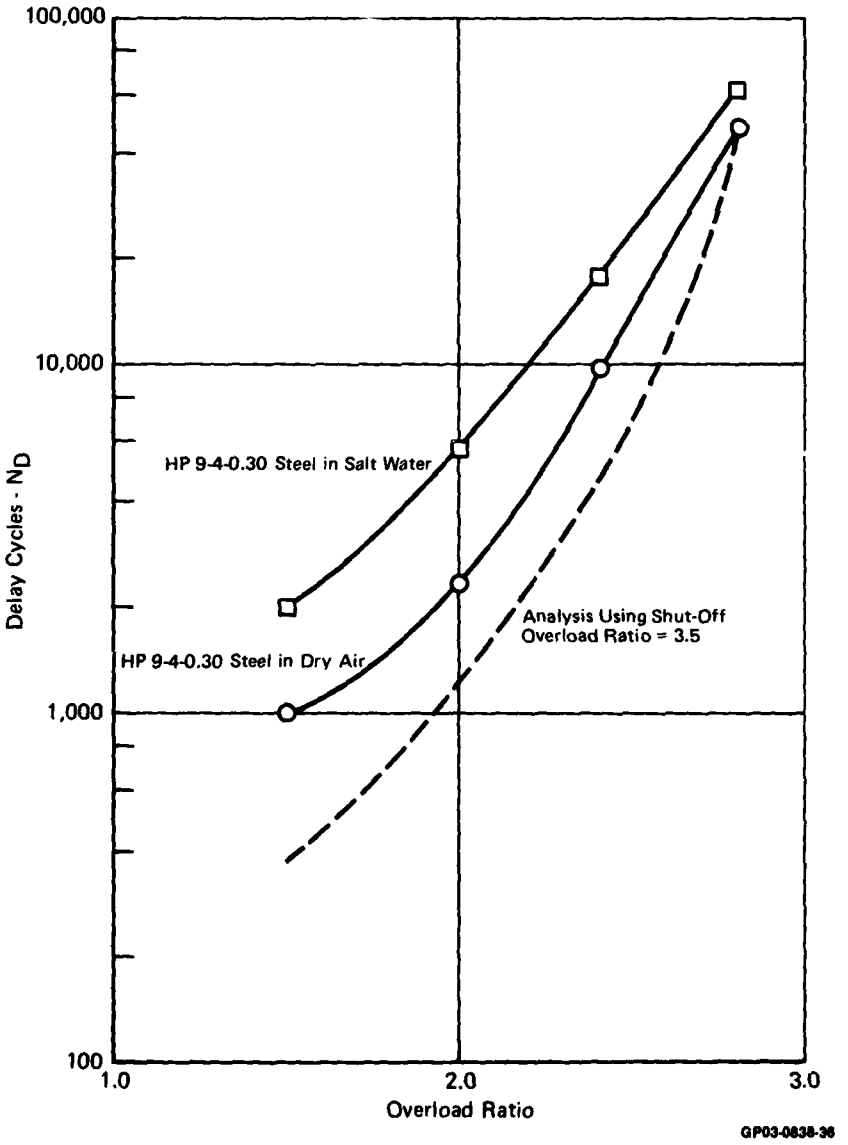

Figure 51. Effect of Overload Ratio on Delay in HP 0-4-0.30 Steel

b. Determination of Overload Interaction Zone Size Using Spectrum Test Data - The overload interaction zone size selected for the analyses was based on the retardation measured in spectrum tests in dry air. Once the shut-off ratios were determined from the overload test results, overload interaction zone sizes were determined by correlating analysis results with results obtained from the center crack panel spectrum tested in dry air to the accelerated stress history. Results of these correlations are discussed in Section VI.

6. SEMI-ELLIPTICAL SURFACE FLAW ANALYSIS

a. Stress Intensity Solutions - Stress intensity solutions for elliptic surface flaws were determined using a slice synthesis technique described in Reference 1. A comparison of these solutions with others is presented in Figure 52. In Figures B-1 and B-2 of Appendix B, the solutions are graphically summarized. Closed form expressions are presented in Appendix B which can be readily used in crack growth prediction computer routines.

The slice synthesis technique described in Appendix B was used to obtain stress intensity solutions. In this approach, the flaw is idealized as a series of center crack "slices" joined through the thickness with edge crack slices to account for the shear coupling between the center crack slices. The results presented in Figure 52 show good agreement with those obtained by Raju and Newman (References 18 and 19) using fine mesh finite element models which are the most detailed employed thus far in the analysis of the surface flaw. The slice synthesis solutions include the effects of finite width as well as thickness.

b. Prediction of Flaw Shape Change - The elliptic surface flaw requires analysis of the growth in both the surface and depth directions. Because the crack aspect ratio changes as the crack grows, the stress intensity relationships at the surface and depth change. It would be unnecessarily complicated in spectrum analysis to track the growth at both locations on a cycle-by-cycle basis. Instead, the changing aspect ratio can be predicted, based on constant amplitude loading analysis. With the aspect ratio known, growth at only one location needs to be tracked, simplifying spectrum crack growth prediction. With this data pre-determined, it is then possible to predict stress intensity relationships as a function of surface length, permitting the two dimensional growth to be characterized by surface growth alone.

Appendix B describes a routine used to predict growth, shape changes, and stress intensity factor corrections for a semi-elliptical surface flaw under constant amplitude loading. This routine was used to determine flaw shape changes and stress intensity factors for both constant amplitude and spectrum crack growth analyses. For spectrum crack growth analyses, the highest stress level in the spectrum and initial flaw size and shape were used for analysis.

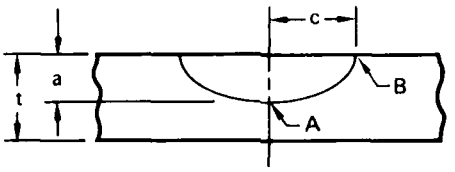

Semielliptical Surface Flaw a/2c = 0.1

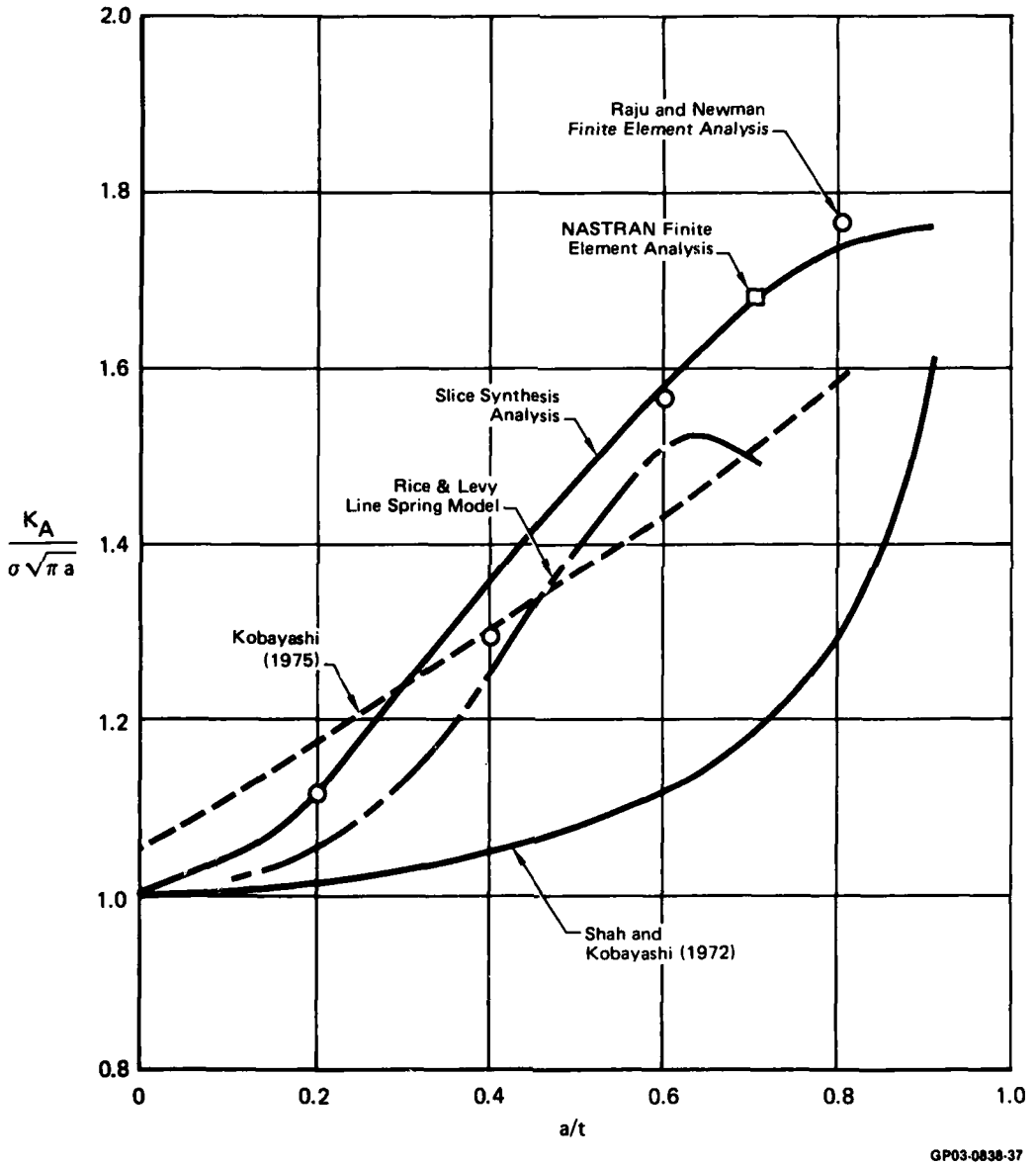

Figure 52. Comparison of Surface Flaw Stress Intensity Solutions

Computation of stress intensity factors at the crack depth and plate surface is based on results from the slice synthesis technique described in Reference 1. Stress intensity factors and crack growth both at flaw depth and surface are computed on a cycle-by-cycle basis. The following assumptions are inherent in this routine:

(1) Constant amplitude, R=0, sinusoidal loading is applied.

(2) Crack growth rates at plate surface and flaw depth are dependent on the K which is applied at those points.

(3) Crack growth rate versus K relationship obtained from a center cracked panel can be used to predict flaw growth at any point along the crack front.

(4) Stress intensity factor expressions are assumed valid until flaw depth exceeds 90% of plate thickness. Values of K_A and K_B at a/t=0.8 and a/t=0.9 are used for extrapolations beyond a/t=0.9.

(5) Fracture is assumed to occur when the stress intensity factor for the input constant amplitude stress level is equal to K_C.

c. Correlation of Analysis and Test - Figures 41 through 44 compare measured and predicted crack growth in the surface flaw specimens under constant amplitude loading. The test data was obtained from the constant amplitude elliptic flaw testing summarized in Section II. Agreement between test and prediction is good.

SECTION IV

LANDING GEAR STRESS HISTORY

The flight-by-flight stress history used in the verification test phase was derived for the axle-piston fork interface area on the F-4J main landing gear system. It was derived from the design fatigue load spectrum for F-4J landing gears and includes estimated times of stress application. The times required to attain the various landing gear loading conditions can vary widely, especially during braking where the pilot establishes load duration. The times computed were the maximum possible for each braking condition.

1. F-4J LANDING GEAR DESCRIPTION - The F-4J main landing gear (Figure 53) is a retractable, single wheel, pneudraulic strut mounted in the wing outboard of the fuselage between the main and rear spars. Retraction of the gear is accomplished by a hydraulic side brace actuator having one end attached to the gear and the other end mounted in the wing. Retraction of the actuator causes the gear to rotate about its trunnion axis inboard and upward into the wing cavity. While in the extended position, the actuator is converted into a rigid brace by means of an internal locking device. Hydraulic pressure unlocks the device prior to retraction.

Energy developed during landing is dissipated by metering fluid through a series of orifices in a tube. Vertical loads encountered during taxiing and ground handling are supported by air pressure. Fore and aft loads, side loads, and moments on the piston-fork applied at the wheel are taken out as a couple by the upper and lower strut main bearings. Torsional moments about the strut centerline are reacted by the torque arm lugs. Vertical loads are reacted by internal fluid and/or air pressure acting against an orifice fitting.

All the components discussed above except the axle-piston fork are fabricated from 4330V steel heat treated to 220-240 ksi ultimate tensile strength. The axle-piston fork is an integral unit fabricated from 300M steel heat treated to 280-300 ksi ultimate tensile strength.

The four areas of the F-4 main gear predicted to sustain the most fatigue damage are identified in Figure 54. The axle-piston fork interface area was predicted by crack growth analyses to have the most severe of the stress spectra considered. The axle-piston fork area of the F-4 main gear is the only area known to have produced cracks in service.

The main landing gear was selected as a representative highly fatigue critical component. A fatigue spectrum was derived for the axle-piston fork region based on design loads. This

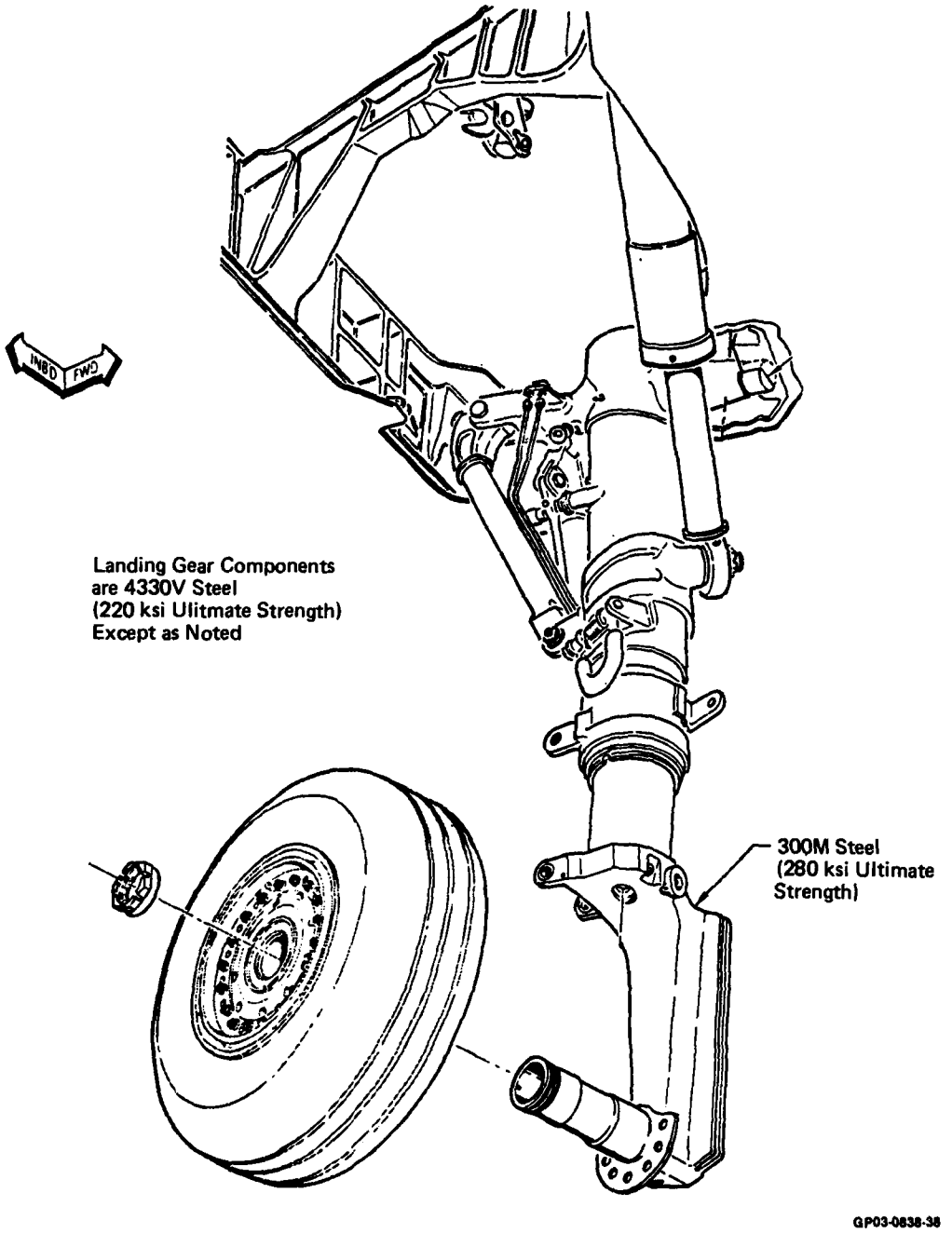

Figure 53. F-4J Main Landing Gear Selected as Study Base

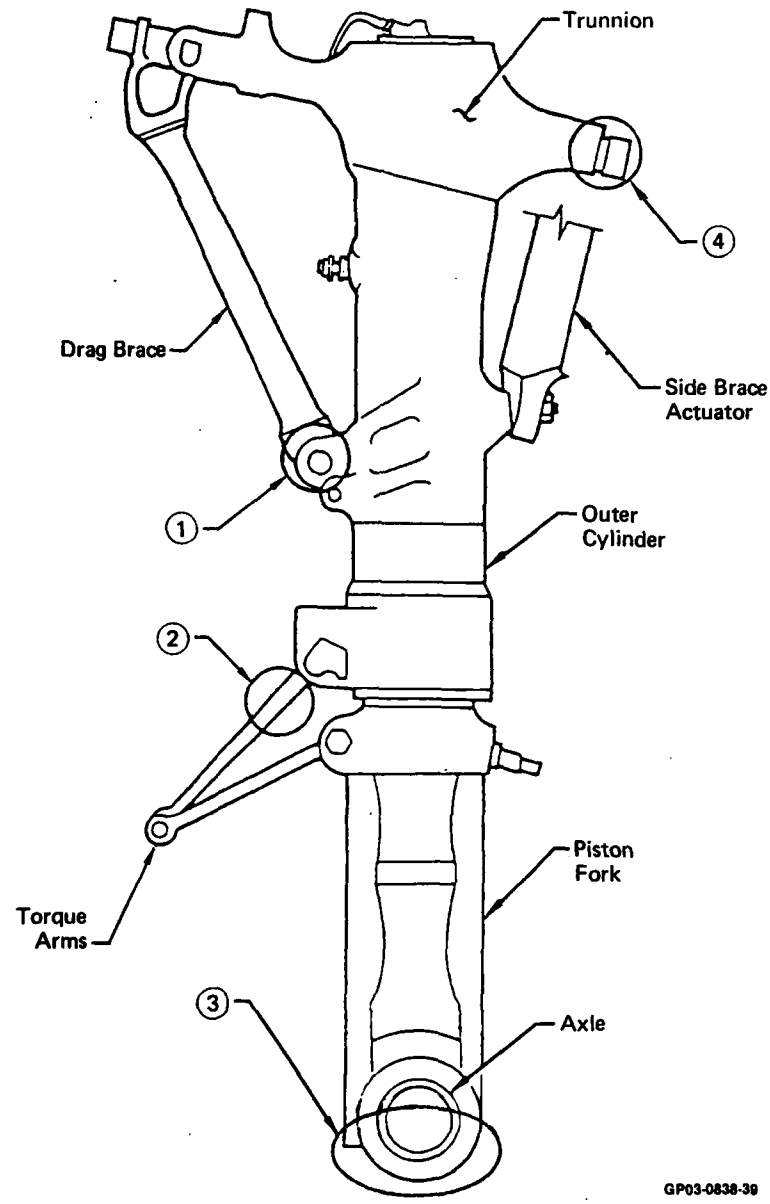

Figure 54. Areas of F-4J Main Gear Predicted to Sustain Greatest Fatigue Damage

region experiences representative loads in each of the major loading conditions for the gear; i.e., landing, braking, turning, etc., and is subject to most of the 1g sustained loads when the aircraft is parked.

2. LOADS SPECTRUM SUMMARY - The F-4J main landing gear were designed to the ultimate strength requirements of MIL-A-8862 and the repeated loads requirements of MIL-A-8866, except that the service life was conservatively selected as 4,000 takeoffs and landings rather than the 3,000 specified in MIL-A-8862. A scatter factor of two was used, resulting in 8,000 takeoffs and landings in the design fatigue spectrum.

The landing gear repeated load conditions for the F-4J main gear are presented in Table 8. These design conditions are in accordance with MIL-A-8866. Side drift landings as defined in MIL-A-8863 were included although not specifically required by MIL-A-8866. Landing condition 19 was separated into three conditions to better represent the highest loads in the spectrum. Landing conditions not defined in Table 8 are assumed to produce 1g stress levels. Turning conditions at design landing gross weight were predicted to produce negligible damage and were omitted. The remaining ground handling loads conditions were conservatively assumed to occur at design takeoff gross weight.

Loads for both ground handling and landing load conditions are summarized in Table 9. The sequence in which loads are applied to the landing gear are defined in Figure 55. The maximum stresses for the axle-piston fork interface area for each loading condition are summarized in Table 10. These stresses are based on design values and not on actual measurements on field hardware.

3. FLIGHT-BY-FLIGHT STRESS HISTORY DEVELOPMENT - The event sequence used to develop the flight stress history for the axle-piston fork interface is summarized in Table 11. This stress sequence is used for every flight in the spectrum, except that pivoting cycles are only applied every tenth flight and hard braking cycles before landing are applied every second flight.

A high stress level landing load cycle is applied every sixth or seventh flight in the spectrum. Stresses for each landing load condition were repeated uniformly throughout the spectrum, the two highest stress levels were placed at the middle and end of the spectrum. The resulting landing stress level distribution is shown in Figure 56.

A comparison of the flight-by-flight stress spectrum with the stresses for the repeated loads spectrum presented in Reference 1 is shown in Figure 57. The only significant differences occur at the largest stresses where the two highest landing stress levels are separately identified in the flight-by-flight history. The occurrences of each loading condition in the reduced design spectrum and the flight-by-flight spectrum are compared in Table 12.

TABLE 8. F-4J LANDING GEAR REPEATED LOAD CONDITIONS

Description	Condition	Sink Rate (ft/sec)	Roll Angle	Number of Cycles (1)	Parameters Defining Loads
Arrested Landing	1	15.6	0°-	330	Landing Weights Vary from 36,000 to 38,000 lb
	2	15.6	2°-Lo Gear	205	
	3	15.6	2°-Hi Gear	153	
	4	15.6	5°-Lo Gear	65	
	5	15.6	5°-Hi Gear	27	
	6	18.5	0°	122	
	7	18.5	2°-Lo Gear	76	
	8	18.5	2°-Hi Gear	53	
	9	18.5	5°-Lo Gear	25	
	10	18.5	5°-Hi Gear	15	
	11	20.4	0°	25	
	12	20.4	2°-Lo Gear	15	
	13	20.4	2°-Hi Gear	13	
	14	20.4	5°-Lo Gear	7	
	15	20.4	5°-Hi Gear	5	
	16	23.4	0°	11	
	17	22.8	2°-Lo Gear	9	
	18	22.4	2°-Hi Gear	11	
	19a	22.8	5°-Lo Gear	1	14° Pitch Angle
	19b	22.4	5°-Lo Gear	1	14° Pitch Angle
	19c	22.8	5°-Lo Gear	7	10.5 Pitch Angle
	20	22.8	5°-Hi Gear	8	
Side Drift Landing	21	–	–	10	Side Reaction = 0.8 Vertical Reaction
	22	–	–	10	Side Reaction = 0.6 Vertical Reaction

Ground Handling Load Conditions

Description	Condition	Aircraft Weight	Number of Cycles	Parameters Defining Loads
Turning	23a, 23b	Takeoff	15,000	Side Reaction = 0.4 Vertical Reaction
Hd Braking	24	Takeoff	12,800	Drag Reaction = 0.8 Vertical Reaction
Md Braking	25	Takeoff	32,000	Drag Reaction = 0.4 Vertical Reaction
Pivoting	26	Takeoff	800	Torque = 0.5 Limit Torque Load

Note: (1) Number of cycles represent 8,000 takeoffs and landings

GP03-0838-40

TABLE 9. F-4J MAIN LANDING GEAR DESIGN FATIGUE SPECTRUM

Description	Condition	Gear Stroke in. from Extended	P_V lb	P_D lb	P_S lb	M_{P_V} in.-lb
Arrested Landing	1	10.0	52,970	−21,190	− 2,500	–
	2	13.5	63,750	−23,370	− 4,370	–
	3	8.5	51,960	−14,700	3,000	–
	4	14.0	56,940	−20,990	− 6,320	–
	5	7.0	68,050	−20,280	2,000	–
	6	13.0	75,130	−30,540	4,500	–
	7	14.0	86,850	−35,700	− 8,280	–
	8	11.0	60,700	−17,320	6,500	–
	9	15.0	71,970	−30,490	−14,890	–
	10	8.5	71,590	−34,590	3,000	–
	11	13.0	96,790	−32,570	− 3,500	–
	12	14.0	101,420	−45,030	−13,370	–
	13	12.0	68,150	−32,330	8,000	–
	14	15.0	82,950	−39,630	−22,600	–
	15	9.5	78,600	−41,810	5,500	–
	16	13.0	119,760	−43,220	− 5,000	–
	17	14.0	119,860	−48,450	−16,000	–
	18	12.0	85,420	−40,490	10,000	–
	19a	15.0	103,690	−53,780	−32,280	
	19b	15.0	98,300	−51,360	−30,760	–
	19c	15.0	105,170	−44,290	−25,020	–
	20	10.0	89,050	−51,300	10,000	–
Side Drift Landing	21	5.0	49,810	−4,613	−40,020	–
	22	5.0	49,240	−4,560	−29,670	–
Turning	23a	16.85	30,370	−2,810	−12,250	–
	23b	16.85	18,170	−1,680	7,310	–
Hard Braking	24	16.85	23,000	15,190	0	–
Medium Braking	25	16.85	23,950	7,070	0	–
Pivoting	26	16.85	24,890	−2,305	0	42,000

Notes: 1 All loads are in Strut Coordinate System. P_V = vertical load, P_D = drag load, P_S = side load, M_{P_V} = moment about vertical load axis

2 Parking load at takeoff weight is P_V = 24,500 lb, at landing weight, P_V = 15,470 lb

GP03-0838-41

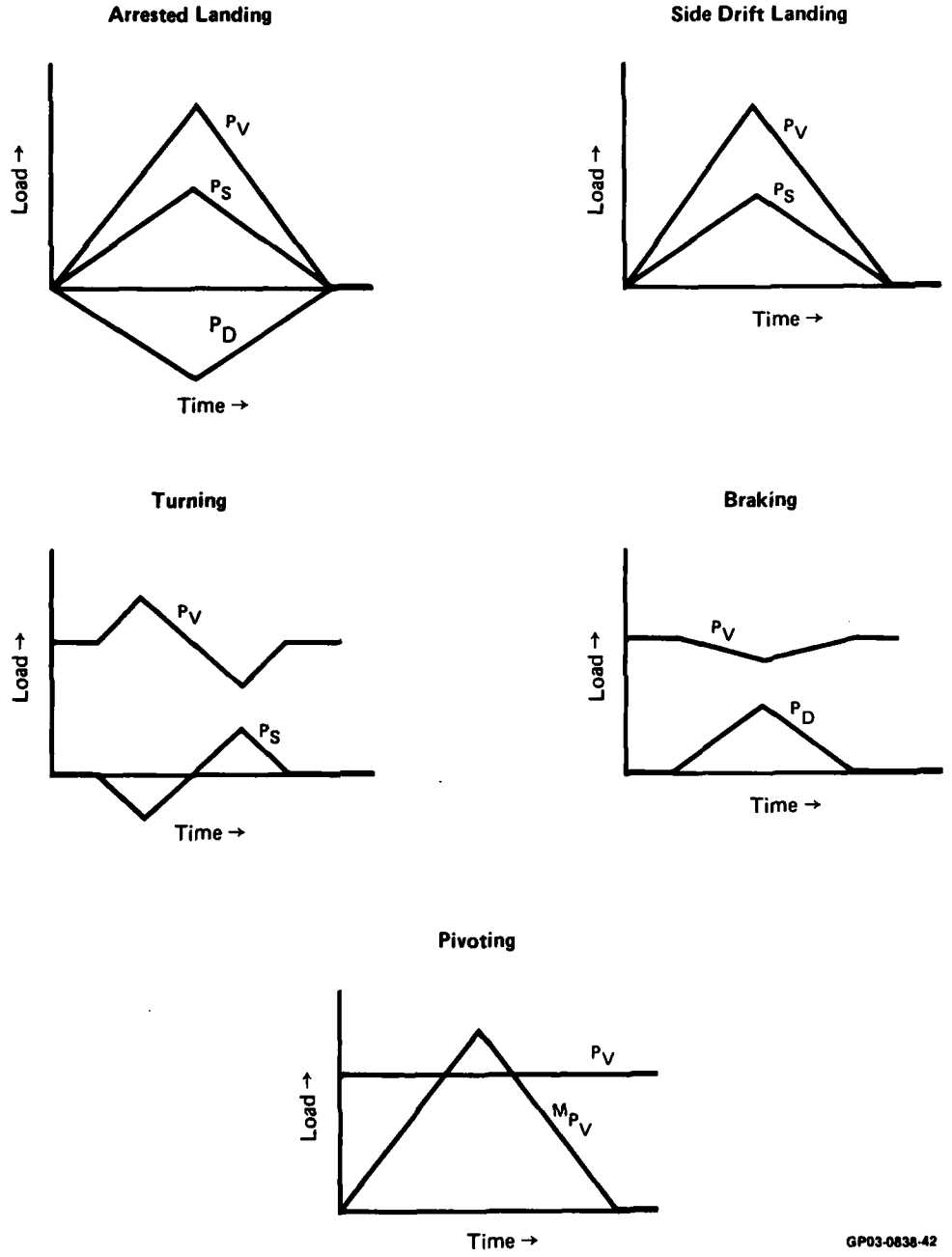

Figure 55. Loading Diagrams for F-4J Main Gear Fatigue Spectrum

TABLE 10. STRESS SPECTRUM FOR AXLE-PISTON FORK AREA

Description	Condition	Stress (Max/Min)	Percent of Maximum Stress	Number of Cycles (1)
Arrested Landing	1	93.8/0	32.5/0	330
	2	116.6/0	40.4/0	205
	3	69.9/0	24.2/0	153
	4	94.3/0	39.1/0	65
	5	65.2/0	34.3/0	27
	6	136.7/0	47.4/0	122
	7	169.1/0	58.7/0	76
	8	7.14/0	24.8/0	53
	9	169.2/0	58.7/0	25
	10	108.0/0	37.5/0	15
	11	164.5/0	57.1/0	25
	12	212.6/0	73.7/0	15
	13	84.7/0	29.4/0	13
	14	217.1/0	75.3/0	7
	15	113.6/0	39.4/0	5
	16	207.3/0	71.9/0	11
	17	249.2/0	86.4/0	9
	18	106.2/0	36.8/0	11
	19a	288.3/0	100.0/0	1
	19b	274.1/0	95.1/0	1
	19c	258.9/0	89.8/0	7
	20	118.9/0	41.2/0	8
Side Drift Landing	21	216.7/0	75.2/0	10
	22	0.0/–35	0.0/–12.1	10
Turning	23	8.85/–8.1	30.7/–2.8	7,500
Hd Braking	24	41.1/36.6	14.3/12.7	12,800
Md Braking	25	37.2/36.6	12.9/12.7	32,000
Pivoting	26	37.2/36.6	12.9/12.7	800

Note: (1) Number of cycles represent 8,000 takeoffs and landings

GP03-0838-43

TABLE 11. FLIGHT STRESS SEQUENCE FOR AXLE-PISTON FORK AREA

Description	Condition	Cycles per 8,000 Flights	Cycles per Flight
Pivoting	26	800	(1)
Turning	23	8,000	1
Hard Braking	24	4,000	(2)
Medium Braking	25	16,000	2
Landing	1 - 22	8,300	(3)
Hard Braking	24	8,000	1
Medium Braking	25	16,000	2

Notes:
(1) Pivoting cycles added every tenth flight
(2) Hard braking cycles added every second flight
(3) 1,204 landing cycles are distributed evenly throughout the 8,000 flight spectrum

GP03-0838-44

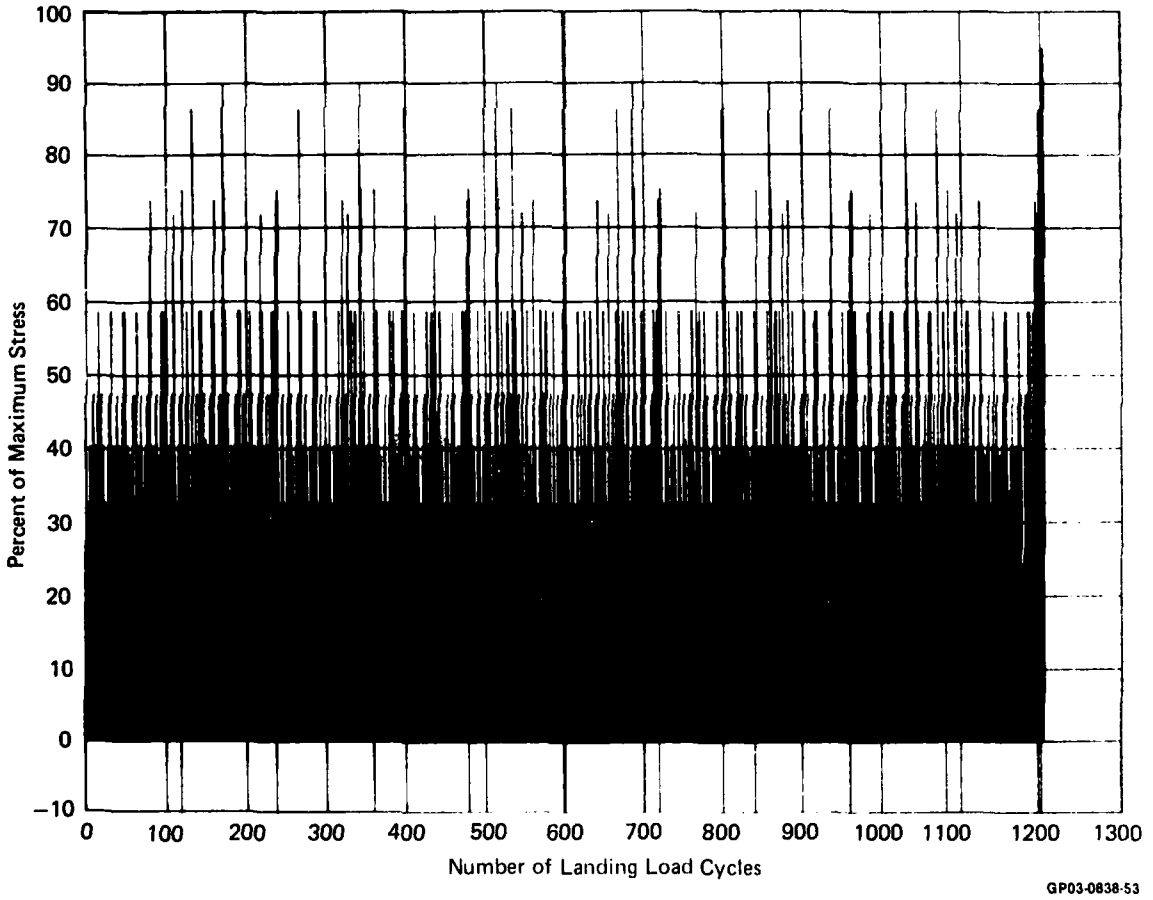

GP03-0838-53

Figure 56. Distribution of Landing Stress Cycles in Stress History

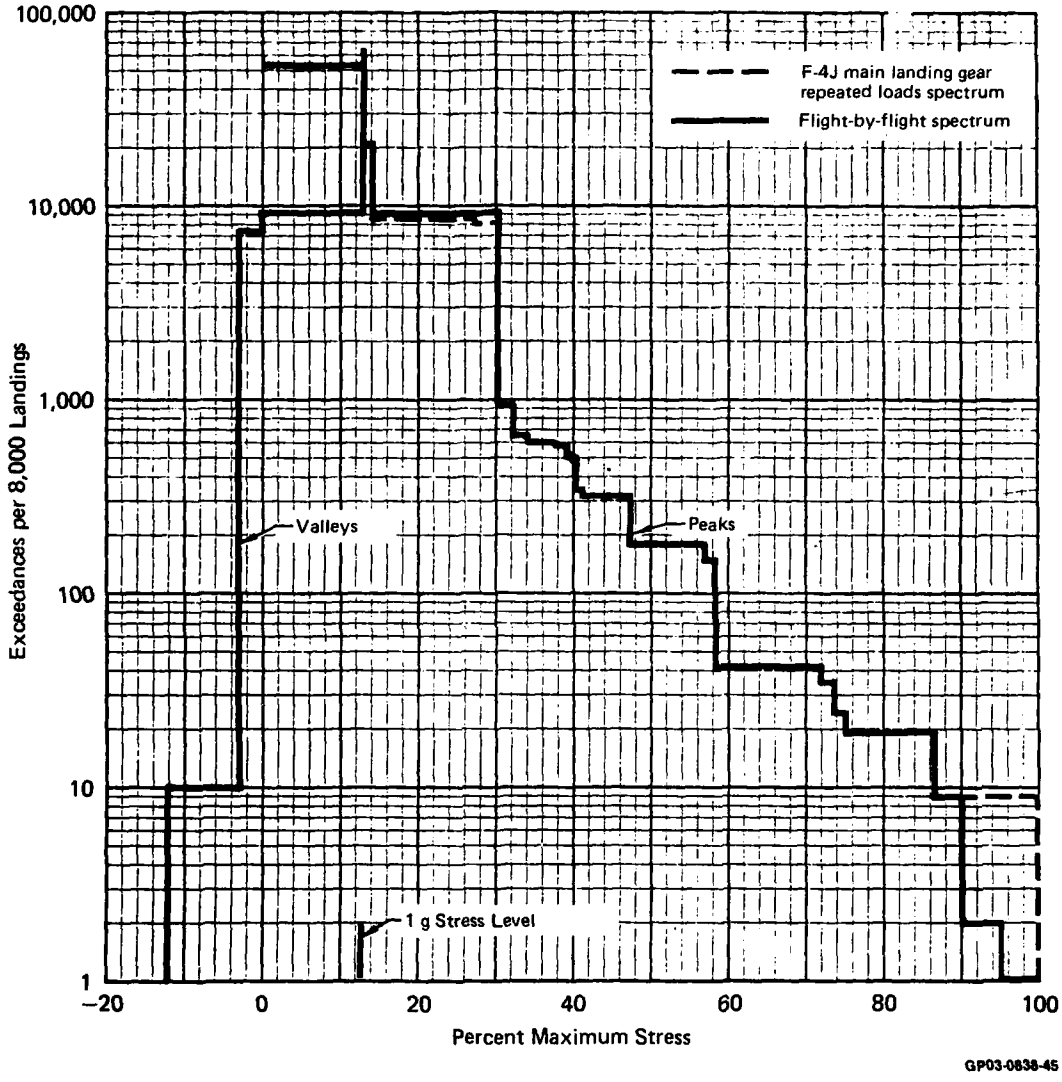

Figure 57. Comparison of Flight-by-Flight Spectrum and Design Spectrum for F-4J Main Landing Gear

TABLE 12. COMPARISON OF DESIGN AND FLIGHT-BY-FLIGHT STRESS SPECTRA F-4J MAIN LANDING GEAR AXLE-PISTON FORK SPECTRA 8,000 TAKEOFF AND LANDINGS

Description	Condition	Percent of Spectrum Maximum Stress	(1) Design Number of Cycles	(2) Flight-by-Flight Number of Cycles
Arrested Landings	1	32.5/0	330	330
	2	40.5/0	205	205
	3	24.2/0	153	153
	4	39.1/0	65	65
	5	34.3/0	27	27
	6	47.4/0	122	122
	7	58.7/0	76	76
	8	24.8/0	53	53
	9	58.7/0	25	25
	10	37.5/0	15	15
	11	57.1/0	25	25
	12	73.7/0	15	15
	13	29.4/0	13	13
	14	75.3/0	7	7
	15	39.4/0	5	5
	16	71.9/0	11	11
	17	86.4/0	9	9
	18	36.8/0	11	11
	19a	100.0/0	9	1
	19b	95.1/0	–	1
	19c	89.8/0	–	7
	20	41.2/0	8	8
Side Drift Landings	21	75.2/0	10	10
	22	0.0/–12.1	10	10
Turning	23	30.7 – 2.8	7,500	8,000
Hd Braking	24	14.3/12.7	12,800	12,000
Md Braking	25	12.9/12.7	32,000	32,000
Pivoting	26	12.9/12.7	800	800

GP03-0838-46

Notes: (1) MCAIR design repeated loads spectrum
(2) Flight-by-flight spectrum

4. TIMES FOR STRESS APPLICATION - The spectrum tests include simulation of the times of stress application as well as the value of stresses. Therefore, an evaluation of the times required to attain the landing gear loading conditions was performed. Load application times vary widely, especially during braking where the pilot dictates the duration of the load. The times for stress application computed herein are the maximum possible times for each braking condition. Two stress-time histories were created - one having the greatest possible duration of stress application, the other having the same stress levels applied as quickly as possible without sustained loads. The time estimates are design estimates and not based on actual measurements on field hardware.

Pivoting - Pivoting was assumed to occur by hard braking of one main gear, simultaneously turning the nose gear such that no drag force is developed on the nose gear. The turning torque due to the locked wheel is

$$T = \mu V_{MG} L_M$$

where μ is the coefficient of friction (specified to be 0.8 for hard braking).

V_{MG} is the main gear vertical load (computed to be 0.44 times the aircraft weight, W) and L_M is the distance between the main gear tire and the aircraft centerline (8.94 feet).

$$T = (0.8)(0.44W)(8.94) = 3.15W, \text{ ft-lb}$$

The rotational acceleration of the aircraft is

$$\dot{\omega} = T/I$$

where ω is the yaw rotational rate

and I is the yaw moment of inertia

$$I = \frac{W}{g} \rho^2$$

where g is gravitational acceleration (32.2 ft/sec^2)

and ρ is the yaw radius of gyration (computed to be 10.74 ft)

$$\dot{\omega} = \frac{(3.15W)(32.2)}{(10.74)^2 W} = 0.879 \text{ rad/sec}^2$$

The relationship of velocities and accelerations are

$$v = R\omega$$

$$a = R\omega^2$$

hence $\omega = a/v$

where $a = F_S/M$

F_S is the side force acting through the aircraft mass centroid = μW

where μ is specified to be 0.4

$M = W/g$

hence $a = \mu g$

and v is the velocity (assumed to be 15 knots, 25.32 ft/sec)

thus $\omega = (0.4)(32.2)/(25.32) = 0.509$ rad/sec.

Assuming that angular acceleration increases linearly with time to the maximum angular velocity, the time required to reach this velocity is

$$t = \omega/\dot{\omega} = (.509)/(0.879) = 0.58 \text{ sec.}$$

Turning - Turning was assumed to occur by turning the nose wheel with no braking of either main gear. It was assumed that the aircraft yaws such that its centerline is tangent to the path of motion at the center of gravity. It was assumed that a constant velocity turn is made and that the turning radius varies such that the total side force linearly increases and decreases with time to and from its maximum value. The turning torque provided by the nose gear is:

$$T = \mu V_{NG} L_N$$

where μ is the coefficient of friction (specified to be 0.4 for side force)

V_{NG} is the nose gear vertical load (computed to be 0.12 times the aircraft weight, W)

and L_N is the distance between the nose gear tire and the centerline of the main gear (20.4 ft).

$T = (0.4)(0.12W)(20.4) = 0.979W$ ft-lbs

The rotational acceleration of the aircraft is

$$\dot{\omega} = T/I$$

where ω is the yaw rotation rate and I is the yaw moment of inertia $(3.58W)$ ft-lb-sec^2)

$\dot{\omega} = (0.979W)(3.58W) = 0.273$ rad/sec^2

$\omega = a/v$

where $a = \mu g = (0.4)(32.2) = 12.88$ ft/sec^2

and v = is the velocity (again assumed to be 15 knots, 25.32 ft/sec^2)

$\omega = (12.88)/25.32 = 0.509$ ft/sec.

The time required to reach this maximum angular velocity is

$t = \omega/\dot{\omega} = 0.509/0.273 = 1.86$ sec.

Hard and Medium Braking - Braking times can vary from very short pulses to the time required to stop the aircraft during high speed landing or a rejected takeoff. Assuming the effect of aerodynamic drag is small in comparison to braking forces, the deceleration is computed as:

$$\ddot{x} = \frac{2\mu V_{MG}}{W} g$$

where x is the stopping distance

μ is the coefficient of friction (specified to be 0.4 for medium braking and 0.8 for hard braking)

V_{MG} is the main gear vertical load (0.44 times the aircraft weight, W)

g is gravitational acceleration

W is aircraft weight

The total main gear load is

$2V_G = 0.88W$

Hence the deceleration rate is:

$\ddot{x} = 0.88\mu g$ ft/sec^2

The time to stop, t, depends on the initial velocity, which can be as high as 185 knots, (312.2 ft/sec) for an aborted takeoff.

$t = v/\ddot{x} = 312.2/(0.88\mu g) = 11.02/\mu$ sec.

Stopping time for medium braking is 27.6 sec.

Stopping time for hard braking is 13.8 sec.

The time to apply or remove braking loads was assumed to be one second.

AD-A093 803 MCDONNELL AIRCRAFT CO ST LOUIS MO F/G 11/6
ENVIRONMENT-LOAD INTERACTION EFFECTS ON CRACK GROWTH IN LANDING--ETC(U)
OCT 80 C R SAFF N62269-79-C-0275
UNCLASSIFIED NADC-79095-60 NL

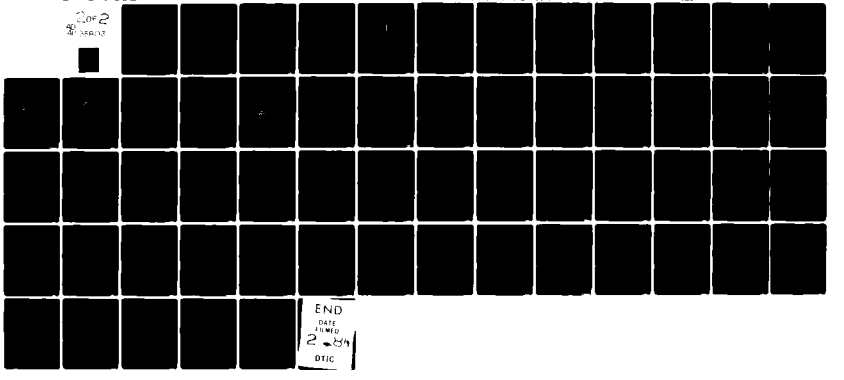

Landing - The time required to reach the peak vertical load for the main gear was found from drop test data to be approximately 0.18 sec. This value is used for all landing loads.

A sustained stress representing a 1g static loading at take-off gross weight was arbitrarily added in equal 0.33 second intervals between loading events. The resulting stress-time profiles used for load conditions are summarized in Figure 58.

5. CYCLE-BY-CYCLE STRESS SPECTRA - The stress-time profiles of Figure 58 were assembled according to the event sequence of Table 11 to produce a cycle-by-cycle stress history. The resulting stress-time history for the landing gear is made up of flight histories of various lengths, depending on which events are included. The stress levels and times for load application for the longest flight are presented in Table 13. Time increments represent the time required to obtain the given load from the previous load level. When successive loads have equal magnitudes, the time increment represents sustained load duration.

The stress-time history for the longest flight is shown in Figure 59; that for the shortest flight is shown in Figure 60. The total time required to apply 8,000 flights of this spectrum including sustained loads is about 338 hours.

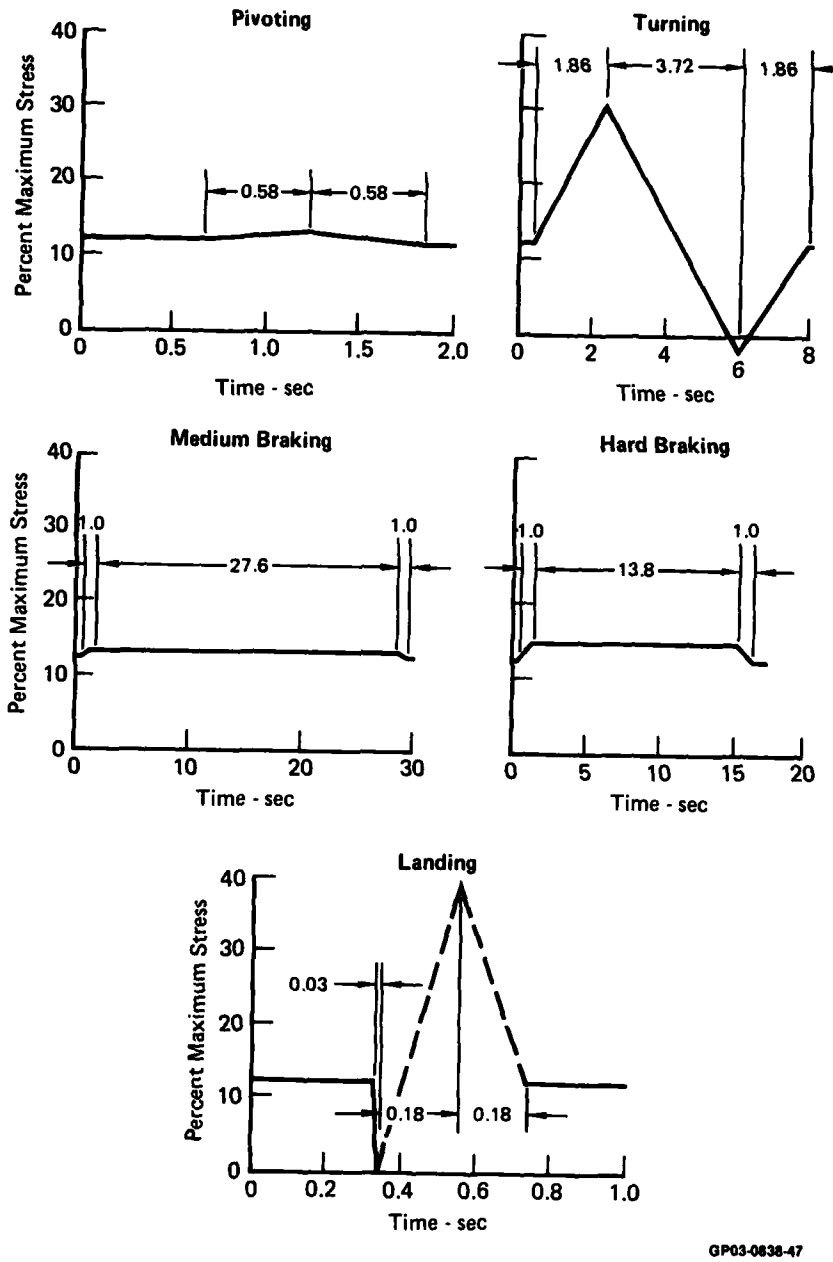

Figure 58. Stress-Time Profiles for Each Loading Condition

TABLE 13. SUMMARY OF STRESS-TIME HISTORY FOR BASELINE FLIGHT

Stress Number	Delta Time	Percent of Maximum Stress	Condition	Description
1	0.33	12.7	26	Take-off
2	0.58	12.9	26	Pivoting
3	0.58	12.7	26	
4	0.33	12.7	23	Turning
5	1.86	30.7	23	
6	3.72	−2.8	23	
7	1.86	12.7	23	
8	0.33	12.7	24	Hard
9	1.00	14.3	24	Braking
10	13.80	14.3	24	
11	1.00	12.7	24	
12	0.33	12.7	25	Medium
13	1.00	12.9	25	Braking
14	27.60	12.9	25	
15	1.00	12.7	25	
16	0.33	12.7	25	
17	1.00	12.9	25	
18	27.60	12.9	25	
19	1.00	12.7	25	
20	0.33	12.7	1 - 22	Landing (2)
21	0.03	0.	1 - 22	
22	0.18	12.7	1 - 22	
23	0.18	12.7	1 - 22	
24	0.33	12.7	24	Hard
25	1.00	14.3	24	Braking
26	13.80	14.3	24	
27	1.00	12.7	24	
28	0.33	12.7	25	Medium
29	1.00	12.9	25	Braking
30	27.60	12.9	25	
31	1.00	12.7	25	
32	0.33	12.7	25	
33	1.00	12.9	25	
34	27.60	12.9	25	
35	1.00	12.7	25	Park

Notes: 1 Stress numbers 1 - 35 are repeated 8,000 times to represent two design lifetimes

(2) Stress level 22 is replaced by a higher landing stress in every sixth or seventh flight

GP03-0838-48

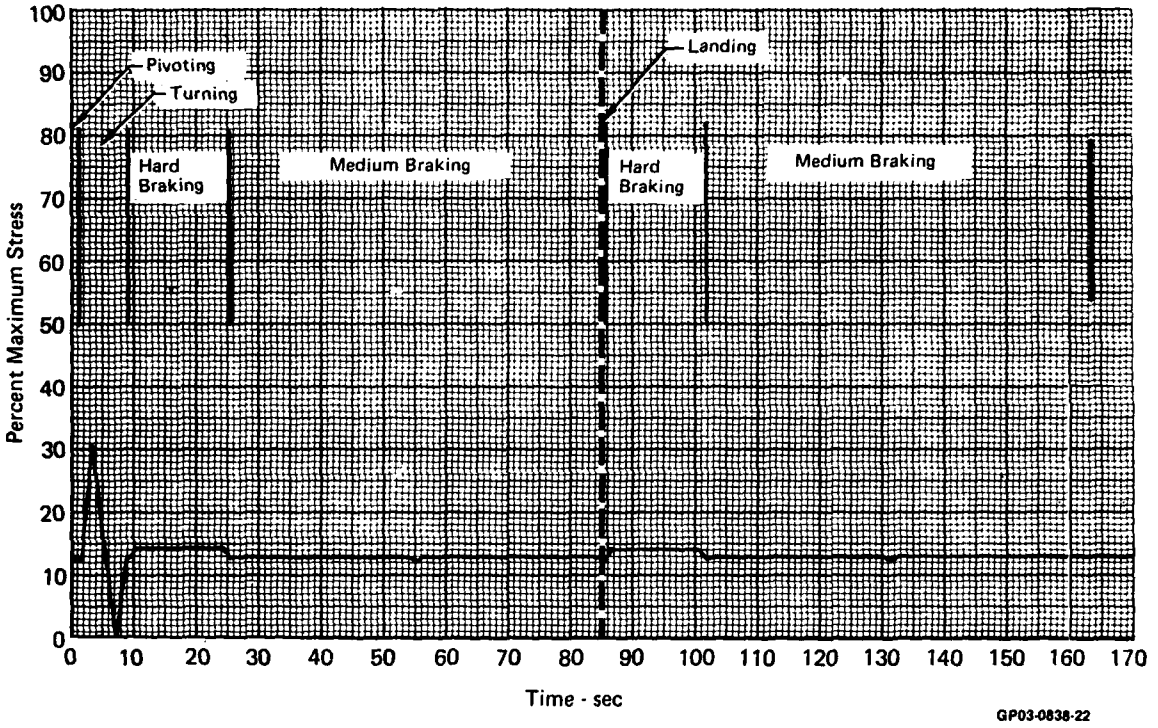

Figure 59. Real Time Stress History for Longest Flight

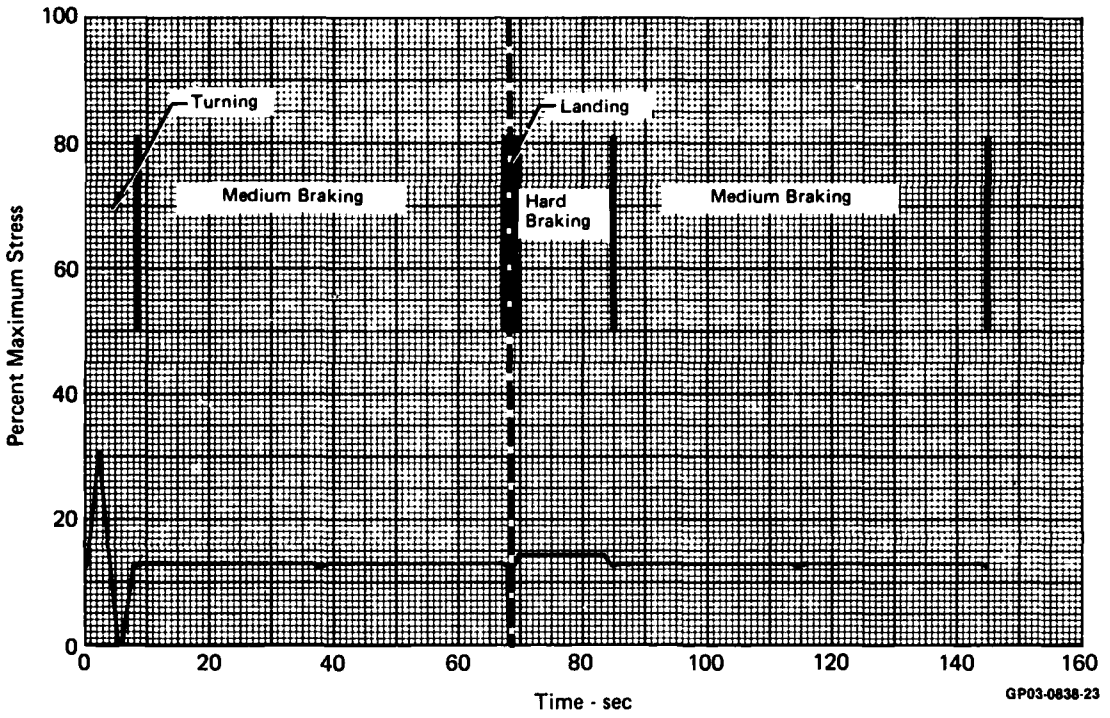

Figure 60. Real Time Stress History for Shortest Flight

SECTION V

VERIFICATION TEST PLAN

1. TEST PROGRAM SUMMARY - The verification test plan is summarized in Table 14. This test program was performed to provide the data required to verify the crack growth prediction methodology. Spectrum fatigue tests on center cracked and surface flawed panels were performed in dry air and synthetic sea water using both accelerated and sustained load stress histories. Five tests in each steel are divided into three series.

- o Test Series 1 - One surface flawed panel in the dry air environment using the accelerated stress history to evaluate predictions of surface flaw growth in an inert environment.
- o Test Series 2 - One center cracked panel and one surface flawed panel in sea water using the accelerated stress history to evaluate the predictions of crack growth in an aggressive environment minimizing sustained load effects.
- o Test Series 3 - One center cracked panel and one surface flawed panel in sea water using the sustained load stress history to evaluate predictions of crack growth under maximum conditions of sustained load and aggressive environment.

TABLE 14. VERIFICATION TEST PROGRAM

Specimen Number	Specimen Type	Environment	Load Frequency (cps)	Objective
1	Surface Flawed Panel	<10% RH Air	∿ 10	Evaluate crack growth in an inert environment
2 3	Center Cracked Panel Surface Flawed Panel	Alternate Immersion in Sea Water	∿ 10 ∿ 10	Evaluate crack growth in an aggressive environment
4 5	Center Cracked Panel Surface Flawed Panel	↓	∿ 0.1 ∿ 0.1	Evaluate crack growth with sustained load in an agressive environment

Test series is identical for each material

GP03-0838-49

2. TEST SPECIMENS AND TEST CONDITIONS

a. Test Specimens - The center cracked panel and surface flawed panel specimens, Figures 1 and 2, were used in this test program. The reduced sections in the surface flawed panel specimens were required in order to properly simulate the stresses experienced in landing gear components and maintain load levels within the capacity of available fatigue test equipment. For both steel alloys, there was minimal specimen width effect on predicted critical flaw sizes, or in the predicted crack growth rates at crack lengths near those critical flaw sizes.

b. Spectrum Stress Levels - The spectrum used in the testing is defined in Section IV. The cycle-by-cycle stress history was derived for the axle-piston fork interface of the F-4J main landing gear system. In order to achieve the desired life (8,000 take-offs and landings in the dry air environment), consistent stress levels had to be selected. The maximum spectrum stress level used in the Air Force landing gear program was approximately 85% of the ultimate strength of the HP 9-4-.30 material. This percentage is representative of the maximum stress level in a landing gear component. To permit direct comparison between the crack growth rates of Air Force and Navy landing gear spectra, as well as maintaining direct comparison between the materials, it is desirable to use the same maximum stress in both steel materials. Therefore 185 ksi was selected as the maximum spectrum stress level for surface flawed panels in both steels.

Stress levels and precrack lengths for the center cracked panels were selected to result in 8,000 take-offs and landings in the dry air environment. The combination of precrack length and stress levels provided initial stress intensity factor levels similar to those of the surface flawed panels.

c. Initial Flaw Sizes - Initial flaw sizes were selected to produce the maximum possible crack growth in 8,000 spectrum landings. Predicted crack growth under the Navy landing gear spectrum (Section IV) was very small because of the small magnitude of frequently applied loads and the infrequent application of the highest loads. In order to obtain the greatest possible growth in 8,000 spectrum landings, initial flaw sizes were selected which result in failure at the end of the 8,000 landing spectrum. Because of the difference in critical stress intensity factor, K_C, between 300M and HP 9-4-.30 steel, the same initial flaw size could not be used for both materials. In fact, initial flaw sizes used for HP 9-4-.30 steel were greater than critical flaw sizes in 300M steel. In center cracked panels, initial flaw lengths were 1.23 inches in 300M and 2.52 inches in HP 9-4-.30 steel.

In surface flawed panels initial flaw geometries were developed from small semi-circular EDM notches, 0.05 inch long by 0.025 inch deep. Semi-circular flaw geometries were used because surface flaws under uniform tensile stress tend to grow in a roughly semi-circular shape. Crack growth in the depth is accompanied by growth at the surface, allowing surface measurements to characterize the overall growth of the flaw. EDM notch and initial flaw geometries used for verification tests are shown in Figure 61.

3. PRECRACKING PROCEDURES - An Electrical Discharge Machined (EDM) notch of size and shape expected to produce the desired initial flaw was introduced on the specimen surface. Specimens were then precracked to obtain the desired surface length. The target EDM and precrack sizes and shapes are indicated in Figure 61. The precracking stress levels were 100 ksi.

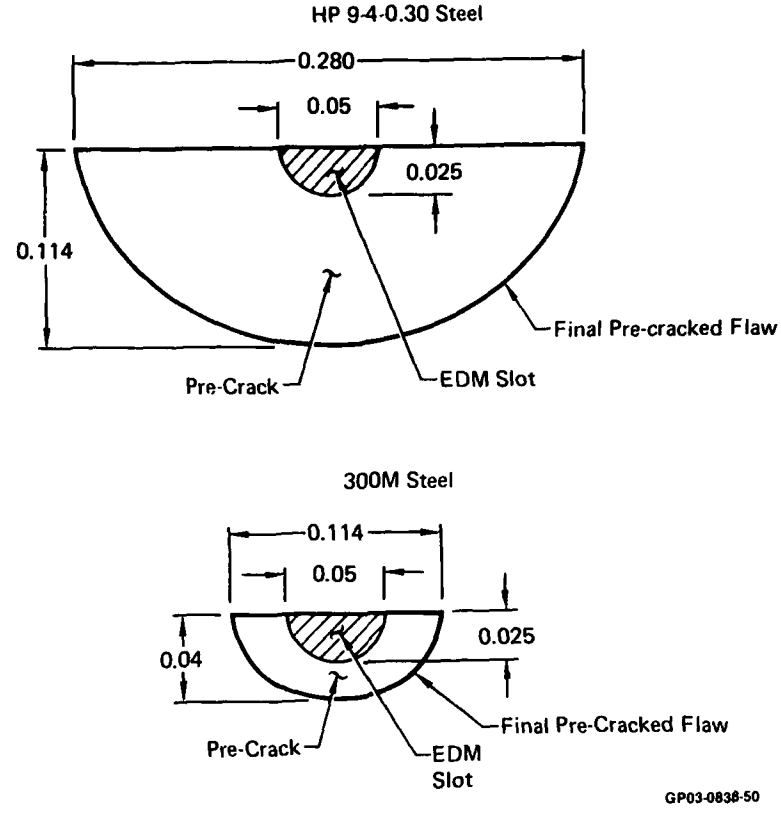

Figure 61. Development of Initial Flaws

4. TEST PROCEDURES, CRACK GROWTH MONITORING, INSTRUMENTATION, AND ENVIRONMENTAL CONTROL - Cyclic testing was performed in a Materials Testing System (MTS) test system. The specimen was loaded through self-aligning hydraulic grips. The load spectrum application was controlled through a mini-computer; the time-sequence load spectrum was defined by the load levels and the time point at which each load was to be applied. A haversine wave shape was used between consecutive loads. Sustained load was defined by two consecutive loads of equal magnitude applied at the beginning and end of the sustained load period.

During the testing, crack lengths were optically monitored using a linear displacement transducer with a 30X microscope. Crack growth measurements were made after every 100 landings for the first 2,000 landings and after every 500 landings thereafter.

The chambers used to maintain environmental conditions are shown in Figures 3 and 4, Pages 8 and 9. The alternate immersion cycle was 10 minutes immersion followed by 50 minutes of blown air drying. Low humidity air was obtained using silica jell dessicant contained in a sealed mylar case enclosing the crack (Figure 3).

SECTION VI

COMPARISON OF SPECTRUM LIFE PREDICTIONS AND TEST RESULTS

1. SUMMARY - The crack growth algorithms described in Section III were calibrated to correlate with the spectrum crack growth data obtained from center crack panels tested in dry air. The calibrated model was then used to predict the crack growth in the center crack panels tested to both the accelerated and real time stress histories in the alternate immersion environment. The real time stress history is the history described in Section IV including sustained stress times. The accelerated stress history uses the same stress levels and sequence but includes no sustained stress periods. In the accelerated stress history, stress levels were applied at about 10 cps. Predictions were based on cycle-by-cycle analyses of the stress spectrum of the F-4J main landing gear axle-piston fork interface. This spectrum involves small peak stresses sustained for up to 27 seconds, as well as high peak stresses rapidly applied. Good correlation was obtained between the predicted and measured growth behavior in the aggressive (alternate immersion in sea water) environment.

The calibrated model was also used to predict crack growth for surface flawed panel tests. Verification tests included application of the stress history both in real time and at accelerated rates to specimens containing surface flaws. Tests were conducted both in lab air and in alternate immersion in sea water. Verification test results confirm the ability of the model to predict the growth of both center cracks and semi-elliptical surface flaws under spectrum loading both in inert and aggressive environments. The relative severity of Navy and Air Force landing gear spectra on crack growth was investigated.

2. CENTER CRACK PANEL SPECIMEN RESULTS

a. Model Calibration - Model calibration is discussed in greater detail in Section III. The load-environment interaction algorithms were calibrated through correlation with constant amplitude test results from the development test program. The Willenborg spectrum crack growth analysis parameters were determined from single overloads tests in dry air and sea water and through correlation with the results of tests of center cracked panels tested to the accelerated stress history in the dry air environment. The load interaction zone size parameter was used to provide correlation with center cracked panel results.

b. Spectrum Crack Growth Analyses And Test Results - Spectrum crack growth was predicted for center crack panels in the alternate immersion environment under the accelerated and sustained load stress histories using the calibrated crack growth algorithms. Table 15 summarizes crack growth life results for all verification tests. Figure 62 summarizes crack growth life results for the center cracked panels. Results of analyses and

tests in each material are presented in Figures 63 and 64. Correlation with dry air test results is good because the model was calibrated to correlate with those results.

TABLE 15. SUMMARY OF SPECTRUM TEST LIVES
Results of Verification Tests

Specimen Type	Environment	Load Frequency (cps)	Life-Landings to Failure			
			300M (1)		HP 9-4-0.30 (2)	
			Test	Analysis	Test	Analysis
Center Cracked Panel	< 10% R H Air	10	12,100	11,780	14,500	10,870
Surface Flawed Panel		10	11,780	11,780	11,300	11,780
Center Cracked Panel	Alternate Immersion in Sea Water	10	3,870	11,780	8,500	10,870
Surface Flawed Panel		10	11,000	11,200	9,370	11,780
Center Cracked Panel		0.1	3,500	3,780	4,380	10,870
Surface Flawed Panel		0.1	4,000	3,780	7,990	11,780

GP03-0838-82

Notes:

(1) Initial flaw lengths in 300M steel were 1.23 in. for center cracked panels (48 ksi maximum stress) and approximately 0.1145 in. in surface flawed panels (185 ksi maximum stress)

(2) Initial flaw lengths in HP 9-4-0.30 steel were 2.52 in. for center cracked panel (48 ksi maximum stress) and approximately 0.278 in. in surface flawed panels (185 ksi maximum stress).

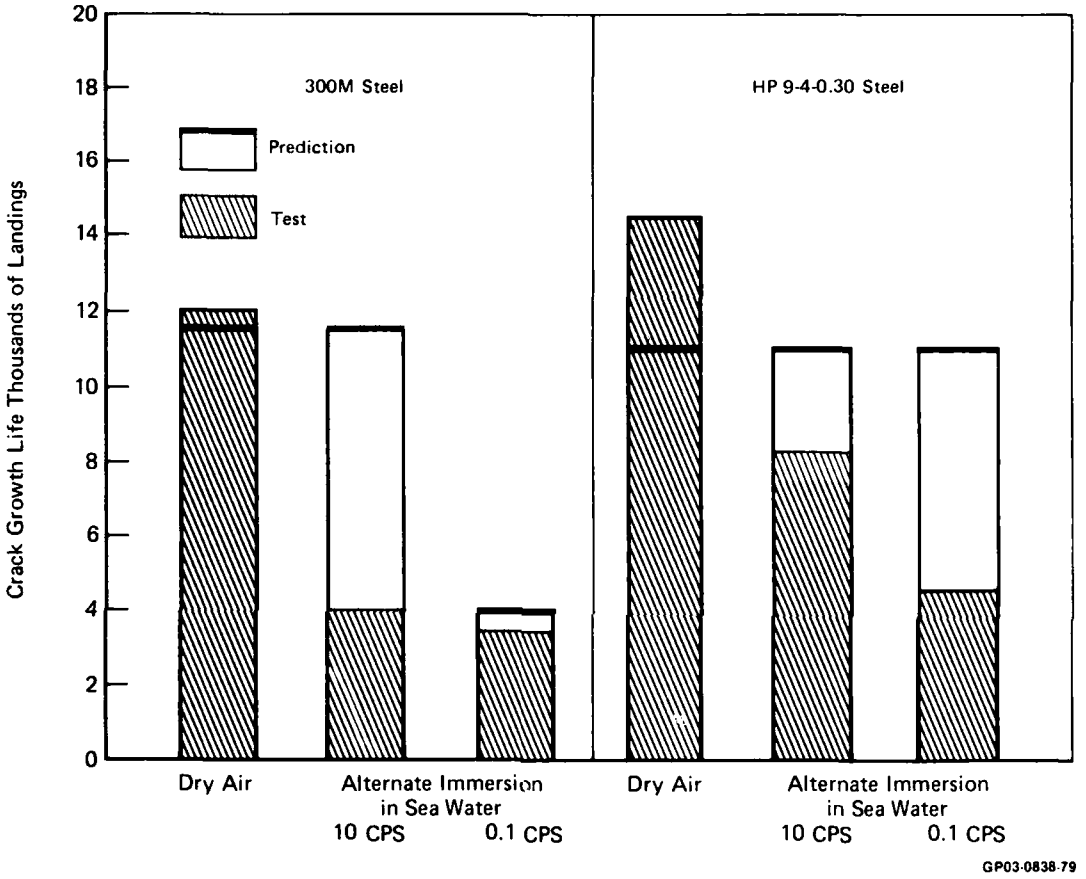

Figure 62. Comparison of Analysis and Verification Test Lives for Center Cracked Panels

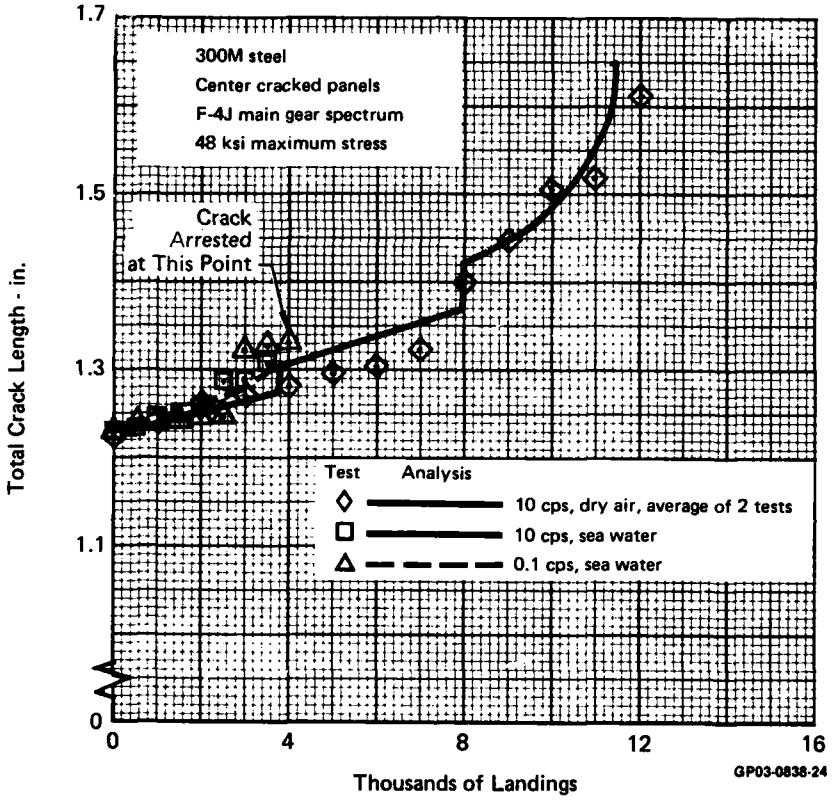

Figure 63. Verification Test Results for 300M Center Cracked Panels

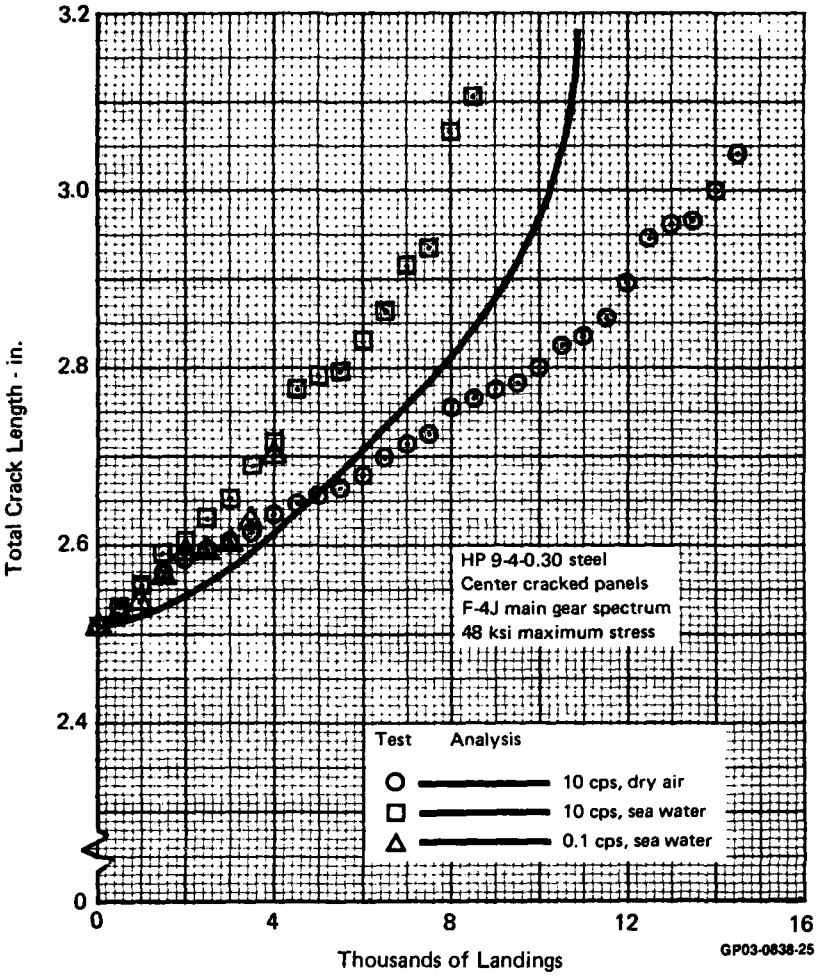

Figure 64. Verification Test Results for HP 9-4-0.30 Center Cracked Panels

Spectrum crack growth predictions for center cracked panels in the alternate immersion environment showed inconsistent correlation with test behavior. Generally, good correlation was obtained in all tests prior to application of the maximum load in the spectrum. Two specimens, one 300M specimen tested to the accelerated time history and one HP 9-4-.30 specimen tested to the real time stress history, failed during, or shortly after, application of the maximum stress level in the spectrum at about 3,870 landings. Both 300M and HP 9-4-.30 steel center cracked panels showed considerable tunneling in alternate immersion tests, increasing stress intensity factor during application of the maximum stress level. Also, both materials showed some variation in failure crack lengths in the constant amplitude tests. Some tunneling coupled with low K_c for individual specimens probably contributed to the early failure of these specimens.

The 300M specimen tested to the real time stress history showed erratic behavior. Between 2500 and 3000 landings crack growth jumped from below that predicted to somewhat above that predicted. The crack continued to grow slowly until after application of the maximum stress level at 3,870 landings. Thereafter the crack growth stopped (at least at the surface). After 8,000 landings were applied under real time loading, the spectrum was accelerated. The alternate immersion cycle was maintained throughout the test. The crack remained essentially stationery until 27,500 landings had been applied. At that point the crack began growing and failure occurred at 28,380 landings. In this case it is expected that the increased stress intensity factor produced by tunneling may produced sufficient plasticity at the crack tip to halt subsequent growth. Several authors (References 9-11) have shown that overloads can arrest a growing crack if the overload is of sufficient magnitude. For purposes of the comparisons shown herein (Figure 62-64), failure of this specimen was said to occur at the application of the maximum spectrum stress level at 3,870 landings.

3. SURFACE FLAW SPECIMEN TEST RESULTS - Using the analysis algorithms described in Section III, spectrum crack growth predictions were made for the surface flaw geometries.

Predictions of the shape change occurring during growth from the given initial flaw geometries are obtained from constant amplitude analysis, as described in Section III. At any surface crack length, the crack aspect ratio is assumed equal to that obtained by constant amplitude analysis.

Table 15 and Figure 65 summarize the predicted and measured crack growth lives for each surface flaw test. The crack growth lives shown in Figure 65 are presented for growth to fracture from the largest initial flaw length in each material type. In 300M steels, this flaw length was 0.114 inch and in HP-9-4-.30, it was 0.278 inch.

Comparisons of predicted and measured crack growth for each surface flaw test are presented in Figures 66 and 67. Correlation of crack growth predictions with the surface flaw test results in 300M as shown in Figure 66 is poor except for the alternate immersion test using the 10 cps spectrum. While correlation with crack growth appears poor, correlation with test lives is good as indicated in Table 15 and Figure 65. This discrepancy was explained by examination of the fracture surfaces of each specimen. These examinations showed that for the dry air test and the slow cycle rate alternate immersion test, crack growth at the surface (where measurements were taken) was arrested, while growth beneath the surface continued. Crack sizes at failure, beneath the surface, approached those predicted. Unfortunately corrosion of the crack surfaces during storage made it impossible to determine subsurface crack lengths accurately.

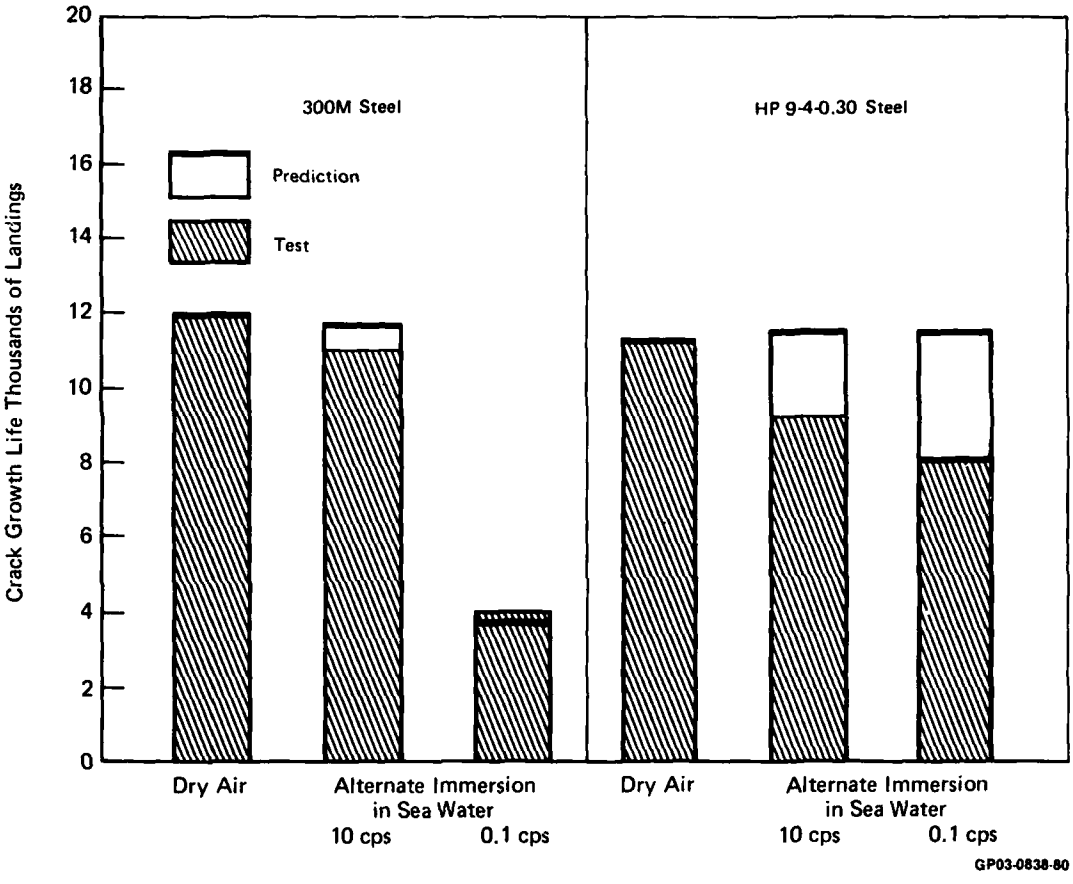

Figure 65. Comparison of Analysis and Verification Test Lives for Surface Flawed Panels

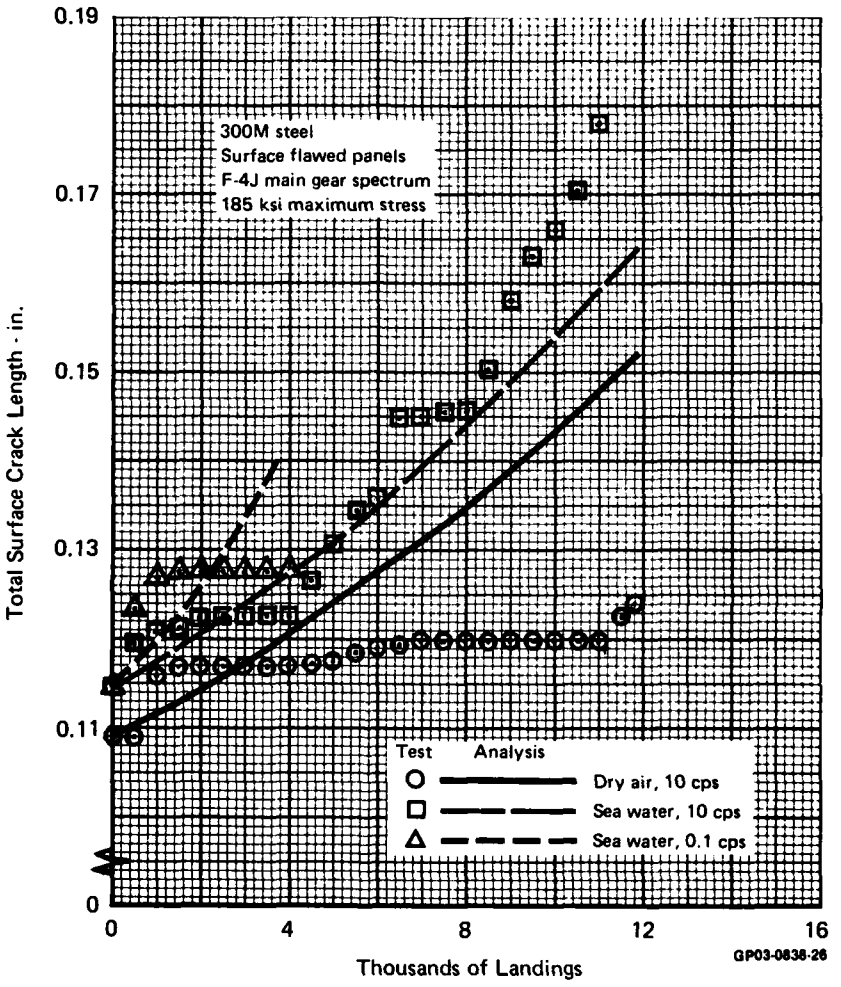

Figure 66. Verification Test Results for 300M Surface Flawed Panels

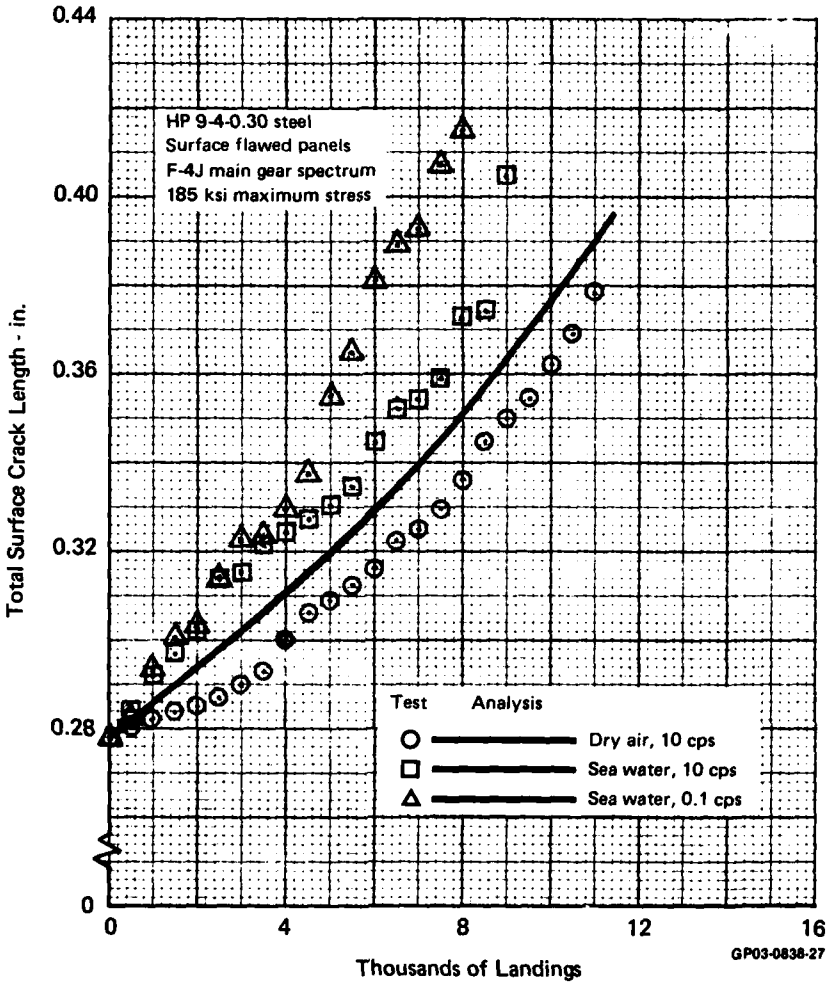

Figure 67. Verification Test Results for HP 9-4-0.30 Surface Flawed Panels

4. CRACK GROWTH UNDER NAVY LANDING GEAR SPECTRUM - This test series verified the slow crack growth rates predicted for cracks growing under the Navy landing gear spectrum. As shown in Figure 68, crack lengths used in verification tests were significantly larger than those found in the initial flaw survey of References 1 and 2. Yet test lives, for both center cracked and surface flawed panels, under the Navy landing gear spectrum are longer than the 8,000 landings desired in the verification tests.

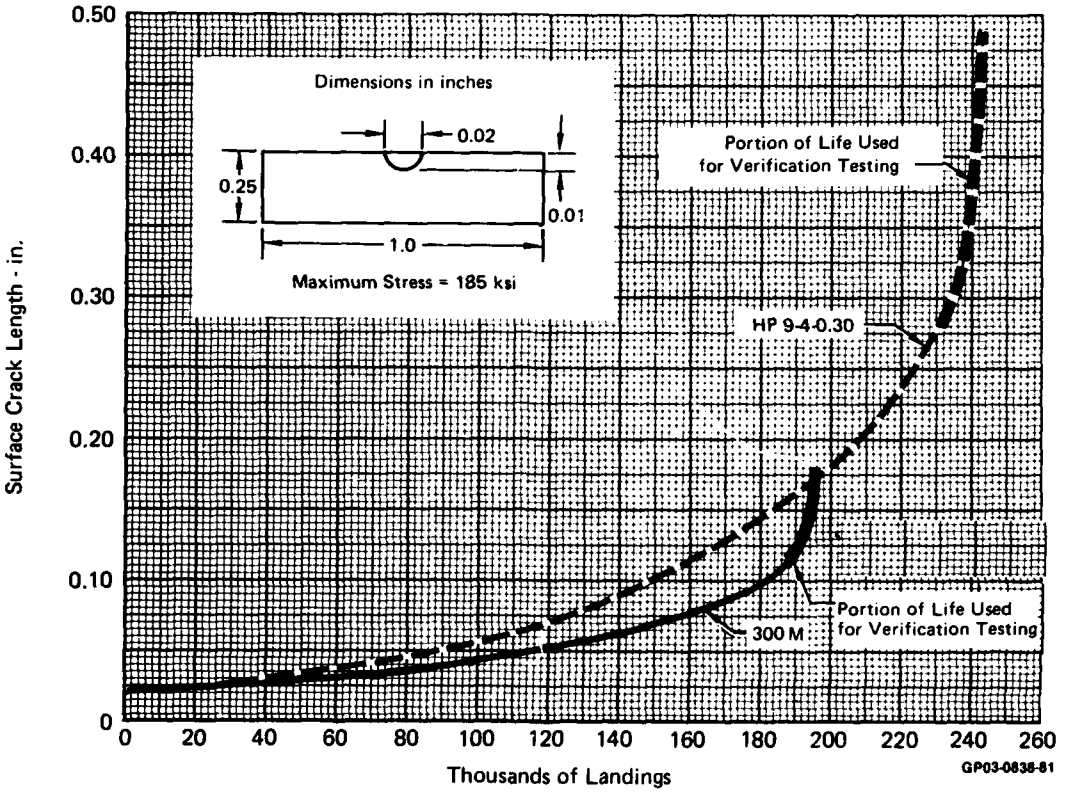

Figure 68. Predicted Growth of Small Surface Flaws Under Navy Landing Gear Spectrum

The Navy landing gear spectrum is characterized by a few occurrences of high stress levels caused by high sink rate (carrier) landings and many occurrences of very low stress levels caused by ground handling loadings (taxiing, turning, pivoting, and braking). As shown in Figure 69, all of the high peak stresses in the Navy gear spectrum are caused by carrier landing loads. In fact, the Navy landing gear spectrum without carrier landing stresses is similar to Air Force landing gear spectrum used in Reference 1, as shown in Figure 70. In this comparison, both stress spectra have been normalized to the parking load stress level so that differences in aircraft weights and design criteria are minimized.

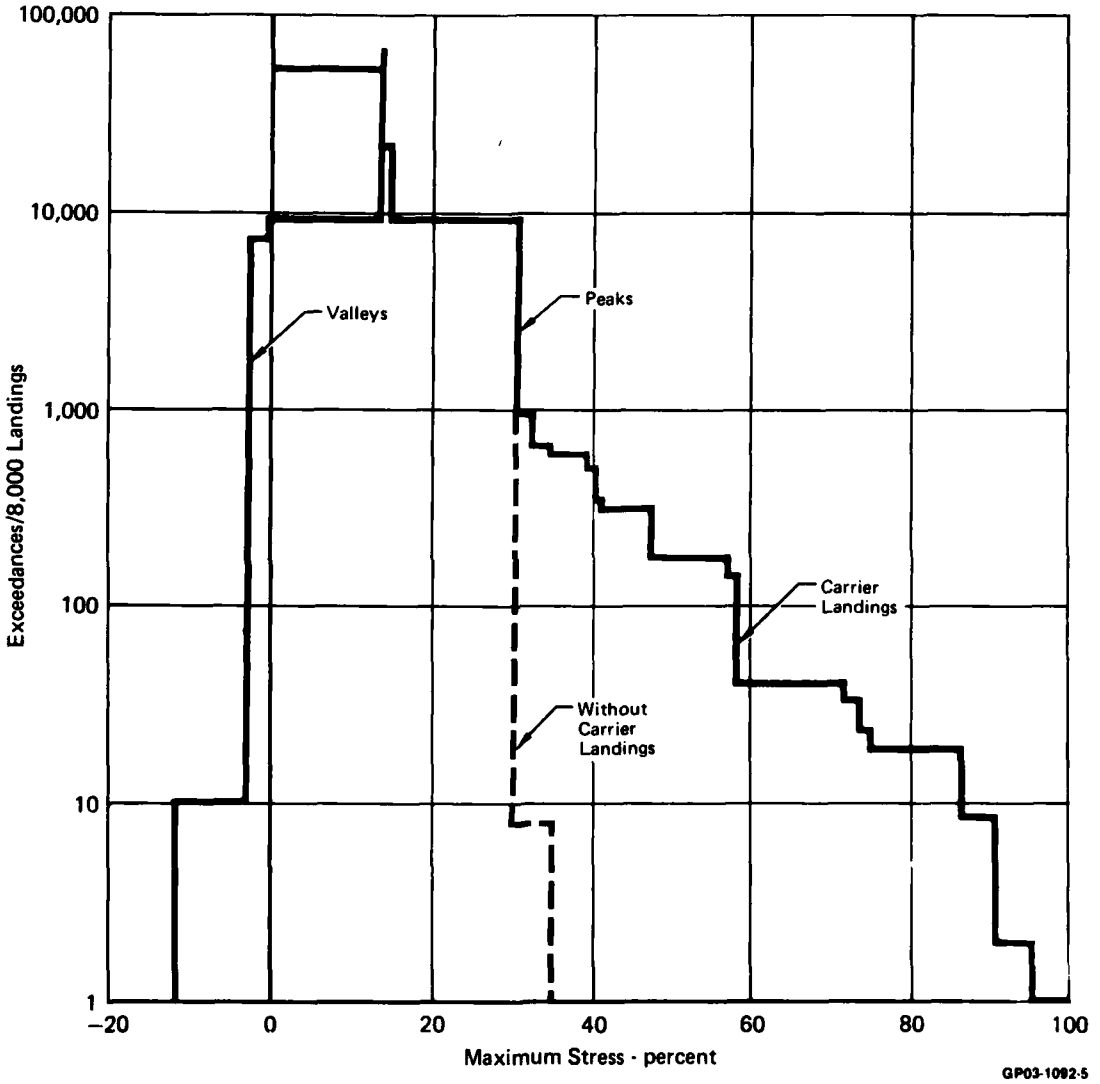

Figure 69. Navy Main Landing Gear Stress Spectra

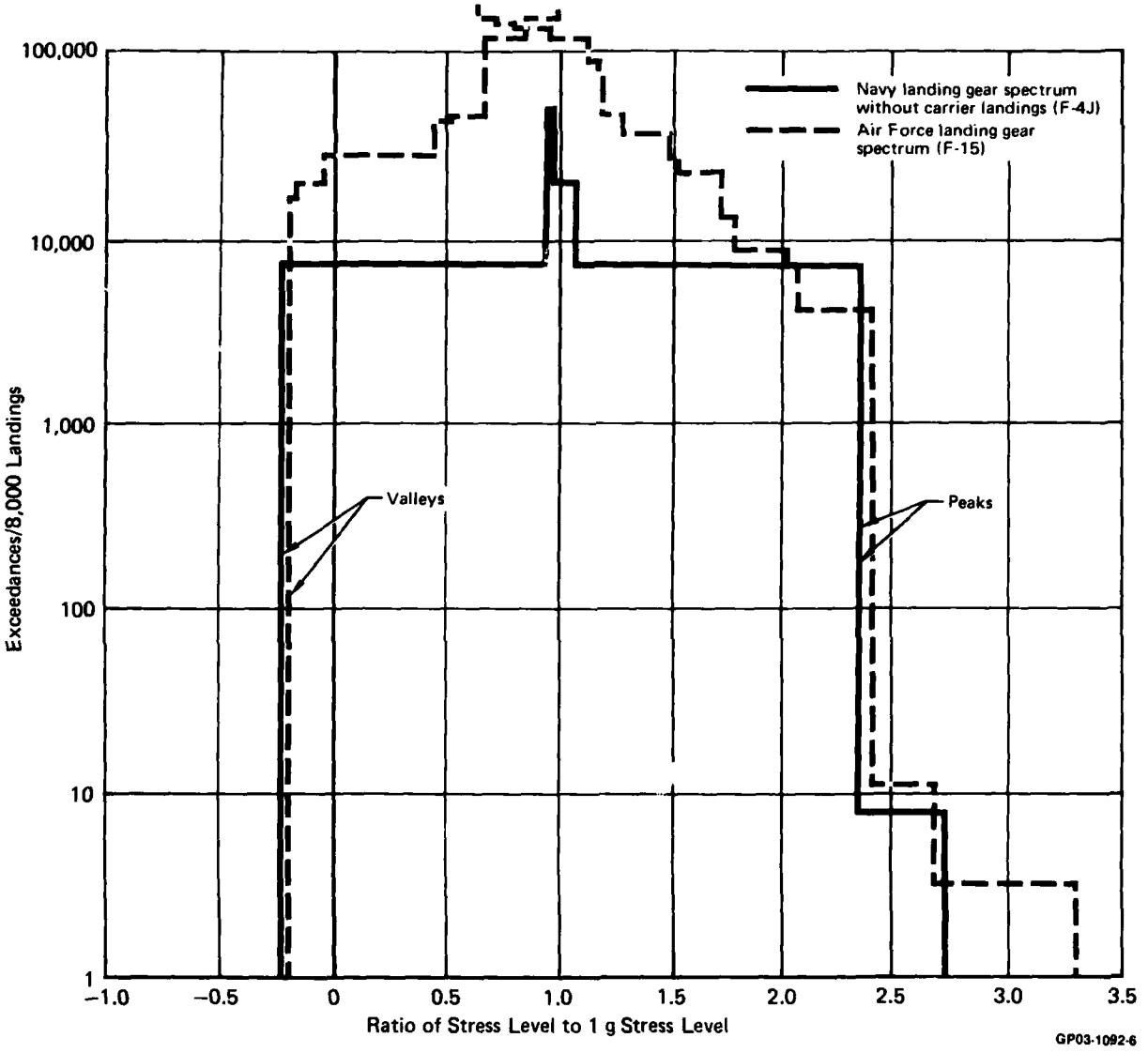

Figure 70. Comparison of Navy Landing Gear Spectrum Without Carrier Landings, and Air Force Landing Gear Spectrum

When carrier landing stress levels are included in the Navy gear spectrum, as they were in this program, the Navy stress spectrum differs significantly from the Air Force gear spectrum used in the program of Reference 1. Exceedance curves for these spectra are compared in Figure 71. Ground handling stress levels in the Navy spectrum are no more than 35 percent of the maximum stress level in the spectrum, while ground handling stress levels in the Air Force spectrum exceed 70 percent of the maximum stress level. This difference in relative stress level due to ground handling loads makes the Navy spectrum much less severe, from a crack growth life point of view, than the Air Force spectrum. This difference in severity is reflected in Table 16 which compares crack growth lives for surface flawed panel tests using the Air Force and Navy spectra.

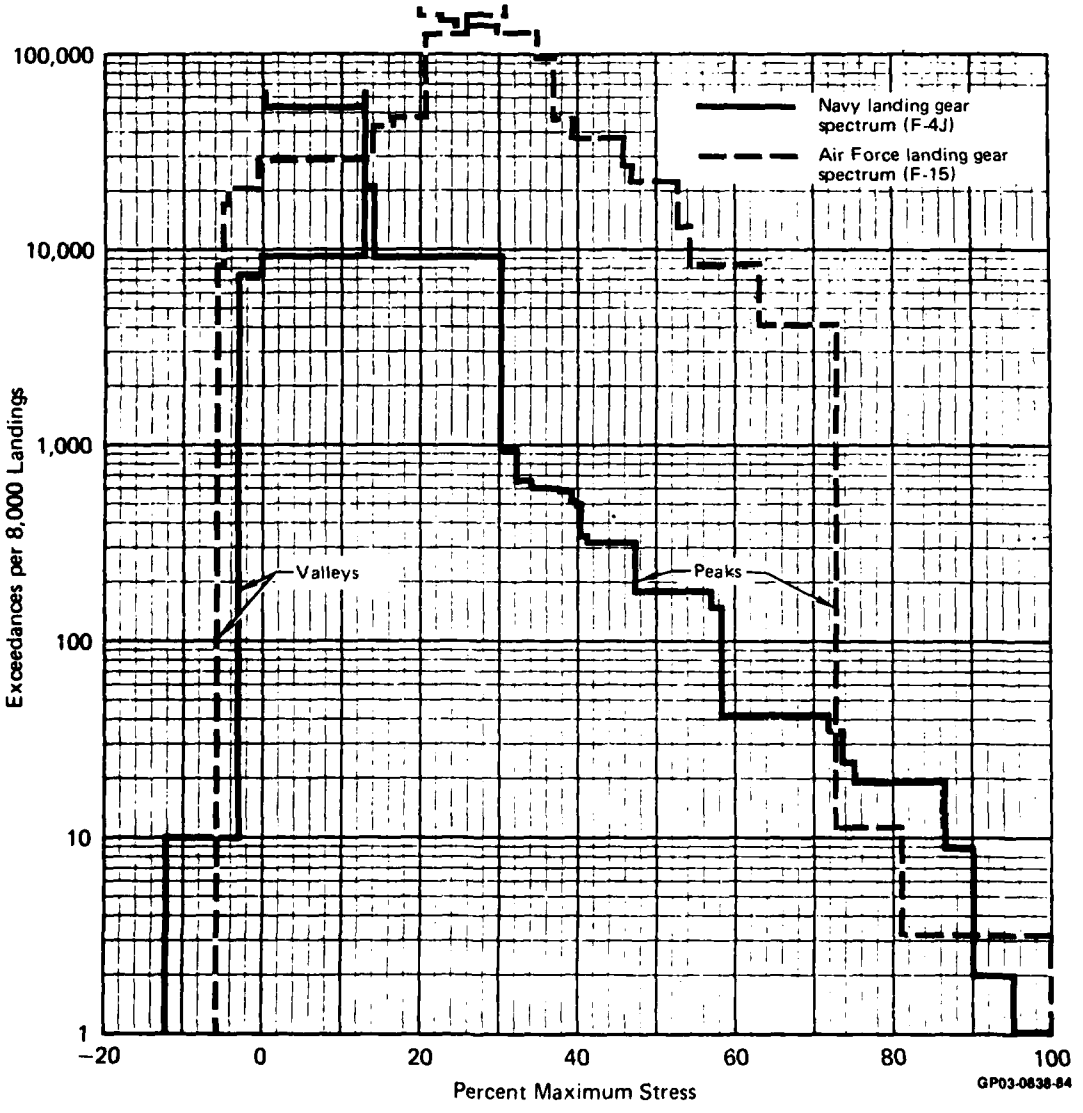

Figure 71. Comparison of Air Force and Navy Main Landing Gear Stress Spectra

TABLE 16. COMPARISON OF TEST LIVES UNDER AIR FORCE AND NAVY LANDING GEAR SPECTRA

Steel Material	Environment (1)	Sustained Loads	Life-Landings (2)	
			Air Force Spectrum	Navy Spectrum
300M	Dry Air	No	60	10,780
	Aggressive	No	20	11,370
	Aggressive	Yes	12	3,780
HP 9-4-0.30	Dry Air	No	500	11,780
	Aggressive	No	510	9,370
	Aggressive	Yes	500	7,990

GP03-0838-83

Notes:

(1) Aggressive environment for the Air Force spectrum is continuous immersion in 3.5% NaCl salt water, for Navy spectrum is alternate immersion in synthetic sea water.

(2) Initial flaw lengths are 0.114 in. in 300M steel and 0.278 in. in HP 9-4-0.30. Maximum stress level for both spectra is 185 ksi.

While the implication of this data is that cracks will not grow in landing gear of Navy aircraft, service experience shows that this is not the case. Corrosion cracking is a primary cause for gear replacement in the field. These flaws are caused by high residual tensile stresses in local regions or by actuator loadings or other loadings independent of the primary loading of the gear during landings. To minimize crack growth in Navy gear, residual stresses, actuator loading, or redundant loads may require more attention during design than stresses caused by primary loading.

SECTION VII

CONCLUSIONS

Immersion in sea water accelerates crack growth in 300M steel. The acceleration decays with drying time after immersion, indicating that continuous immersion is a more aggressive environment for crack growth in 300M steel than is alternate immersion.

Immersion in sea water has little impact on crack growth rate in HP-9-4-.30 steel except at stress intensity factor ranges below 30 ksi $\sqrt{in}$. Alternate immersion at low cycle rates tends to increase threshold stress intensity factor from below 7 ksi $\sqrt{in}$ at 10 cps to 25 ksi $\sqrt{in}$ at 0.1 cps. When the maximum stress intensity factor is below these threshold values, crack growth arrests during the drying portion of the immersion cycle and does not reinitiate during subsequent immersions.

Currently, we conjecture that the drying cycle of the alternate immersion environment served to dry corrosion products on the crack faces, increasing crack closure to the point that the crack could not grow in the dry air environment. Subsequent ten minute immersion times were not sufficient to dissolve the product such that the crack could grow. Once the specimen was precracked beyond the apparent threshold, the crack growth rates closely approached those found in the dry air tests.

Crack growth in alternate immersion environments, such as that applied in this program, can be accurately predicted using linear summation of sustained load crack growth rates derived from cyclic tests in an aggressive environment and cyclic crack growth rates determined from tests in an inert environment. The decay in crack growth rate following removal from an aggressive environment is accurately predicted by a function which decays exponentially with time after removal.

The main landing gear stress history used in this program is based on Navy specified sink rates for carrier-based fighter aircraft and so is typical of that for landing gear of many carrier-based fighter aircraft. This stress history is characterized by few applications of high stress levels caused by high sink rate landings and numerous applications of low stress levels produced by ground handling (taxiing, turning, pivoting, braking) load cycles. This stress history is typical of many landing gear components. However, nose gear, actuators, and some redundant components can be subjected to significantly different stress histories.

This stress history produces very little crack growth over the aircraft service liftime, except for crack lengths near critical flaw size. Large flaw sizes were used in the verification tests reported herein. So little growth occurs under sustained loads in this stress history that crack growth lives are not as sensitive to environment as were those reported in previous work with Air Force fighter aircraft landing gear (Reference 1).

APPENDIX A

CRACK GROWTH ANALYSIS ROUTINE INCLUDING ENVIRONMENT-LOAD INTERACTION EFFECTS

1. INPUT DEFINITIONS - The computer program has the following inputs:

Analysis inputs include

a. title identifying problem (TITLE)

b. threshold stress intensity factor, critical stress intensity factor for material thickness (DELKTH, KSUBC)

c. initial crack length (AZERO)

d. stress ratio correction parameter, plastic zone size correction factor, and shut-off overload ratio (ALPHA, ROOT, OLMAX)

e. stress intensity correction factor type (ICOR)

f. for single and double cracks from holes (ICOR = 1 or 2, respectively), radius of the hole and shortest distance perpendicular to the load from hole center to the plate edge (RADIUS, ECCEN) are input; for constant shape semi-elliptical surface flaws (ICOR = 3) the flaw aspect ratio, plate thickness, and shortest distance from crack center to plate edge, (A, C, THICK, ECCEN) are input; and for a through crack (ICOR = 4), the shortest distance from the crack center to plate edge (ECCEN) is input.

g. if a stress intensity factor correction table is to be used, the number of points in the table (NPTS), and the crack length and K correction factors for each point (TABLEA(I), TABLEB(I)), are input.

h. number of spectrum repetitions to be analyzed (NBLKS)

i. design limit stress (DLS)

j. number of flights between printouts of accumulated time, crack length, and reference K (PRTFLTS)

k. index for consideration of environmental effects, 0 if no load-environment interaction is to be considered, 1 if load-environment interaction will be considered.

Material data inputs include one data set if load-environment interaction is not considered, two data sets if load-environment interaction is considered. The two data sets describe high frequency, sinusoidal wave crack growth rate data from tests in an inert environment and low frequency, trapezoidal wave data from tests in an aggressive environment. The single data set used for anaysis without load-environment interaction is the same as the first of the following sets.

High frequency, sinusoidal wave data (used with or without load-environment interaction effects)

a. title identifying material, product form, and loading (TITLE)

b. monotonic tensile yield stress, cyclic tensile yield stress (TYLD, CYLD)

c. number of points in da/dN table and sine wave frequency (NDADNA, FA)

d. ΔK and da/dN values of points in table (DKA(I), DADNA(I)).

Low frequency, trapezoidal wave data (used only for load-environment interaction effects)

a. title identifying material, product form, and loading (TITLE 2)

b. monotonic tensile yield stress, cyclic tensile yield stress (TYLD, CYLD)

c. number of points in da/dN table and trapezoidal wave frequency (NDADNB, FB)

d. ΔK and da/dN values of points in table (DKB(I), DADNB(I)).

Spectrum inputs include:

a. title identifying spectrum (TITLE)

b. number of stress levels in spectrum and number of flights (landings) represented by spectrum (NLYR, FLTS)

c. stress level and time increment for each half cycle (SMAX(I), TIME (I)).

2. DESCRIPTION OF OUTPUT - The program outputs include titles of analysis, material, and spectrum input data sets, design limit stress (DLS), initial flaw length (AZERO), and a table of elapsed flights (landings), crack length, and reference stress intensity factor printed at the interval specified by PRTFLTS. When K_{max} exceeds K_c, fracture is predicted to occur and the flight in the spectrum, crack length at fracture, and K_{max} is printed.

LISTING OF PROGRAM

```
C
C     THIS PROGRAM COMPUTES SPECTRUM CRACK GROWTH
C     INCLUDING ACCELERATION DUE TO SUSTAINED LOADING
C     IN AN AGGRESSIVE ENVIRONMENT.  THE WILLENBORG
C     MODEL IS USED TO PREDICT SPECTRUM LOAD
C     INTERACTION EFFECTS.  A LINEAR SUMMATION APPROACH
C     IS USED TO PREDICT ENVIRONMENTAL ACCELERATION.
C     CYCLE-BY-CYCLE ANALYSIS IS USED.  PROGRAM WAS
C     DEVELOPED BY C.R.SAFF OF MCDONNELL AIRCRAFT CO.,
C     ST. LOUIS, MISSOURI, TELEPHONE (314) 232-3356.
C
      DIMENSION SMAX(1000),TIME(1000),CARRAY(100),SNARAY(100)
      DIMENSION SLAND(1500)
      INTEGER RETARD,TITLE(20)
      REAL KMAX,KMIN,KSUBC,KMXEFF,KMNEFF
      COMMON/A/A,RADIUS,ECCEN,AOC,THICK,NPTS,TABLEA(50),TABLEB(50)
      COMMON/B/DKC(32),DKD(32),DADND(32),DADT(32),NDADT,NEN,DELKTH
      PI=3.14159265
      RETARD=0
C
C     READ AND ECHO INPUT DATA
C
C     ANALYSIS INPUTS INCLUDE-
C
C     TITLE WHICH IDENTIFIES PROBLEM
C     DELKTH=THRESHOLD STRESS INTENSITY FACTOR
C     KSUBC=CRITICAL STRESS INTENSITY FACTOR FOR MATERIAL THICKNESS
C     AZERO=INITIAL CRACK LENGTH
C     RC=STRESS RATIO CORRECTION
C     ROOT2=PLASTIC ZONE SIZE FACTOR
C     OLMAX=SHUT-OFF OVERLOAD RATIO
C     ICOR=STRESS INTENSITY FACTOR CORRECTION TYPE
C          1=SINGLE CRACK FROM HOLE
C          2=DOUBLE CRACK FROM HOLE
C          3=SEMI-ELLIPTICAL SURFACE FLAW (FIXED A/C)
C          4=THROUGH CRACK
C     RADIUS=RADIUS OF CRACKED HOLE
C     ECCEN=SHORTEST DISTANCE PERPENDICULAR TO LOAD
C           FROM HOLE CENTER TO PLATE EDGE
C     AOC=RATIO OF SURFACE CRACK DEPTH TO HALF LENGTH
C     THICK=PLATE THICKNESS
C     ECCEN=SHORTEST DISTANCE FROM CRACK CENTER TO PLATE EDGE
C     NPTS=NO. OF POINTS IN STRESS INTENSITY FACTOR CORRECTION TABLE
C     TABLEA(I),TABLEB(I)=CRACK LENGTH AND K-CORRECTION
C                         FACTOR VALUE FOR TABLE
C     NBLKS=NO. OF SPECTRUM REPETITIONS TO BE ANALYZED
C     DLS=DESIGN LIMIT STRESS
C     PRT FLTS=NO. OF FLIGHTS BETWEEN PRINTOUTS OF ACCUMULATED
C              TIME,CRACK LENGTH,AND REFERENCE K
C     NEN=INDEX FOR CONSIDERATION OF ENVIRONMENTAL EFFECTS
C         0=SINGLE DA/DN CURVE IS TO BE USED
C           NO FREQUENCY EFFECT CONSIDERED
C         1=ENVIRONMENTAL EFFECT WILL BE CONSIDERED
C           INPUT HIGH FREQ. SINE WAVE DATA &
C           LOW FREQ. TRAPEZOIDAL WAVE DATA
C     ALFA=RATE OF DECAY OF ENVIRONMENTAL ACCELERATION
C     FREF=REFERENCE FREQUENCY FOR ENVIRONMENTAL ACCELERATION
C     P=EXPONENT OF FREQUENCY RATIO USED TO DETERMINE
C     ENVIRONMENTAL ACCELERATION
C
```

```
      READ(1,2200)  TITLE
      READ(1,1000) DELKTH,KSUBC
      READ(1,1000) AZERO
      READ(1,1000) RC,ROOT2,OLMAX
      IF(RC.LT.-1.85) RC=-1.85
      READ(1,2000) ICOR
      GO TO (10,10,20,30),ICOR
   10 READ(1,1000) RADIUS,ECCEN
      GO TO 40
   20 READ(1,1000) AOC,THICK,ECCEN
      GO TO 40
   30 READ(1,1000) ECCEN
   40 READ(1,2000) NPTS
      IF(NPTS.LE.0) GO TO 60
      DO 50 I=1,NPTS
   50 READ(1,1000) TABLEA(I),TABLEB(I)
   60 READ(1,2000) NBLKS
      READ(1,1000) DLS
      READ(1,1000) PRTFLTS
      READ(1,2000) NEN
      IF(NEN.NE.0) READ(1,1000) ALP,FREF,P
      WRITE(6,2300) TITLE
C
C     READ MATERIAL GROWTH RATE DATA
C
C     COMPUTE DA/DT AND DA/DN
C
      CALL ENVIR(CARRAY,SNARAY,NDADN,KSUBC,TYLD,CYLD)
      DO 70 I=1,NDADN
      SNARAY(I)=ALOG10(SNARAY(I)*(KSUBC-CARRAY(I))/KSUBC)
   70 CARRAY(I)=ALOG10(CARRAY(I))
C
C     READ SPECTRUM INPUT DATA
C
C     SPECTRUM DATA INPUTS INCLUDE-
C
C     TITLE WHICH IDENTIFIES SPECTRUM INPUT
C     NLYR=NO. OF STRESS LEVELS IN SPECTRUM
C     FLTS=NO. OF FLIGHTS (LANDINGS) REPRESENTED BY SPECTRUM
C     SMAX(I)=STRESS LEVEL FOR EACH HALF CYCLE
C     TIME(I)=TIME INCREMENT FOR EACH HALF CYCLE
C
  100 READ(4,2200) TITLE
      READ(4,2000) NLYR,FLTS
      DO 110 I=1,NLYR
      READ(4,1000) SMAX(I),TIME(I)
      SMAX(I)=SMAX(I)*DLS/100.
  110 CONTINUE
      READ(5,5000) (SLAND(I),I=1,1204)
 5000 FORMAT(10F6.1)
      WRITE(6,2300) TITLE
      WRITE(6,3460) NBLKS,DLS
```

```
C
C       SET UP FOR CYCLIC GROWTH ANALYSIS
C
        ZK=0.33045+0.15164*RC-0.01476*RC**2
        FR=CYLD/TYLD-1.
        ZK=ZK*(1.+0.6*FR-0.156*FR**2)
        SIGMAY=CYLD
        A=AZERO
        ASUBP=AZERO
        CALL BETA(ICOR,BETAT)
        WRITE(6,4300) A
        PFLTS=0.
        WRITE(6,3500)
C
C       THESE LINES ARE USED TO SET UP COUNTERS FOR ENVIRONMENT
C       AND RANDOM LANDING LOADS
C
        SMIN=0.
        NCYC=0
        KEY=1
        TIME1=0.
        TYME=0.
        TYM1=3600.
        TYM2=600.
        LSTRS=0
        KONT3A=6
        J3A=2568
        J3B=8000
        KONT1=0
        KONT2=0
        KONT3=0
        DO 230 J1=1,NBLKS
        KONT1=KONT1+1
        KONT2=KONT2+1
        KONT3=KONT3+1
        IF(KONT1.GT.10) KONT1=1
        IF(KONT1.LT.10) KEY1=0
        IF(KONT1.EQ.10) KEY1=1
        IF(KONT2.GT.2) KONT2=1
        IF(KONT2.LT.2) KEY2=0
        IF(KONT2.EQ.2) KEY2=1
        IF(J1.GT. J3A) KONT3A=7
        IF(J1.LE.J3B) GO TO 119
        KONT3A=6
        J3A=J3A+8000
        J3B=J3B+8000
  119   IF(KONT3.GT.KONT3A) KONT3=1
        IF(KONT3.LT.KONT3A) KEY3=0
        IF(KONT3.EQ.KONT3A) KEY3=1
        DO 220 J4=1,NLYR
        TYME=TYME+TIME(J4)
        IF(KEY.EQ.1) GO TO 120
        IF(TYME.LT.TYM1) GO TO 125
        KEY=1
        TYM1=TYM1+3600.
        TYM2=TYM2+3600.
        GO TO 125
  120   IF(TYME.LT.TYM2) GO TO 125
        KEY=0
  125   CONTINUE
```

```
C
C     CYCLIC GROWTH ANALYSIS
C
      DADN=0.
      SIGMAX=SMAX(J4)
      IF(J4.LT.4.AND.KEY1.EQ.0) GO TO 220
      IF(J4.LT.8.OR.J4.GT.11) GO TO 126
      IF(KEY2.EQ.0) GO TO 220
  126 IF(J4.NE.22.OR.KEY3.NE.1) GO TO 129
      LSTRS=LSTRS+1
      IF(LSTRS.GT.1204) LSTRS=1
      SIGMAX=SLAND(LSTRS)*DLS/100.
C
C     COMPUTE KMAX & KMIN
C
  129 CONTINUE
  130 IF(SIGMAX.LT.SMIN) GO TO 210
      KMIN=SMIN*SQRT(PI*A)*BETAT
      R=SMIN/SIGMAX
      IF(KMIN.LT.SKMIN) SKMIN=KMIN
      KMAX=SIGMAX*SQRT(PI*A)*BETAT
      RETARD = 1
      IF(A.GE.ASUBP) GO TO 160
C
C     COMPUTE EFFECTIVE KMAX & KMIN
C
      SIGREF=(SIGMAY*SQRT(2.*(ASUBP-A)/A))/BETAT/SQRT(ROOT2)
      SIGRED=SIGREF-SIGMAX
      IF(OLMAX.NE.0.) GO TO 140
      PHI=1.
      GO TO 150
  140 THRSLD=DELKTH*(1.-R**2)
      PHI=(1.-THRSLD/KMAX)/(OLMAX-1.)
      SIGRED=PHI*SIGRED
  150 IF(SIGRED.LT.0.) SIGRED=0.
      SIGMAX=SIGMAX-SIGRED
      IF(SIGMAX.LE.0.) GO TO 210
      KMNEFF=KMIN-SIGRED*SQRT(PI*A)*BETAT
      IF(KMNEFF.LT.0.) KMNEFF=0.
      KMXEFF=SIGMAX*SQRT(PI*A)*BETAT
      REFF=KMNEFF/KMXEFF
C
C     COMPARE EFFECTIVE PLASTIC ZONE INTERFACE WITH PREVIOUS
C     INTERFACE
C
      RSUBY1=(KMAX**2-3./32.*SKMIN**2)/2./PI*ROOT2/SIGMAY**2
      IF(A+RSUBY1.LT.ASUBP) GO TO 170
C
C     THIS CYCLE IS NOT RETARDED
C
  160 RETARD=0
      RSUBY=(KMAX**2-3./32.*SKMIN**2)/2./PI*ROOT2/SIGMAY**2
      ASUBP=A+RSUBY
      SKMIN=1.E20
      KMXEFF=KMAX
      KMNEFF=KMIN
      REFF=KMIN/KMAX
C
C     COMPUTE DA/DN
C
  170 IF(KMXEFF.LE.1.001*KMNEFF) GO TO 180
      IF(KMAX.GE.KSUBC) GO TO 240
      THRSLD=DELKTH*(1.-R**2)
      DELTAK=KMXEFF*(1.-REFF)
      DELK=(1.-REFF)*(1.-(1.-REFF)*ZK)/(1.-ZK)*KMXEFF
      IF(REFF.LT.0.) DELK=(1.-ZK*EXP(0.1*REFF))*KMXEFF/(1.-ZK)
      DELTAK=ALOG10(DELK)
      CALL TLU(CARRAY,SNARAY,NDADN,DELTAK,DADN)
      DADN=10.**DADN*KSUBC/(KSUBC-KMAX)
```

```
C
C       COMPUTE ENVIRONMENTAL ACCELERATION
C
  180 IF(NEN.EQ.0) GO TO 210
      IF(KMXEFF.LT.DELKTH) GO TO 210
      IF(TIME(J4).EQ.0.) GO TO 210
      F=0.5/TIME(J4)
      XKMX=ALOG10(KMXEFF)
      IF(R.GT.0.9) GO TO 190
      CALL TLU(DKD,DADND,NDADT,XKMX,DADTL)
      GO TO 200
  190 CALL TLU(DKC,DADT,NDADT,XKMX,DADTL)
      F=1./TIME(J4)
  200 IF(DADTL.LT.-99.) DADTL=-99.
      DADT1=10.**DADTL
      IF(KEY.NE.0) GO TO 205
      T1=TIME1
      T2=TIME1+TIME(J4)
      DADT1=DADT1*(EXP(-ALP*T1)-EXP(-ALP*T2))/ALP/(T2-T1)
      GO TO 206
  205 TIME1=0.
  206 EDADN=DADT1/F*(FREF/F)**P
      DADN=DADN+EDADN
C
C       INCREMENT A AND COMPUTE STRESS INTENSITY CORRECTION
C
  210 A=A+DADN
      TIME1=TIME1+TIME(J4)
      SMIN=SMAX(J4)
      IF(DADN.LE.0.) GO TO 220
      IF(RDADN.LT.DADN) RDADN=DADN
      CALL BETA(ICOR,BETAT)
      REFK=DLS*SQRT(PI*A)*BETAT
      IF(RETARD.EQ.0) ASUBP=ASUBP+DADN
  220 CONTINUE
C
C       PRINT RESULTS
C
      CFLTS=FLTS*J1
      IF(CFLTS-PFLTS.LT.PRTFLTS) GO TO 230
      PFLTS=PFLTS+PRTFLTS
      WRITE(6,4400) CFLTS,A,REFK
  230 CONTINUE
      GO TO 250
  240 WRITE(6,4100)
      CFLTS=FLTS*J1
      WRITE(6,4200) CFLTS,A,REFK
  250 STOP 1776
 1000 FORMAT(5F10.0)
 2000 FORMAT(I10,5F10.0)
 2200 FORMAT(20A4)
 2300 FORMAT(/1X,20A4)
 3460 FORMAT(/T2,I8,' BLOCKS AT ',E12.5,' PSI DESIGN LIMIT STRESS')
 3500 FORMAT('   FLIGHTS     A       REFK'/)
 4100 FORMAT(/68(1H*)/1X,'KMAX EXCEEDS KSUBC. PROBLEM ',
     +'TERMINATED'/68(1H*)/,1X,'LAST CALCULATED VALUES ARE'/)
 4200 FORMAT(1X,'FLIGHT IN SPECTRUM ',F16.2/
     +       1X,'CRACK LENGTH       ',E16.8/
     +       1X,'REFK               ',E16.8)
 4300 FORMAT(//'  BEGIN SPECTRUM CRACK GROWTH ANALYSIS, A =',F10.5/)
 4400 FORMAT(F8.0,F10.5,F10.5)
 4500 FORMAT(/)
      END
```

```
C
C
C
      SUBROUTINE TLU(X,Y,N,XVAL,YVAL)
C
C     TABLE LOOK UP ROUTINE
C
      DIMENSION X(N),Y(N)
      IF(X(N).GE.XVAL) GO TO 10
      I=N
      GO TO 30
   10 DO 20 I=1,N
      IF(X(I).GE.XVAL) GO TO 30
   20 CONTINUE
   30 IF(I.EQ.1) I=2
      YVAL=(Y(I)-Y(I-1))/(X(I)-X(I-1))*(XVAL-X(I-1))+Y(I-1)
      RETURN
      END
C
C
C
C
      SUBROUTINE BETA(ICOR,BETAT)
C
C     STRESS INTENSITY FACTOR CORRECTIONS
C
      COMMON/A/A,RADIUS,ECCEN,AOC,THICK,NPTS,TABLEA(50),TABLEB(50)
      DATA PI/3.14159265/
      GO TO (10,20,30,40),ICOR
C
C     SINGLE THROUGH CRACK FROM OPEN HOLE
C
   10 AA1=1./COS(PI*(A+2.*RADIUS)/2./(2.*ECCEN-A))
      IF(AA1.LE.0.) AA1=1.E20
      BOWIE=0.6762062+(0.8733015/(0.3245442+A/RADIUS))
      BETAT=BOWIE*SQRT(AA1)
      GO TO 50
C
C     DOUBLE THROUGH CRACK FROM OPEN HOLE
C
   20 AA1=1./COS(PI*(A+RADIUS)/2./ECCEN)
      IF(AA1.LE.0.) AA1=1.E20
      BOWIE=0.9438510+(0.6805078/(0.2771965+A/RADIUS))
      BETAT=BOWIE*SQRT(AA1)
      GO TO 50
C
C     NEWMAN'S SEMI-ELLIPTICAL SURFACE FLAW CORRECTION
C
   30 AT=A/THICK
      IF(AT.GT.0.95) GO TO 35
      XMW=1./SQRT(COS(PI*A/2./AOC/ECCEN))
      XM1=1.13-0.09*AOC
      Q=1.+1.47*AOC**1.64
      XME=XM1+SQRT(Q/AOC-XM1)*AT**(2.+8.*AOC**3)
      BETAT=XMW*XME/SQRT(Q)
      GO TO 50
   35 A=(SQRT(AOC)+1.)**2*BETAT**2*A/4.
      ICOR=4
C
C     CENTER CRACK -FINITE WIDTH
C
   40 AA1=1./COS(PI*A/2./ECCEN)
      IF(AA1.LT.0.) AA1=1.E20
      BETAT=SQRT(AA1)
C
C     TABULAR CORRECTION
C
   50 IF(NPTS.EQ.0) GO TO 60
      CALL TLU(TABLEA,TABLEB,NPTS,A,COR1)
      BETAT=BETAT*COR1
   60 RETURN
      END
```

```
C
C
C
      SUBROUTINE ENVIR(DKA,DADNA,NDADNA,KSUBC,TYLD,CYLD)
C
C     COMPUTATION OF SUSTAINED LOAD GROWTH DATA
C     FOR AGGRESSIVE ENVIRONMENT
C
      DIMENSION AK(32),DADNA(50),DADNB(50),DKA(50),DKB(50)
      INTEGER TITLE1(20),TITLE2(20)
      REAL KSUBC
      COMMON/B/DKC(32),DKD(32),DADND(32),DADT(32),NDADT,NEN,DELKTH
      DATA AK/1.,2.,3.,4.,5.,6.,7.,8.,9.,10.,12.,14.,16.,18.,20.,22.5,
     &25.,30.,35.,40.,45.,50.,60.,70.,80.,90.,100.,110.,120.,130.,
     &140.,150./
C
C
C     READ DA/DN DATA FOR 10 CPS , R=0, IN DRY AIR
C
C     INPUT DATA INCLUDES -
C
C     TITLE1 WHICH IDENTIFIES MATERIAL  & PRODUCT FORM FOR REFERENCE
C     TYLD=MONOTONIC TENSILE YIELD STRESS
C     CYLD=CYCLIC TENSILE YIELD STRESS
C     NDADNA=NO. OF POINTS IN DA/DN TABLE (SINE WAVE)
C     FA=LOAD CYCLE FREQUENCY
C     DKA(I)=DELTA K VALUES OF POINTS IN DA/DN TABLE
C     DADNA(I)=DA/DN VALUES OF POINTS IN DA/DN TABLE
C
C
      READ(2,1000) TITLE1
 1000 FORMAT(20A4)
      READ(2,3000) TYLD,CYLD
      READ(2,2000) NDADNA,FA
 2000 FORMAT(I10,5F10.0)
      NR=0
      DO 10 I=1,NDADNA
      READ(2,3000) DKA(I),DADNA(I)
 3000 FORMAT(8F10.4)
      IF(DKA(I).GE.KSUBC) GO TO 5
      GO TO 10
    5 NR=NR+1
   10 CONTINUE
      NDADNA=NDADNA-NR
      IF(NEN.NE.0) GO TO 15
   12 WRITE(6,1050) TITLE1
 1050 FORMAT(/2X,20A4)
      GO TO 999
   15 WRITE(6,1100) TITLE1
 1100 FORMAT(/1X,' DA/DT IS DETERMINED FROM '/1X,20A4)
```

```
C
C     READ DA/DN DATA FOR 0.1 CPS, R=0, IN AGGRESSIVE ENVIRONMENT
C
C     INPUT DATA INCLUDES -
C
C     TITLE2 WHICH IDENTIFIES MATERIAL & PRODUCT FORM FOR REFERENCE
C     NDADNB=NO. OF POINTS IN DA/DN TABLE (TRAPEZOIDAL WAVE)
C     FB=LOAD CYCLE FREQUENCY
C     DKB(I)=DELTA K VALUES OF POINTS IN DA/DN TABLE
C     DADNB(I)=DA/DN VALUES OF POINTS IN DA/DN TABLE
C
C
      READ(3,1000) TITLE2
      READ(3,2000) NDADNB,FB
      DO 20 I=1,NDADNB
      READ(3,3000) DKB(I),DADNB(I)
      DKB(I)=ALOG10(DKB(I))
   20 DADNB(I)=ALOG10(DADNB(I))
      WRITE(6,1200) TITLE2
 1200 FORMAT('  AND'/1X,20A4)
      DO 25 I=1,NDADNA
      DKA(I)=ALOG10(DKA(I))
   25 DADNA(I)=ALOG10(DADNA(I))
C
C     DETERMINE DA/DT
C
      DNLIM=ALOG10(1.01*DELKTH)
      UPLIM=ALOG10(KSUBC)
      DO 40 J=1,32
      DO 30 I=1,32
      BK=ALOG10(AK(I))
      IF(BK.LT.DNLIM) GO TO 30
      IF(BK.GT.UPLIM) GO TO 45
      CALL TLU(DKA,DADNA,NDADNA,BK,DADN1)
      CALL TLU(DKB,DADNB,NDADNB,BK,DADN2)
      DADN1=10.**DADN1
      DADN2=10.**DADN2
      IF(DADN2.LE.DADN1) GO TO 30
      GO TO 35
   30 CONTINUE
   35 DADT(J)=(DADN2-DADN1)*FB
      DKC(J)=BK
      DNLIM=ALOG10(AK(I+1))
   40 CONTINUE
   45 NDADT=J-1
      DO 50 I=1,NDADT
      DADT(I)=ALOG10(DADT(I))
   50 CONTINUE
      IF(NDADT.GT.0) GO TO 46
      NEN=0
      GO TO 999
C
C     INTEGRATE DA/DT FOR R=0, 1 CPS SINE WAVE
C
   46 DO 130 I=1,NDADT
      DKX=10.**DKC(I)
      CALL GAUSS(DKX,CC)
      DADND(I)=ALOG10(CC)
      DKD(I)=DKC(I)
  130 CONTINUE
      DO 150 I=1,NDADNA
      DKA(I)=10.**DKA(I)
      DADNA(I)=10.**DADNA(I)
  150 CONTINUE
  999 RETURN
      END
```

```
C
C
C
      SUBROUTINE GAUSS(X4,CC)
C
C     10 POINT GAUSS' RULE INTEGRATION ROUTINE
C
      DIMENSION U(5),R(5)
      COMMON/B/DKC(32),DKD(32),DADND(32),DADT(32),NDADT,NEN,DELKTH
      DATA U/0.0744371695,0.216697697,0.339704784,0.432531683,
     &0.486953264/
      DATA R/0.147762112,0.13463336,0.109543181,0.0747256746,
     &0.0333356722/
      DATA PI/3.14159265/
      A=0.
      B=0.55
      C1=0.5*(B+A)
      C2=B-A
      S=0.
      DO 20 I=1,5
      W=C2*U(I)
      X=C1+W
      J=1
   10 XK=X4/2.*(1.-COS(2.*PI*X))
      XKL=ALOG10(XK)
      IF(XKL.GT.0.) GO TO 12
      Y=1.E-99
      GO TO 14
   12 CALL TLU(DKC,DADT,NDADT,XKL,YL)
      Y=10.**YL
   14 S=S+R(I)*Y
      IF(J.EQ.2) GO TO 20
      X=C1-W
      J=2
      GO TO 10
   20 CONTINUE
      CC=S*C2
      RETURN
      END
```

SAMPLE INPUT

ANALYSIS FILE

```
SURFACE FLAWED PANEL ANALYSIS
    15.5          60.
 0.05725
      0.        0.028          3.5
       4
     0.5
       7
   .0545        .6696
   .0614        .6836
   .0705        .6945
    .083         .705
   .0998        .7172
   .1243        .7292
   .1457        .7295
  100000
     135.
     500.
       1
 0.00175          0.1          0.25
```

HIGH FREQUENCY DA/DN DATA FILE

```
DA/DN DATA - 300M STEEL - 10 CPS - DRY AIR
    248.          228.
      13            10.
     12.       .63E-6
     14.       .90E-6
     16.      1.31E-6
     18.      1.85E-6
     20.      2.55E-6
   22.5       3.6E-6
     25.      4.75E-6
     30.       7.5E-6
     35.      12.8E-6
     40.      18.2E-6
     45.      25.5E-6
     50.      40.0E-6
     60.      600.E-6
```

LOW FREQUENCY DA/DN DATA FILE

DA/DN DATA - 300M STEEL - 0.1 CPS - ALTERNATE IMMERSION IN SEA WATER

10	0.1
18.	200.E-6
20.	330.E-6
22.5	400.E-6
25.	430.E-6
30.	475.E-6
35.	525.E-6
40.	570.E-6
45.	600.E-6
50.	650.E-6
60.	710.E-6

SPECTRUM FILE

F-4J MAIN GEAR AXLE-PISTON FORK STRESS HISTORY - FAST

35	1.
12.7	0.001
12.9	0.05
12.7	0.05
12.7	0.001
30.7	0.05
-0.28	0.05
12.7	0.05
12.7	0.001
14.3	0.05
14.3	0.001
12.7	0.05
12.7	0.001
12.9	0.05
12.9	0.001
12.7	0.05
12.7	0.001
12.9	0.05
12.9	0.001
12.7	0.05
12.7	0.001
0.	0.05
12.7	0.05
12.7	0.05
12.7	0.001
14.3	0.05
14.3	0.001
12.7	0.05
12.7	0.001
12.9	0.05
12.9	0.001
12.7	0.05
12.7	0.001
12.9	0.05
12.9	0.001
12.7	0.05

RANDOM LANDING STRESS LEVELS

32.5	32.5	32.5	32.5	40.4	32.5	24.2	32.5	47.4	32.5
40.4	32.5	32.5	24.2	58.7	32.5	40.4	39.1	47.4	32.5
40.4	24.8	24.2	32.5	32.5	32.5	32.5	40.4	47.4	24.2
58.7	32.5	32.5	32.5	40.4	32.5	39.1	24.2	47.4	32.5
40.4	40.4	24.2	34.3	24.8	58.7	57.1	58.7	47.4	32.5
32.5	40.4	32.5	24.2	39.1	32.5	32.5	40.4	47.4	32.5
32.5	24.2	58.7	40.4	32.5	32.5	40.4	24.8	47.4	24.2
32.5	32.5	32.5	39.1	40.4	24.2	47.4	58.7	37.5	73.7
32.5	40.4	32.5	32.5	40.4	24.2	40.4	47.4	34.3	24.8
39.1	29.4	24.2	58.7	57.1	58.7	32.5	47.4	40.4	32.5
32.5	24.2	32.5	40.4	40.4	24.2	47.4	36.8	71.9	58.7
39.1	32.5	24.8	32.5	32.5	40.4	24.2	47.4	-12.1	75.2
32.5	32.5	40.4	32.5	24.2	58.7	40.4	47.4	39.1	32.5
24.2	34.3	86.4	32.5	40.4	24.8	32.5	47.4	32.5	40.4
24.2	58.7	57.1	58.7	32.5	40.4	47.4	39.1	24.2	41.2
32.5	40.4	32.5	40.4	24.2	47.4	58.7	24.8	37.5	73.7
32.5	32.5	32.5	40.4	24.2	39.1	47.4	32.5	32.5	40.4
89.8	75.3	24.2	58.7	32.5	40.4	47.4	34.3	32.5	24.2
24.8	40.4	32.5	39.1	29.4	40.4	47.4	24.2	32.5	58.7
57.1	58.7	40.4	32.5	32.5	24.2	47.4	32.5	40.4	32.5
40.4	24.2	39.1	24.8	58.7	32.5	47.4	32.5	32.5	32.5
40.4	24.2	32.5	32.5	40.4	47.4	36.8	71.9	24.2	58.7
39.1	34.3	40.4	40.4	40.4	47.4	24.8	24.2	40.4	24.2
47.4	58.7	39.1	57.1	58.7	37.5	73.7	-12.1	75.2	39.4
32.5	32.5	24.2	32.5	40.4	47.4	32.5	32.5	24.8	32.5
24.2	40.4	58.7	32.5	32.5	47.4	40.4	24.2	39.1	32.5
32.5	32.5	40.4	24.2	47.4	34.3	86.4	32.5	58.7	40.4
32.5	24.8	40.4	24.2	47.4	39.1	29.4	32.5	32.5	32.5
40.4	32.5	24.2	40.4	58.7	47.4	57.1	58.7	32.5	32.5
24.2	32.5	40.4	47.4	24.8	39.1	32.5	40.4	24.2	58.7
41.2	32.5	32.5	40.4	47.4	24.2	32.5	32.5	32.5	32.5
40.4	34.3	24.2	39.1	47.4	58.7	40.4	24.8	32.5	37.5
73.7	24.2	40.4	32.5	47.4	40.4	36.8	71.9	32.5	24.2
32.5	58.7	39.1	40.4	47.4	57.1	58.7	24.2	40.4	24.8
32.5	40.4	89.8	75.3	47.4	24.2	32.5	58.7	32.5	32.5
39.1	40.4	32.5	24.2	47.4	34.3	32.5	40.4	24.2	-12.1
75.2	40.4	24.8	58.7	47.4	32.5	40.4	24.2	39.1	29.4
32.5	32.5	32.5	40.4	47.4	32.5	24.2	32.5	32.5	58.7
40.4	24.2	47.4	57.1	58.7	24.8	40.4	39.1	32.5	32.5
32.5	40.4	24.2	47.4	40.4	58.7	24.2	34.3	37.5	73.7
86.4	32.5	32.5	47.4	40.4	32.5	39.1	24.8	24.2	40.4
58.7	32.5	32.5	47.4	32.5	40.4	24.2	32.5	32.5	32.5
32.5	40.4	24.2	47.4	32.5	39.1	58.7	40.4	40.4	24.2
24.8	57.1	58.7	47.4	32.5	36.8	71.9	32.5	40.4	24.2
32.5	47.4	58.7	39.1	34.3	40.4	32.5	24.2	32.5	32.5
41.2	40.4	47.4	24.8	32.5	24.2	32.5	40.4	58.7	40.4
47.4	39.1	29.4	24.2	32.5	40.4	40.4	40.4	24.2	24.2
47.4	58.7	39.1	24.8	57.1	58.7	37.5	73.7	-12.1	75.2
39.4	32.5	47.4	32.5	32.5	40.4	24.2	32.5	32.5	34.3
58.7	40.4	47.4	32.5	24.2	32.5	32.5	40.4	24.8	39.1

32.5	24.2	47.4	32.5	40.4	57.7	32.5	32.5	32.5	40.4
24.2	32.5	47.4	40.4	89.8	75.3	32.5	39.1	24.2	40.4
58.7	24.8	47.4	32.5	32.5	40.4	24.2	57.1	58.7	32.5
40.4	47.4	24.2	34.3	57.1	32.5	39.1	57.7	32.5	40.4
24.2	47.4	32.5	40.4	24.8	36.8	71.9	32.5	32.5	24.2
40.4	47.4	58.7	39.1	29.4	32.5	40.4	24.2	32.5	37.5
73.7	47.4	40.4	32.5	32.5	24.2	24.8	32.5	40.4	58.7
32.5	47.4	24.2	39.1	40.4	57.1	58.7	32.5	34.3	40.4
24.2	47.4	32.5	32.5	32.5	58.7	40.4	32.5	24.2	24.8
47.4	39.1	40.4	32.5	40.4	24.2	47.4	58.7	-12.1	75.2
41.2	100.0	32.5	40.4	24.2	32.5	32.5	32.5	40.4	47.4
39.1	24.2	24.8	32.5	32.5	40.4	58.7	32.5	32.5	24.2
47.4	40.4	32.5	34.3	57.1	58.7	40.4	24.2	39.1	32.5
47.4	32.5	58.7	40.4	32.5	24.8	24.2	32.5	40.4	47.4
37.5	73.7	32.5	32.5	24.2	40.4	39.1	29.4	58.7	40.4
47.4	32.5	24.2	32.5	36.8	71.9	40.4	24.8	32.5	24.2
47.4	32.5	40.4	24.2	58.7	39.1	34.3	86.4	40.4	32.5
47.4	32.5	57.1	58.7	40.4	24.2	32.5	40.4	47.4	58.7
24.8	32.5	32.5	24.2	39.1	40.4	89.8	75.3	32.5	47.4
32.5	24.2	40.4	32.5	32.5	32.5	58.7	40.4	24.2	47.4
32.5	40.4	39.1	24.8	32.5	40.4	40.4	24.2	40.4	47.4
24.2	58.7	34.3	47.4	39.1	57.1	58.7	37.5	73.7	-12.1
75.2	39.4	24.2	32.5	32.5	24.8	40.4	58.7	32.5	47.4
24.2	32.5	32.5	40.4	32.5	40.4	24.2	47.4	39.1	29.4
32.5	32.5	32.5	58.7	40.4	32.5	24.2	32.5	24.8	47.4
40.4	41.2	32.5	32.5	24.2	40.4	47.4	34.3	39.1	58.7
32.5	40.4	24.2	32.5	36.8	71.9	40.4	47.4	57.1	58.7
24.2	24.8	32.5	32.5	40.4	58.7	39.1	24.2	47.4	32.5
40.4	32.5	32.5	32.5	32.5	24.2	40.4	32.5	47.4	32.5
40.4	58.7	40.4	24.2	24.8	39.1	24.2	47.4	34.3	37.5
73.7	86.4	32.5	40.4	32.5	32.5	58.7	40.4	47.4	24.2
32.5	32.5	40.4	24.2	39.1	24.8	57.1	58.7	47.4	32.5
32.5	40.4	58.7	32.5	32.5	24.2	40.4	47.4	32.5	32.5
40.4	39.1	29.4	24.2	32.5	40.4	24.2	47.4	58.7	24.8
-12.1	75.2	32.5	32.5	40.4	32.5	34.3	47.4	24.2	32.5
40.4	39.1	32.5	32.5	58.7	40.4	24.2	47.4	89.8	75.3
32.5	40.4	24.8	24.2	57.1	58.7	32.5	47.4	40.4	39.1
58.7	40.4	24.2	36.8	71.9	32.5	32.5	47.4	40.4	24.2
37.5	73.7	32.5	40.4	24.8	24.2	58.7	47.4	39.1	32.5
34.3	40.4	32.5	32.5	32.5	40.4	24.2	47.4	32.5	32.5
40.4	58.7	41.2	24.2	32.5	47.4	39.1	24.8	32.5	40.4
32.5	24.2	32.5	57.1	58.7	40.4	47.4	58.7	32.5	24.2
32.5	40.4	32.5	40.4	39.1	29.4	47.4	24.2	32.5	32.5
24.8	40.4	24.2	58.7	34.3	86.4	47.4	32.5	40.4	32.5
32.5	32.5	24.2	39.1	40.4	32.5	47.4	40.4	40.4	58.7
40.4	24.2	24.2	24.8	47.4	39.1	57.1	58.7	37.5	73.7
-12.1	75.2	39.4	32.5	24.2	58.7	47.4	32.5	40.4	32.5
32.5	32.5	32.5	40.4	24.2	24.8	47.4	40.4	40.4	39.1
34.3	58.7	24.2	36.8	71.9	47.4	32.5	32.5	32.5	32.5
24.2	40.4	32.5	32.5	40.4	47.4	24.2	58.7	24.8	39.1
32.5	32.5	32.5	40.4	32.5	47.4	24.2	32.5	40.4	57.1
58.7	32.5	58.7	40.4	24.2	47.4	39.1	29.4	32.5	32.5

40.4	24.8	24.2	32.5	34.3	47.4	40.4	32.5	58.7	24.2
89.8	75.3	40.4	32.5	32.5	47.4	39.1	24.2	40.4	40.4
24.2	37.5	73.7	24.8	58.7	47.4	32.5	32.5	32.5	32.5
40.4	24.2	41.2	47.4	39.1	32.5	40.4	57.1	58.7	32.5
58.7	24.2	40.4	32.5	47.4	40.4	24.8	24.2	34.3	86.4
32.5	32.5	40.4	39.1	47.4	32.5	58.7	24.2	32.5	40.4
32.5	-12.1	75.2	24.2	47.4	40.4	32.5	40.4	24.2	24.8
58.7	39.1	36.8	71.9	47.4	32.5	32.5	40.4	32.5	32.5
24.2	32.5	40.4	40.4	47.4	57.1	58.7	58.7	24.2	39.1
29.4	40.4	24.8	34.3	47.4	32.5	24.2	32.5	32.5	40.4
24.2	37.5	73.7	58.7	47.4	32.5	40.4	32.5	39.1	32.5
32.5	40.4	24.2	47.4	24.8	32.5	32.5	32.5	40.4	58.7
24.2	32.5	32.5	47.4	40.4	32.5	24.2	39.1	32.5	32.5
40.4	24.2	47.4	57.1	58.7	58.7	40.4	24.8	34.3	32.5
32.5	40.4	24.2	47.4	40.4	39.1	40.4	40.4	40.4	40.4
24.2	58.7	40.4	47.4	40.4	24.2	24.2	24.2	24.2	47.4
24.8	47.4	47.4	58.7	39.1	58.7	39.1	24.8	34.3	57.1
58.7	37.5	73.7	29.4	36.8	71.9	-12.1	75.2	86.4	41.2
89.8	75.3	39.4	95.1						

OUTPUT FOR SAMPLE INPUT

```
SURFACE FLAWED PANEL ANALYSIS

DA/DT IS DETERMINED FROM
DA/DN DATA - 300M STEEL - 10 CPS - DRY AIR
AND
DA/DN DATA - 300M STEEL - 0.1 CPS - ALTERNATE IMMERSION IN SEA WATER

F-4J MAIN GEAR AXLE-PISTON FORK STRESS HISTORY - FAST

 100000 BLOCKS AT    .18500E+03 PSI DESIGN LIMIT STRESS


BEGIN SPECTRUM CRACK GROWTH ANALYSIS, A =     .05725

 FLIGHTS      A       REFK

   500.     .05801   53.89398
  1000.     .05883   54.42016
  1500.     .05969   54.97040
  2000.     .06052   55.49924
  2500.     .06141   56.07418
  3000.     .06225   56.54943
  3500.     .06315   57.06480
  4000.     .06416   57.64067
  4500.     .06513   58.19100
  5000.     .06607   58.72416
  5500.     .06701   59.25124
  6000.     .06803   59.82860
  6500.     .06902   60.38621
  7000.     .07008   60.98072
  7500.     .07116   61.56888
  8000.     .07301   62.54464
  8500.     .07409   63.11053
  9000.     .07532   63.75800
  9500.     .07670   64.47853
 10000.     .07797   65.14455
 10500.     .07965   66.01905
 11000.     .08098   66.70664

**************************************************************************
 KMAX EXCEEDS KSUBC. PROBLEM TERMINATED
**************************************************************************
 LAST CALCULATED VALUES ARE

 FLIGHT IN SPECTRUM          11171.00
 CRACK LENGTH           .81412181E-01
 REFK                   .66932839E+02
```

APPENDIX B

STRESS INTENSITY SOLUTIONS FOR ELLIPTIC SURFACE FLAWS

1. SUMMARY OF RESULTS - Stress intensity solutions computed from a slice synthesis model and NASTRAN three dimensional finite element results were compared with those obtained from three dimensional finite element analyses of Raju and Newman, References 16 and 17 to substantiate the model. Results of these comparisons are shown in Figures B-1 and B-2. Good agreement is obtained for the stress intensity at the flaw depth, Figure B-1, and reasonable agreement is obtained for the stress intensity at the surface for all but deep flaws, Figure B-2. The results reported in Reference 17b are based on the most detailed model employed thus far in the analysis of the surface flaw.

Because good agreement is shown between the results of Raju and Newman, and the slice synthesis model, as shown in Figures B-1 and B-2, the slice synthesis model results are expected to be reasonably accurate. The slice synthesis model has the advantage that finite width as well as thickness can be included in the analysis.

In order to readily use these results in crack growth prediction computer routines, equations relating stress intensity to crack shape, and depth to plate thickness ratio, have been empirically established based on the slice synthesis model results:

$$K_A = \beta_A \sigma\sqrt{\pi a}$$

$$K_B = \beta_B \sigma\sqrt{\pi c}$$

where: K_A = stress intensity at the depth

K_B = stress intensity at the surface

a = crack depth

c = half surface length

t = thickness

w = width

$\beta_A = M1_A*(1 + M2_A)/\sqrt{Q}$

$\beta_B = M1_B*(1 + M2_B)/\sqrt{Q}$

σ = applied stress

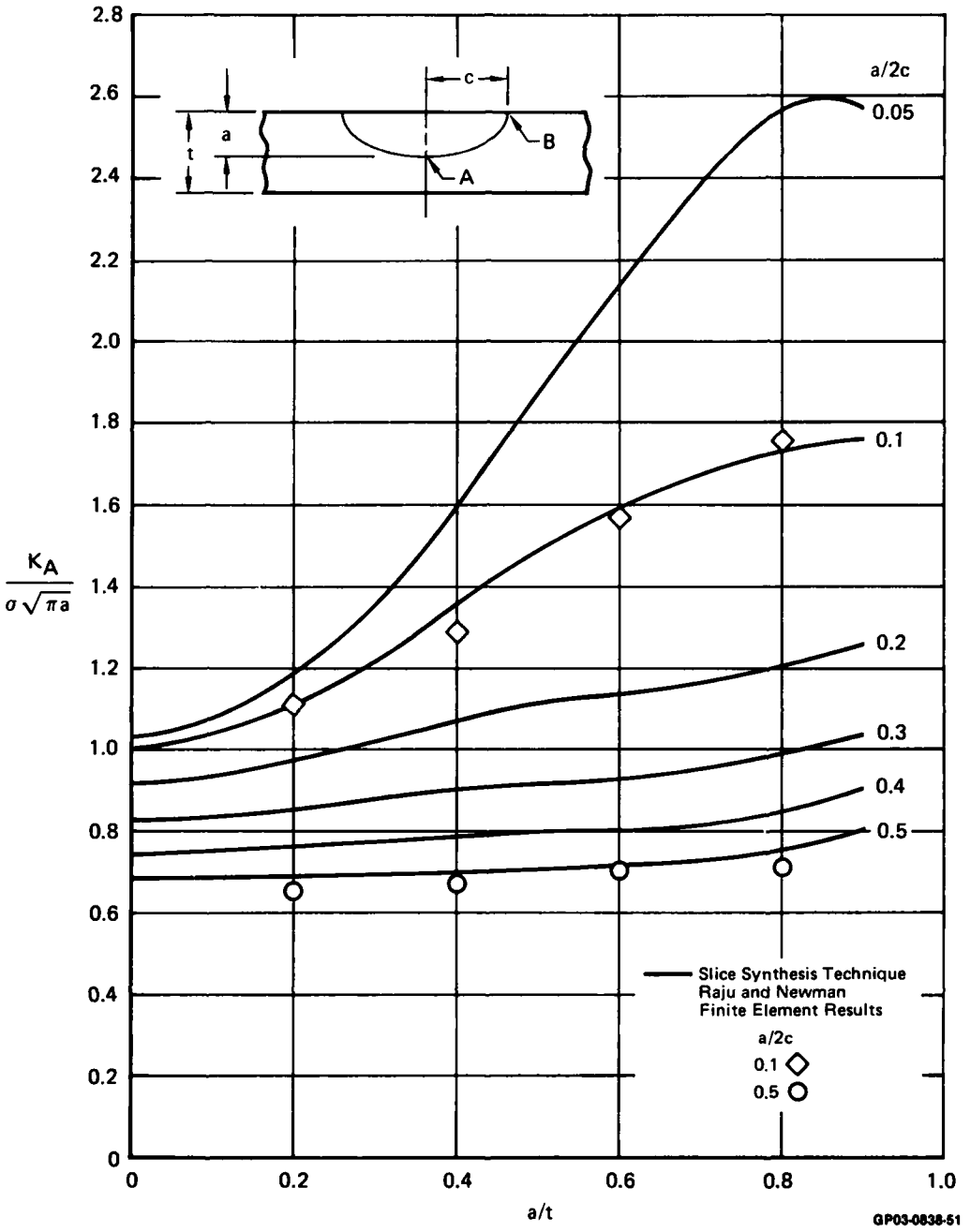

Figure B-1. *Surface Flaw Stress Intensity Solution of Depth*

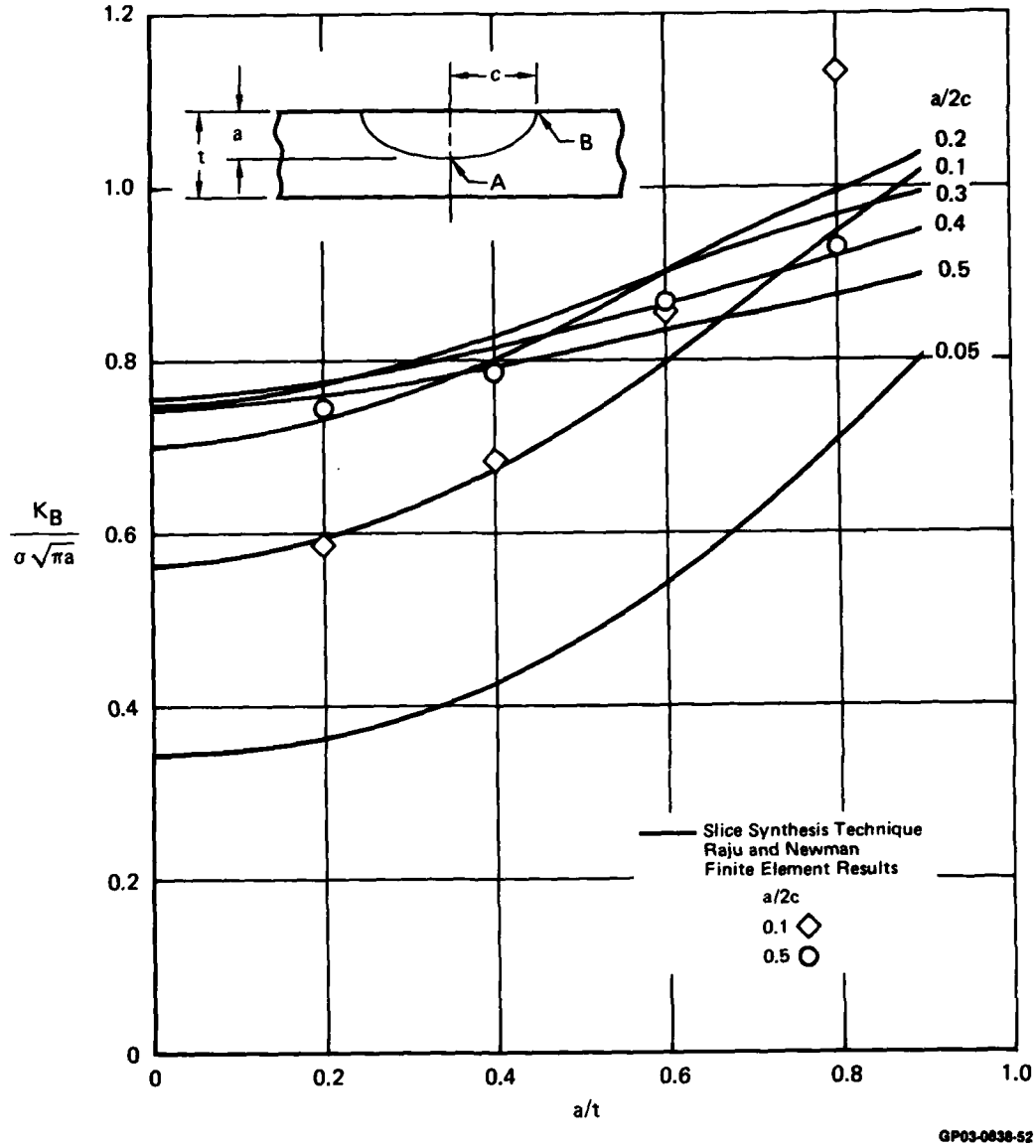

Figure B-2. Surface Flaw Stress Intensity Solution at Surface

and:	for $(a/c \leq 1.0)$	$(a/c > 1.0)$
	$Q = 1.0 + 1.47\ (a/c)^{1.64}$	$1.0 + 1.47\ (c/a)^{1.64}$
	$M1_A = 1.14 - 0.1\ (a/c)$	$1.04\ (c/a)$
	$M1_B = (a/c)\ (1.36 - 0.172(a/c))$	$1.0 + 0.188\ (c/a)$

$$M2_A = (a/t)^2\ [-0.166 + 0.258(a/t)^2 + 0.358(c/a) - 0.242(c/a)(a/t)^2]$$

$$M2_B = (c/t)\ [0.0935 + 0.162\ (a/t) - 0.0097\ (c/a)]$$

The form of these equations is the same as presented in Reference 20.

2. SURFACE FLAW GROWTH ANALYSIS ROUTINE

Input Definitions - The computer program has the following inputs:

a. title describing material and product form for reference (TITLE)

b. number of points in da/dN table (NDADN)

c. stress intensity factor range and crack growth rate for each point in da/dN table (DK(I), DADNA (I)).

d. initial surface flaw depth and length, material thickness, width and maximum stress in spectrum of interest (A, C, T, W, SMAX, KSUBC)

e. number of cycles analyzed between printout of stress intensity factor and crack growth (NPRNT).

Description of Output - The program outputs include title, A, C, T, W, SMAX, and a summary of a, β_A, K_A, and c, β_B, K_B printed at the end of each specified print interval. The print interval is reduced by a factor of ten where a exceeds 0.8t and again when transition to a through crack occurs. The stress intensity correction factors, β_A, and β_B are defined as

$$\beta_A = \frac{K_A}{\sigma\sqrt{\pi a}}$$

$$\beta_B = \frac{K_B}{\sigma\sqrt{\pi c}}$$

LISTING OF PROGRAM

```
C     THIS PROGRAM COMPUTES CRACK GROWTH AT SURFACE AND THROUGH DEPTH
C     FOR A SEMIELLIPTICAL SURFACE FLAW. STRESS INTENSITY FACTORS
C     ARE BASED ON MCAIR SLICE SYNTHESIS MODEL RESULTS. CRACK
C     FRONT PENETRATION OF BACK FACE IS PREDICTED BY LINEAR EXTRAPOLATION
C     OF STRESS INTENSITY FACTOR RESULTS. ASSUMED LOADING IS CONSTANT
C     AMPLITUDE, R=0., SINUSIODAL LOADING. PROGRAM WAS DEVELOPED BY
C     C.R.SAFF OF MCDONNELL AIRCRAFT CO., ST. LOUIS, MISSOURI,
C     TELEPHONE (314) 232-3356.
C
      INTEGER TITLE(20)
      REAL DADNA(25),DK(25),KSUBC
      PI=3.14159265
C
C      INPUTS ARE - TITLE
C                   FTY,FCY
C                   NDADN,FREQ
C                   DK(25),DADNA(25)
C                   A,C,T,W,SMAX,KSUBC
C                   NPRNT
C
C     MATERIAL PARAMETERS
C
C     TITLE DESCRIBES MATERIAL & PRODUCT FORM FOR REFERENCE
C     FTY=MONOTONIC TENSILE YIELD STRENGTH
C     FCY=CYCLIC TENSILE YIELD STRENGTH
C     NDADN=NO. OF POINTS IN DA/DN TABLE
C     FREQ=LOAD CYCLE FREQUENCY
C     DK(I)=DELTA K VALUES OF POINTS IN DA/DN TABLE
C     DADNA(I)=DA/DN VALUES OF POINTS IN DA/DN TABLE
C
C     GEOMETRIC PARAMETERS
C
C     A=INITIAL SURFACE FLAW DEPTH
C     C=INITIAL SURFACE FLAW LENGTH
C     T=MATERIAL THICKNESS - CRACK DEPTH DIRECTION
C     W=MATERIAL WIDTH - CRACK SURFACE DIRECTION
C     SMAX=MAXIMUM SPECTRUM STRESS APPLIED
C     KSUBC=CRITICAL STRESS INTENSITY FACTOR FOR MATERIAL THICKNESS
C
C     NPRNT=NO. OF CYCLES BETWEEN PRINTOUT OF K DATA AND GROWTH
C
      READ(5,1000) TITLE
      WRITE(6,1010) TITLE
      READ(5,1020) FTY,FCY
      READ(5,1030) NDADN,FREQ
      DO 10 I=1,NDADN
      READ(5,1020) DK(I),DADNA(I)
      DK(I)=ALOG10(DK(I))
   10 DADNA(I)=ALOG10(DADNA(I))
      OUTPUT,'INPUT A,C,T,W,SMAX,KSUBC'
      READ(5,1020) A,C,T,W,SMAX,KSUBC
      OUTPUT,'INPUT NO. OF CYCLES BETWEEN OUTPUT'
      READ(5,1030) NPRNT
      WRITE(6,1040) A,C,T,W,SMAX
      ICHK=0
      IBRK=0
      CYC=0.
      NP=0
      WRITE(6,1050)
```

```
C
C     DO LOOP 80 COMPUTES STRESS INTENSITY FACTORS AND GROWTH AT
C     DEPTH AND SURFACE OF FLAW
C
      DO 80 I=1,100000
      IF(I.EQ.1) NINC=1
      IF(I.EQ.2) NINC=NPRNT/1000-1
      IF(I.GT.2) NINC=NPRNT/1000
      IF(NINC.LT.1) NINC=1
      CYC=CYC+NINC
      ICYC=CYC
      IF(ICHK.EQ.1) GO TO 40
      AOC=A/C
      COA=1./AOC
      AOT=A/T
      IF(AOC.GT.1.) GO TO 20
      Q=1.+1.47*(AOC**1.64)
      XM1A=1.13-0.09*AOC
      XM1B=(1.36-0.185*AOC)*AOC
      GO TO 25
   20 Q=1.+1.47*COA**1.64
      XM1A=1.04*COA
      XM1B=1.+0.188*COA
   25 XM2A=(-0.166+0.258*AOT*AOT+0.358*COA-0.242*COA*AOT*AOT)*(AOT*AOT)
      XM2B=(0.0935+0.162*AOT-0.0097*COA)*(COA*AOT)
      BETAA=XM1A*(1.+XM2A)/SQRT(Q)
      BETAB=XM1B*(1.+XM2B)/SQRT(Q)
C
C     STRESS INTENSITY FACTOR EXPRESSIONS ARE ASSUMED GOOD UNTIL
C     FLAW DEPTH EXCEEDS 90% OF THICKNESS. VALUES AT A/T=0.8 AND
C     A/T=0.9 ARE USED FOR EXTRAPOLATIONS BEYOND A/T=0.9.
C
      IF(A.LT.0.8*T) GO TO 50
      NPRNT=NPRNT/10
      IF(NPRNT.LT.1) NPRNT=1
      ICHK=1
      A1=0.8*T
      A2=0.9*T
      IF(AOC.GT.1.) GO TO 30
      Q=1.+1.47*(AOC**1.64)
      XM1A=1.13-0.09*AOC
      XM1B=(1.36-0.185*AOC)*AOC
      GO TO 35
   30 Q=1.+1.47*COA**1.64
      XM1A=1.04*COA
      XM1B=1.+0.188*COA
   35 XM2A1=(-.166+.258*A1/T*A1/T+.358*COA-.242*COA*A1/T*A1/T)*(A1/T)**2
      XM2A2=(-.166+.258*A2/T*A2/T+.358*COA-.242*COA*A2/T*A2/T)*(A2/T)**2
      XM2B1=(0.0935+0.162*A1/T-0.0097*COA)*(COA*A1/T)
      XM2B2=(0.0935+0.162*A2/T-0.0097*COA)*(COA*A2/T)
      BA1=XM1A*(1.+XM2A1)/SQRT(Q)
      BA2=XM1A*(1.+XM2A2)/SQRT(Q)
      BB1=XM1B*(1.+XM2B1)/SQRT(Q)
      BB2=XM1B*(1.+XM2B2)/SQRT(Q)
   40 BETAB=(A-A1)/(A2-A1)*(BB2-BB1)+BB1
      BETAA=(A-A1)/(A2-A1)*(BA2-BA1)+BA1
```

```
   50 AK=BETAA*SMAX*SQRT(PI*A)
      BK=BETAB*SMAX*SQRT(PI*C/COS(PI*C/W))
      IF(IBRK.NE.1) GO TO 60
      WRITE(6,1070) CYC,A,BETAA,AK,C,BETAB,BK
      WRITE(6,1100)
      IBRK=IBRK+1
      GO TO 70
   60 IF(ICYC.LT.NP) GO TO 70
      NP=NP+NPRNT
      WRITE(6,1070) CYC,A,BETAA,AK,C,BETAB,BK
C
C     FRACTURE IS ASSUMED TO OCCUR WHENEVER THE STRESS INTENSITY
C     FACTOR AT EITHER THE SURFACE OR THE DEPTH EXCEEDS KSUBC.
C
   70 IF(AK.GT.KSUBC) GO TO 120
      IF(BK.GT.KSUBC) GO TO 130
C
C     DA/DN LOOK UP IS LOG(DA/DN) VS. LOG(DELTA K). CRACK GROWTH RATE
C     CURVE IN THE DEPTH DIRECTION IS ASSUMED SAME AS ALONG SURFACE.
C
      IF(BK.GT.0.8*KSUBC.OR.AK.GT.0.8*KSUBC) NINC=1
      AK1=ALOG10(AK)
      BK1=ALOG10(BK)
      CALL TLU(DK,DADNA,NDADN,AK1,ADADN)
      CALL TLU(DK,DADNA,NDADN,BK1,BDADN)
      ADADN=10.**ADADN
      BDADN=10.**BDADN
      A=A+ADADN*NINC
      C=C+BDADN*NINC
C
C     CRACK IS ASSUMED TO GROW AT A FIXED A/C RATIO AFTER CRACK
C     FRONT BREAKTHROUGH UNTIL BETAB EXCEEDS 1. THEN FLAW IS TREATED
C     AS A CENTER CRACK OF LENGTH 2C.
C
      IF(BETAB.GE.1.) GO TO 90
      IF(A.LT.T) GO TO 80
      IF(IBRK.GE.1) GO TO 80
      WRITE(6,1060)
      IBRK=IBRK+1
   80 CONTINUE
   90 WRITE(6,1080)
      WRITE(6,1070) CYC,A,BETAA,AK,C,BETAB,BK
      A=C
      WRITE(6,1090)
      WRITE(6,1070) CYC,A
      DO 110 I=1,100000
      CYC=CYC+NINC
      ICYC=CYC
      CK=SMAX*SQRT(PI*A/COS(PI*A/W))
      IF(ICYC.LT.NP) GO TO 100
      WRITE(6,1070) CYC,A
      NP=NP+NPRNT-1
```

```
  100 IF(CK.GT.KSUBC) GO TO 140
      IF(CK.GT.0.9*KSUBC) NINC=1
      CK=ALOG10(CK)
      CALL TLU(DK,DADNA,NDADN,CK,DADN)
      DADN=10.**DADN
      A=A+DADN*NINC
  110 CONTINUE
      STOP
  120 WRITE(6,1110)
      WRITE(6,1070) CYC,A,BETAA,AK,C,BETAB,BK
      STOP
  130 WRITE(6,1120)
      WRITE(6,1070) CYC,A,BETAA,AK,C,BETAB,BK
      STOP
  140 WRITE(6,1130)
      WRITE(6,1070) CYC,A
      STOP
 1000 FORMAT(20A4)
 1010 FORMAT(1H1,/20A4)
 1020 FORMAT(10F10.0)
 1030 FORMAT(I10)
 1040 FORMAT(/'     A0 = ',F8.3,'     C0 = ',F6.3,
     &/'      T = ',F8.3,'      W = ',F6.3,/'  SMAX = ',F8.3)
 1050 FORMAT(/T4,'CYC',T16,'A',T24,'BETAA',T34,'KA',T44,'C',T52,
     &'BETAB',T62,'KB'/)
 1060 FORMAT(' CRACK FRONT PENETRATES BACK FACE AT')
 1070 FORMAT(F8.0,2F10.4,F8.2,2F10.4,F8.2)
 1080 FORMAT(' SURFACE CRACK BECOMES THROUGH CRACK AT')
 1090 FORMAT(//' EQUIVALENT THROUGH CRACK LENGTH IS'/,
     &T4,'CYC',T16,'A'/)
 1100 FORMAT(1H )
 1110 FORMAT(/' FRACTURE AT A')
 1120 FORMAT(/' FRACTURE AT C')
 1130 FORMAT(/' THROUGH CRACK FRACTURE')
      END
C
C
C
      SUBROUTINE TLU(X,Y,N,XVAL,YVAL)
      DIMENSION X(N),Y(N)
      IF(X(N).GE.XVAL) GO TO 10
      I=N
      GO TO 30
   10 DO 20 I=1,N
      IF(X(I).GE.XVAL) GO TO 30
   20 CONTINUE
   30 IF(I.EQ.1) I=2
      YVAL=(Y(I)-Y(I-1))/(X(I)-X(I-1))*(XVAL-X(I-1))+Y(I-1)
      RETURN
      END
```

SAMPLE INPUT

```
DA/DN DATA - 300M STEEL - 10 CPS - DRY AIR
     248.       228.
      13         10.
     12.      .03E-6
     14.      .90E-6
     16.     1.31E-6
     18.     1.85E-6
     20.     2.55E-6
    22.5      3.6E-6
     25.     4.75E-6
     30.      7.5E-6
     35.     12.8E-6
     40.     18.2E-6
     45.     25.5E-6
     50.     40.0E-6
     60.     600.E-6
   0.04      0.0545        0.25          1.          100.          60.
    500
```

OUTPUT FOR SAMPLE INPUT

DA/DN DATA - 300M STEEL - 10 CPS - DRY AIR

A0 = .040 C0 = .055
T = .250 W = 1.000
SMAX = 100.000

CYC	A	BETAA	KA	C	BETAB	KB
1.	.0400	.7813	27.69	.0545	.6696	27.91
500.	.0432	.7758	28.57	.0578	.6769	29.08
1000.	.0466	.7712	29.52	.0614	.6836	30.32
1500.	.0504	.7681	30.57	.0656	.6893	31.64
2000.	.0547	.7661	31.76	.0705	.6945	33.10
2500.	.0596	.7651	33.11	.0762	.6996	34.74
3000.	.0653	.7648	34.65	.0830	.7050	36.61
3500.	.0720	.7651	36.38	.0907	.7111	38.75
4000.	.0795	.7669	38.34	.0998	.7172	41.18
4500.	.0883	.7712	40.62	.1107	.7233	43.99
5000.	.0988	.7793	43.41	.1243	.7292	47.39
5500.	.1120	.8025	47.60	.1457	.7295	52.10
FRACTURE AT C						
5767.	.1284	.8825	56.05	.1934	.6986	60.11

REFERENCES

1. Dill, H. D., and Saff, C. R., "Environment-Load Interaction Effects on Crack Growth", AFFDL-TR-78-137, November 1978.

2. Fujimoto, W. T., and Gallagher, J. P., "Summary of Landing Gear Initial Flaws", AFFDL-TR-77-125, December 1977.

3. Ryder, J. T., and Pickel, F. M., "Effect of Temperature on Stress Corrosion Cracking of 300M Steel", Journal of Testing and Evaluation, Vol. 6, No. 2, March 1978, pp. 129-133.

4. "Damage Tolerant Design Handbook", MCIC HB-01, Part 1, January 1975.

5. Dill, H. D., and Saff, C. R., "Spectrum Crack Growth Prediction Method Based on Crack Surface Displacement and Contact Analyses", Fatigue Crack Growth Under Spectrum Loads, ASTM STP 595, American Society for Testing and Materials, 1976, pp. 306-319.

6. Forman, R. G., Kearney, V. E., and Engle, R. M., "Numerical Analysis of Crack Propagation in Cylic-Loaded Structures", Journal of Basic Engineering, September 1967.

7. Wei, R. P., and Landes, J. D., "Correlation Between Sustained-Load and Fatigue Crack Growth in High Strength Steels", Materials Research and Standards, Vol. 9, No. 7, pp. 25-28, July 1969.

8. Willenborg, J., Engle, R. M., and Wood, H. A., "A Crack Growth Prediction Model Using an Effective Stress Concept", AFFDL-TM-71-1-FBR, 1971.

9. Gallagher, J. P., and Hughes, T. F., "Influence of Yield Strength on Overload Affected Fatigue Crack Behavior in 4340 Steel", AFFDL-TR-74-27, March 1974.

10. Probst, E. P., and Hillberry, B. M., "Fatigue Crack Delay and Arrest Due to Single Peak Tensile Overloads", AIAA Paper 73-325, AIAA Dynamics Specialists Conference, Williamsburg, Va., March 19-20, 1973.

11. Wei, R. P., and Shih, T. T., "Delay in Fatigue Crack Growth", International Journal of Fracture, Vol. 10, No. 1, March 1974, pp. 77-85.

12. Alzos, W. X., Skat, A. C., Jr. and Hillberry, B. M., "Effect of Single Overload/Underload Cycles on Fatigue Crack Propagation", Fatigue Crack Growth Under Spectrum Loads, ASTM STP 595, American Society for Testing and Materials, 1976, pp. 41-60.

13. McGee, W. M., and Hsu, T. M., "Effects of Underloads on Fatigue Crack Growth", AFFDL-TR-77-2, March 1977.

14. Gallagher, J. P., and Stalnaker, H. D., "Methods for Analyzing Fatigue Crack Growth Rate Behavior Associated with Flight-by-Flight Loading", AIAA Paper 74-367, presented at the 15th Structure, Structural Dynamics and Materials Conference, April 17-19, 1974.

15. Engle, R. M., "CRACKS II, User's Manual", AFFDL-TM-74-173.

16. Dill, H. D., and Saff, C. R., "Effect of Fighter Attack Spectrum on Crack Growth", AFFDL-TR-76-112, March 1977.

17. Hsu, T. M., and Lassiter, L. W., "Effects of Compressive Overloads on Fatigue Crack Growth", AIAA Paper No. 74-365, AIAA/ASME/SAE Structures, Structural Dynamics and Materials Conference, Las Vegas, Nevada, April 17-19, 1974.

18. Raju, I. S., and Newman, J. C., Jr., "Improved Stress-Intensity Factors for Semi-Elliptical Surface Cracks in Finite-Thickness Plates", NASA TM X-72825, August 1977.

19. Newman, J. C., Jr. and Raju, I. S., "Analysis of Surface Cracks in Finite Plates Under Tension or Bending Loads", NASA Technical Paper 1578, 1979.

20. Newman, J. C., Jr. "Fracture Analysis of Surface and Through Cracks in Cylindrical Pressure Vessels", NASA TN D-8325, December 1976.

DISTRIBUTION LIST

Naval Sea Systems Command
Washington, DC 20362
(Attn: C. H. Pohler)

Bell Helicopter Corporation
Box 482
Fort Worth, Texas 76101

Boeing Company
Vertol Division
P.O. Box 16858
Philadelphia, PA 19142

Goodyear Aerospace Corp.
1210 Massillon Road
Akron, Ohio 44350

Kaman Aircraft Corporation
Old Windsor Road
Bloomfield, CT 06002

McDonnell-Douglas
McDonnell Aircraft Corp.
P.O. Box 516
St. Louis, MO 63166

Republic Aviation Division
Fairchild-Hiller Corp.
Farmingdale
Long Island, NY 11735

Naval Research Lab
Washington, DC 20375
(Attn: T. W. Crooker 6384)

Administrator
Natl. Aeron. & Space Admin.
600 Independence Ave., SW
Washington, DC 20546

Naval Air Systems Command
Department of the Navy
Washington, DC 20361
(Attn: Code 5303)

Naval Air Systems Command
Department of the Navy
Washington, D.C. 20361
(Attn: Code 5203)

Naval Air Systems Command
Department of the Navy
Washington, DC 20361
(Attn: Code 320B)

Naval Air Systems Command
Department of the Navy
Washington, D.C. 20361
(Attn: Code 320A)

Office of Naval Research
Washington, D.C. 20362
(Attn: Dr. N. Perrone)

University of Illinois
College of Engineering
Urbana, Illinois 61803
(Attn: Theoretical & Applied
Mechanics Dept.)

University of Minnesota
107 Aeronautical Bldg.
Minneapolis, MN 55455
(Attn: Eng. Library)

Cornell Aeronautical Lab
4455 Genesee Street
Buffalo, New York 14221
(Attn: Tech. Library)

Naval Postgraduate School
Monterey, CA 93940
(Attn: Prof. Lindsay)

Vought Corp.
P.O. Box 5907
Dallas, Texas 75222
(Attn: Mr. D. White)

Naval Research Lab
Washington, DC 20375
(Attn: Mr. R. Judy 6382)

University of Dayton
Research Institute
300 College Park
Dayton, OH 45469
(Attn: Dr. J. Gallagher)

Lehigh University
Sinclair Lab. Bldg. 7
Bethleham, PA 18015
(Att [illegible] Weil)

DISTRIBUTION LIST (Continued)

Director
Naval Research Lab
Washington, DC 20375

Department of Mech. Engrg.
University of Kansas
Lawrence, Kansas 66044
(Attn: Eng. Library)

Aluminum Company of America
Alcoa Labs
Alcoa Center, PA 15069
(Attn: Mr. J. G. Kaufman)

Metals & Ceramics Info. Center
Battelle Memorial Institute
505 King Avenue
Columbus, Ohio 43201

LeHigh University
Bethlehem, PA 18015
(Attn: Prof. G. C. Sih)

Lockheed Aircraft Corp.
2555 N. Hollywood Way
Burbank, CA 91503
(Attn: Dr. T. Brussat)

Northrop Corporation
Aircraft Division
3901 Broadway
Hawthorne, CA 90250
(Attn: Mr. Levi-MN.3605/34)

Fracture Research Inc.
2992 Heatherleaf Way
Columbus, OH 43229
(Attn: Dr. D. Brock)

Midwest Research Institute
425 Volker Boulevard
Kansas City, Missouri 64110

Department of Aeron. Engrg.
University of Michigan
Ann Arbor, Michigan 48105
(Attn: Eng. Library)

Belfour Stulen, Inc.
13919 W. Bay Shore Drive
Traverse City, MI 49684

Natl. Aero. & Space Admin.
Lewis Research Center
21000 Brookpark Road
Cleveland, OH 44135

General Dynamics
Convair Division
San Diego, CA 92112
(Attn: Mr. G. Kruse)

Rockwell International
Columbus Aircraft Division
4300 East Fifth Avenue
Columbus, OH 43216
(Attn: Mr. F. Kaufman)

Air Force Flight Dynamics Laboratory
Wright Patterson AFB, Ohio 45433
(AFWAL/FIBEC)

Lockheed Georgia Co.
Marietta, Georgia 30064
(Attn: Mr. T. Adams
D71/20 Z407)

Commander
Naval Air Test Center
Patuxent River, MD 20670

Chief of Naval Air Basic Training
Naval Air Station
Pensacola, FL 32508

Naval Air Systems Command
Representative, Atlantic
Naval Air Station
Norfolk, VA 23511

Commanding Officer
Naval Air Rework Facility
Naval Air Station
Jacksonville, FL 32212

Commanding Officer
Naval Air Rework Facility
Naval Air Station
Quonset Point, R.I. 02819

Commander, Naval Air Force
U.S. Atlantic Fleet
Naval Air Station
Norfolk, VA 23511

Air Force Wright Aero. Lab
Air Force Systems Command
Wright-Patterson Air Force
Base, Ohio 45433
(Attn: FB)

Air Force Wright Aero. Lab
Air Force Systems Command
Wright-Patterson Air Force
Base, Ohio 45433
(Attn: LAM)

U. S. Army
Aberdeen Proving Ground
Aberdeen, Maryland

Commander
Naval Air Safety Center
Naval Air Station
Norfolk, VA 23511

Chief of Naval Air Res. Trg.
Naval Air Res. Trg. Command
Naval Air Station
Glenview, IL 60026

Naval Air Systems Command
Representative, Pacific
Naval Air Station, N. Island
San Diego, CA 92135

Commanding Officer
Naval Air Rework Facility
Naval Air Station
Norfolk, VA 23511

Commanding Officer
Naval Air Rework Facility
Naval Air Station, N. Island
San Diego, CA 92135

Commander, Naval Air Force
U.S. Pacific Fleet
Naval Air Station, N. Island
San Diego, CA 92135

Commander
Naval Weapons Laboratory
Dahlgren, VA 22248
(Attn: Mr. Morton)

Air Force Wright Aero. Lab
Air Force Systems Command
Wright-Patterson Air Force
Base, Ohio 45433
(Attn: SEFS)

Air Force Wright Aero. Lab
Air Force Systems Command
Wright-Patterson Air Force
Base, Ohio 45433
(Attn: FBA)

U. S. Army
AMMRC
Watertown, Massachusetts

Chief of Naval Air Advanced
Training
Naval Air Station
Corpus Christi, Texas 78419

Chief of Naval Air Training
Naval Air Station
Pensacola, FL 32508

Commanding Officer
Naval Air Rework Facility
Naval Air Station
Pensacola, FL 32508

Commanding Officer
Naval Air Rework Facility
Marine Corps Air Station
Cherry Point, N.C. 28533

U. S. Army
Aviation Systems Command
St. Louis, MO

Air Force Wright Aero. Lab
Air Force Systems Command
Wright-Patterson Air Force
Base, Ohio 45433
(Attn: FBR)

DISTRIBUTION LIST (Continued)

Naval Air Systems Command
Department of the Navy
Washington, D.C. 20361
(Attn: Code 5302)

Officer in Charge
Carderock Laboratory
Naval Ship Res. & Dev. Ctr.
Bethesda, MD 20034
(Attn: A. Stavovy 730)

Boeing Commercial Airplane Company
P.O. Box 3707
Seattle, Washington 98124
(Attn: Mr. T. Porter)

McDonnell Douglas Aircraft Corporation
3855 Lakewood Blvd.
Long Beach, CA 90846
(Attn: Mr. Abelkis-MC35-41)

Grumman Aerospace Corp.
Bethpage, Long Island, NY 11714
(Attn: Mr. Gomza)

Lockheed Aircraft Corp.
Lockheed-California Co.
2555 N. Hollywood Way
Burbank, CA 91503

Rockwell International
Los Angeles Division
International Airport
Los Angeles, CA 90009
(Attn: Mr. G. Fitch)

Sikorsky Aircraft Company
Stratford, CT 06497

Federal Aviation Agency
(FS-120)
800 Independence Ave., SW
Washington, DC 20553

NASA-Langley Research Ctr.
Fatigue Branch
Langley Field, VA 23365
(Attn: Dr. J. Davidson)

AFIAS-B
Directorate of Aerospace Safety
Norton AFB, CA 92409

Bell Aerosystems Company
Div. of Bell Aerospace Corp.
P.O. Box 1
Buffalo, N.Y. 14205

Boeing Company
Airplane Division
3801 S. Oliver Street
Wichita, Kansas 67210
(Mr. D. Bryan, K16-29)

General Dynamics Corporation
P.O. Box 748
Fort Worth, Texas 76101
(Attn: Dr. S. Manning)

Aircraft-Missiles Div.
Fairchild-Hiller Corp.
Hagerstown, MD 21740

Lockheed Aircraft Corp.
Lockheed-Georgia Co.
86 S. Cobb Drive
Marietta, Georgia 30061

Northrop Corporation
Aircraft Division
3901 W. Broadway
Hawthorne, CA 90250

Headquarters
Res. & Tech. Division
Air Force Systems Command
Bolling AFB, WA 20332

Federal Aviation Agency
Technology Center
Atlantic City, NJ 08405
(ACT-330, Mr. D. Nesterok)

National Bureau of Standards
Washington, DC 20234

DISTRIBUTION LIST (Continued)

Air Force Wright Aero. Lab
Air Force Systems Command
Wright-Patterson Air Force
Base, Ohio 45433
(Attn: FYA)

Air Force Wright Aero. Lab
Air Force Systems Command
Wright-Patterson Air Force
Base, Ohio 45433
(Attn: LPH)

U. S. Army
AMRDL
Fort Eustis, VA 23604

Air Force Wright Aero. Lab
Air Force Systems Command
Wright-Patterson Air Force
Base, Ohio 45433
(Attn: LLD)

Commanding Officer
Naval Air Rework Facility
Naval Air Station
Alameda, CA 994501